Cortical Reorganization Characterization Using Multimodal EEG − FNIRS Integration Analysis

by
Rihui Li

A dissertation submitted to the Department of Biomedical Engineering,
Cullen College of Engineering
in partial fulfillment of the requirements for the degree of

DOCTOR OF PHILOSOPHY

in Biomedical Engineering

Chair of Committee: Yingchun Zhang, Ph.D.

Committee Member: Joseph T. Francis, Ph.D.

Committee Member: Jinsook Roh, Ph.D.

Committee Member: Luca Pollonini, Ph.D.

Committee Member: Sheng Li, M.D., Ph.D.

University of Houston
May 2020

Copyright 2020, Rihui Li

ACKNOWLEDGMENTS

First and foremost, I wish to express my deepest gratitude toward my academic advisor, Dr. Yingchun Zhang, for his endless support, knowledge, help and kindness through my PhD study. I would like to thank him for his willingness to share knowledge and for being such an encouraging supervisor. He has not only been a caring and dedicated supervisor, but also a great supportive mentor allowing me to pursue my ideas and interests. In retrospect, I have a very fruitful PhD career experience, both in academic achievements and personal development.

I would also like to thank my committee members, Dr. Sheng Li, Dr. Jinsook Roh, Dr. Joe Francis and Dr. Luca Pollonini for their advices and comments on my dissertation, as well as critical questions incented to widen my research from various perspectives.

I greatly appreciate the funding and resources that support my research and laboratory through the University of Houston, Baylor College of Medicine and National Institute of Health.

I also greatly appreciate the Department of Biomedical Engineering, as well as its enthusiastic and friendly staffs, who have always been very informative and helpful whenever I met difficulties during my PhD life.

I would like to give my genuine gratitude to all the members of my lab, for being great colleagues and friends, who have contributed greatly to my very fruitful and enjoyable PhD experience. Special thanks to Thinh Nguyen and Thomas Potter for their invaluable insights and knowledge that have helped me greatly in improving my scientific research.

At the end, a special thanks to my family, my father Jianxiong Li, my mother Yundi Huang, my brother Rifeng Li for all their love, encouragement and endless support. I dedicate my dissertation work to you. It was a long journey and we did it!

ABSTRACT

Introduction

Electroencephalography (EEG) and functional near-infrared spectroscopy (fNIRS) stand as state-of-the-art techniques for non-invasive functional neuroimaging. On a unimodal basis, EEG suffers from poor spatial resolution while presenting high temporal resolution. In contrast, fNIRS offers better spatial resolution though it is constrained by its poor temporal resolution. One important merit shared by the EEG and fNIRS is that, both modalities have favorable portability and could be integrated into a compatible experimental setup, providing a compelling ground for the development of a multimodal EEG-fNIRS integration analysis approach. The main goal of this dissertation is to develop and implement multimodal EEG/fNIRS integration analysis method for the characterization of cortical reorganization.

Methods

The first part of the dissertation primary focuses on the experimental validation of the inherent correlation between neuronal activity and hemodynamic response from views of fNIRS-guided and EEG-guided, respectively. After that, we develop a novel fNIRS-informed EEG source imaging approach, by fusing the high spatial resolution of fNIRS and high temporal resolution of EEG, to investigate the cortical activity with good spatiotemporal resolution. Leveraging the high spatiotemporal resolution cortical activity, detailed cortical network alterations, can be subsequently estimated, providing a complete cortical-level characterization of the brain activity.

Results

Through an fNIRS-guided hybrid EEG-fNIRS brain computer interface (BCI) study and an EEG-guided fNIRS analysis study, we validate that the complementary information offered by EEG and fNIRS is beneficial to the investigation of cortical activity. In addition, the novel fNIRS-informed EEG source imaging, is developed,

validated and applied in studying the brain network alterations induced by Alzheimer's disease and stroke.

Conclusion

The novel fNIRS/EEG integration methods and subsequent brain network analysis presented in this dissertation have provided the tools and technologies for cortical-level assessment of normal brain activity and characterizing cortical reorganization associated with brain disorders.

TABLE OF CONTENTS

LIST OF TABLES

LIST OF FIGURES

Chapter 1 ─ Basis of Brain Imaging

1.1 Background

The human brain comprises billions of neurons [1]. Each of these forms a number of synapses, establishing a complicated network with quadrillions of connections and thus enabling our brains to function as they do [2]. Although there is an increasing understanding of neurons on a microscopic scale in recent decades, little is known about how these huge numbers of neurons (and synapses) work collectively to generate macroscopic brain signals and human behaviors as observed.

It is believed that human brain functions and relevant behaviors are carried out by complex neural activations and interactions. This internal activities generally elevate electrical activity (direct effects) accompanied by hemodynamic and metabolic response (indirect effects), which serve as the basic sources for all noninvasive neuroimaging techniques. Depending on the sources of the signals, these brain imaging techniques can be roughly divided into two categories. On one hand, the first category refers to imaging techniques that directly capture the neural electrical activities by detecting the induced electrical signal fluctuations over the scalp. The most representative method in this category is electroencephalography (EEG). On the other hand, the second category comprises indirect imaging approaches that rely on hemodynamic (cerebral blood flow, cerebral blood volume) anr metabolic (glucose and oxygen utilization) response induced by neural activity. Commonly-available techniques in this category are functional near-infrared spectroscopy (fNIRS), functional magnetic resonance imaging (fMRI), and positron emission tomography (PET).

1.2 Electroencephalography

Electroencephalography (EEG), first found by Hans Berger in 1929 [3], is thought to result primarily from the synchronization of post-synaptic potentials at cortical pyramidal neurons [4]. The recorded EEG signal is not representing the single neuron depolarization inside the brain. Instead, it is assumed that tens of thousands of synchronized pyramidal neurons at cortex are firing when the brain is activated, wherein dendritic trunks of the neurons are coherently orientated, parallel with each other and perpendicular to the cortical surface so as to induce sufficient summation and propagation of electrical signals to the scalp (Figure 1-1) [5].

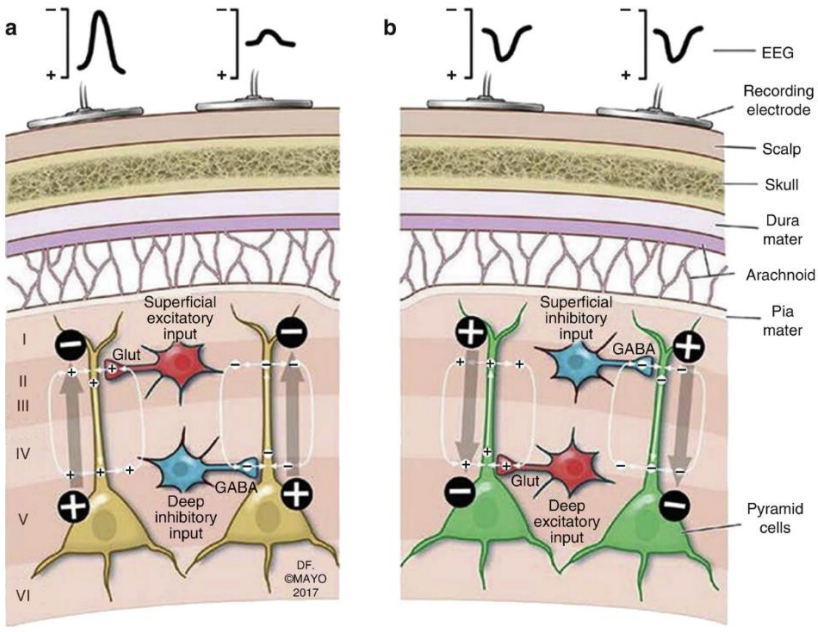

Figure 1-1. Generation of EEG signal [6].

Typically, EEG signals is measured through EEG electrodes (including a reference electrode and a ground electrode) which are placed over a person's scalp. Voltages differences between the electrodes and the reference electrode are then measured and amplified (Figure 1-1). In general, the recorded EEG signals which represent the large-

scale neural oscillatory activity, can be divided into various rhythms depending on characteristic frequency bands, including theta (4–7 Hz), alpha (8–14 Hz), beta (15–25 Hz) and gamma (> 25 Hz) [7]. These brain rhythms contain information associated with the ongoing neuronal processing in specific brain areas, which allows EEG to be used as a non-invasive method for the characterization of cortical reorganization induced by various brain disorders, particularity in the diagnosis of epilepsy and stroke [7, 8].

1.3 Functional Near-infrared Spectroscopy

Functional Near-infrared Spectroscopy (fNIRS), first reported by Jobsis in 1977 [9], is an optical imaging technique to non-invasively investigate the hemodynamics response in humans brain. fNIRS usually utilizes lights with distinct wavelengths (between 600 and 1000 nm) that can penetrate the scalp and reach the cortical surface to measure the concentration changes of oxygenated hemoglobin (HbO) and deoxygenated hemoglobin (HbR) that are coupled with the metabolic activity of neurons in the outer layers of the cortex. This technique is particularly useful for studying the functional activation within the brain due to the inherent relationship between neural activity and hemodynamic response in the brain [10]. Specifically, fNIRS is capable of measuring the regional changes of HbO and HbR concentration, which can serve as an indicator of hemodynamic changes associated with neural activity in the brain.

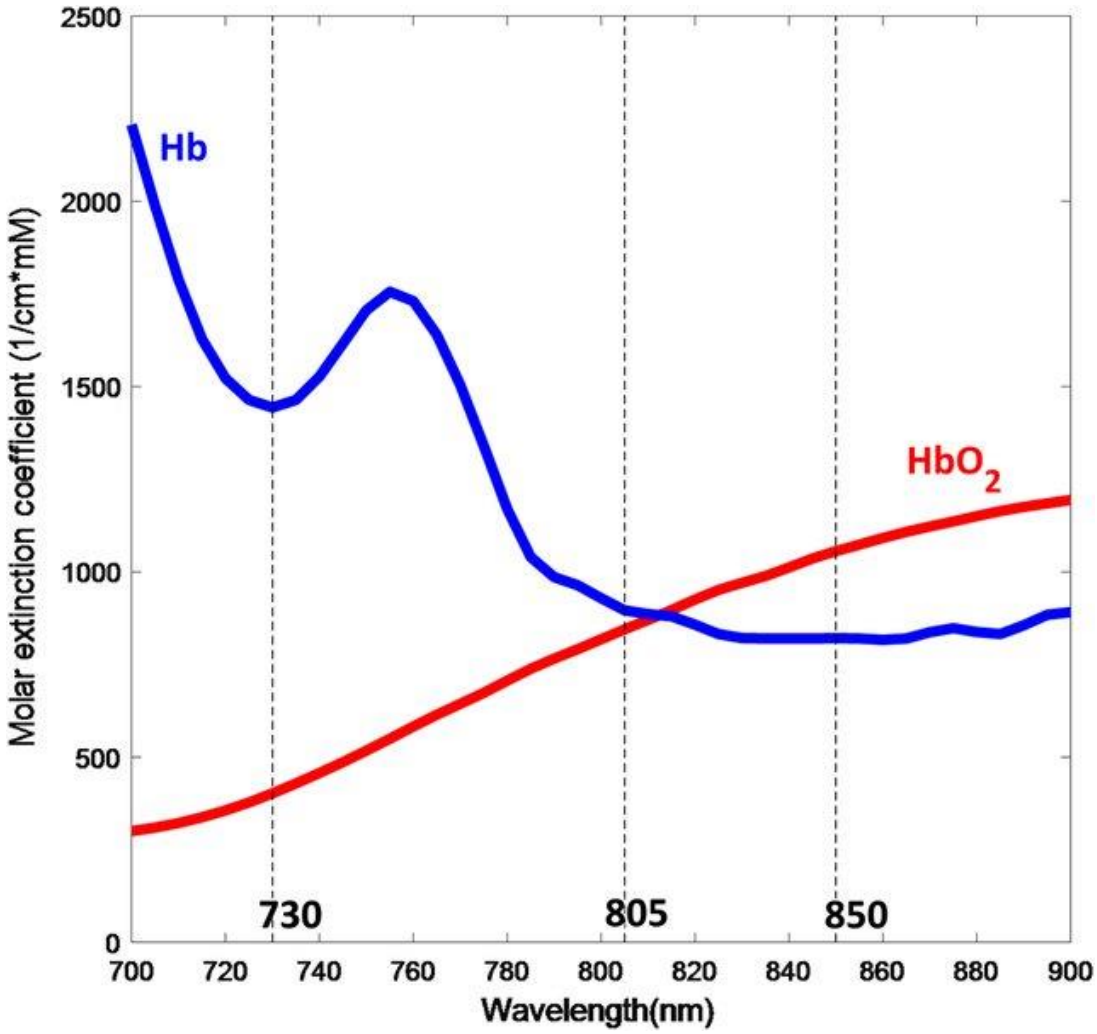

Figure 1-2. Absorption of light by oxygenated and deoxygenated hemoglobin (blue and red lines) and common NIRS light source wavelengths (730 and 850 nm) [11].

Currently, the continuous wave NIRS (CW-NIRS) is extensively used in the research and clinical settings due to its low-cost and simplicity. The measurement of the hemoglobin concentration (Hbo and HbR) in CW-NIRS primary relies on the physical basis that chromophores inside the brain, in particular the HbO and HbR, have specific and sensitive absorption characteristics in the near-infrared range (between 600 and 1000 nm, Figure 1-2). With this in mind, lights at different wavelengths can be injected into the brain via the sources (illuminators) placed on the scalp, and the attenuated lights

are detected by the optical detectors placed near the illuminators (Figure 1-3), from which the concentration changes of HbO and HbR can be computed based on Modified Beer-Lambert Law [12]. Specifically, CW-NIRS systems typically utilize laser/LED sources to shine two distinct wavelengths into the brain at a constant intensity and uses detectors to measure the intensity of diffusely reflected light continuously.

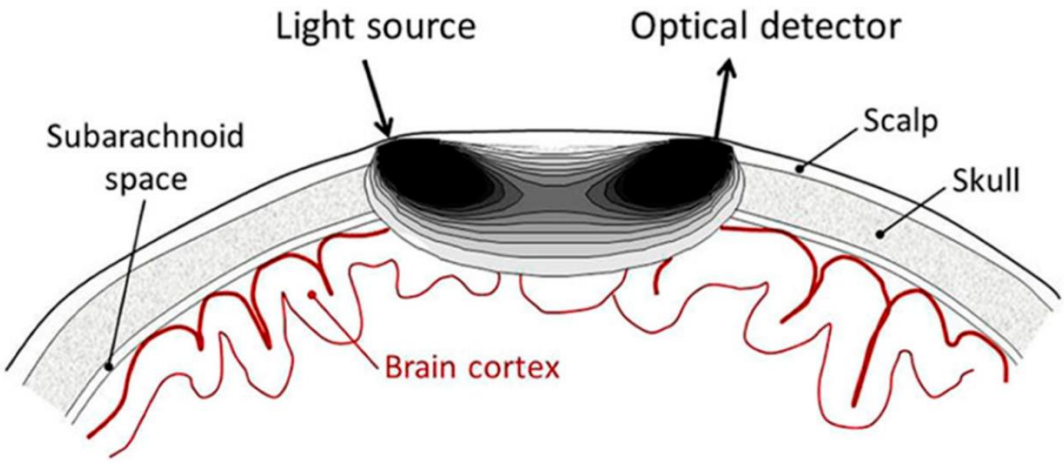

Figure 1-3. Schematic demonstration of fNIRS measurement [13].

1.4 Multimodal Brain Imaging Approach

The functional activity of the cerebral cortex can be investigated using various imaging techniques including EEG, fNIRS and fMRI. Each of these techniques has its own advantages and disadvantages. Compared to fMRI, fNIRS features higher temporal resolution (1 cm), good portability, low-cost, good resistance to motion artifacts, which is applicable to various measurement scenarios including clinical setting as well as natural environment [12]. More importantly, fNIRS measurements have been proven to be similar to the blood oxygen level dependent (BOLD) response obtained by fMRI [14]. However, there are also several limitations of fNIRS techniques; the limited penetration depth, low signal-noise ratio, relatively low temporal resolution compared

to EEG. On the other hand, EEG presents a number of advantages over fMRI for exploring the dynamic brain activity: it is highly-portable, inexpensive, and features a very high temporal resolution (millisecond) compared to fNIRS and fMRI [15], though EEG is highly vulnerable to motion artifacts that would inhibit the EEG measurement in a practical setting [16].

Single-modality imaging techniques can only capture limited information associated with neural activity due to their technical limitations and the complex neural processing within the brain. In order to comprehensively explore the functional activity of the brain, multimodal approaches are needed. Generally, integrated EEG-fNIRS approaches offer various benefits over single-modality methods by exploiting their individual strengths; EEG provides favorable temporal resolution, while fNIRS offers better spatial resolution and is robust to noise [17, 18]. Additionally, EEG and fNIRS signals are associated with different aspects of cortical activity, providing a built-in validation for identified activity. Measurements obtained from each of these two modalities thereby provide complementary information related to functional activity of the brain.

1.5 Neurovascular Coupling

Apart from their complementary technical properties, the rationale behind the combination of EEG and fNIRS relies on a physiological phenomenon called neurovascular coupling within the brain [19]. Briefly, neural activity is inherently accompanied with the fluctuation of the cerebral blood flow (CBF) that carries oxygen and nutrients to neurons for their function. Specifically, when the neurons are activated within a specific brain region, blood will flow to that brain region in order to meet the

increased demand of glucose and oxygen, resulting in the fluctuations of the hemoglobin concentration (HbO and HbR) that could be pick up by the functional imaging techniques such as fNIRS and fMRI (Figure 1-4). The so-called neurovascular coupling forms the theoretical basis for multimodal-based imaging of brain activity, such as combined EEG-fMRI and combined EEG-fNIRS imaging approaches. It has been shown in recent studies that the impairment of neurovascular coupling could serve as a sign for several neurological diseases such as Alzheimer's disease and stroke [19-21], which might provide a new prospective for evaluation and diagnosis of neurological diseases as well as increase our understanding of the mechanism of the neurovascular coupling.

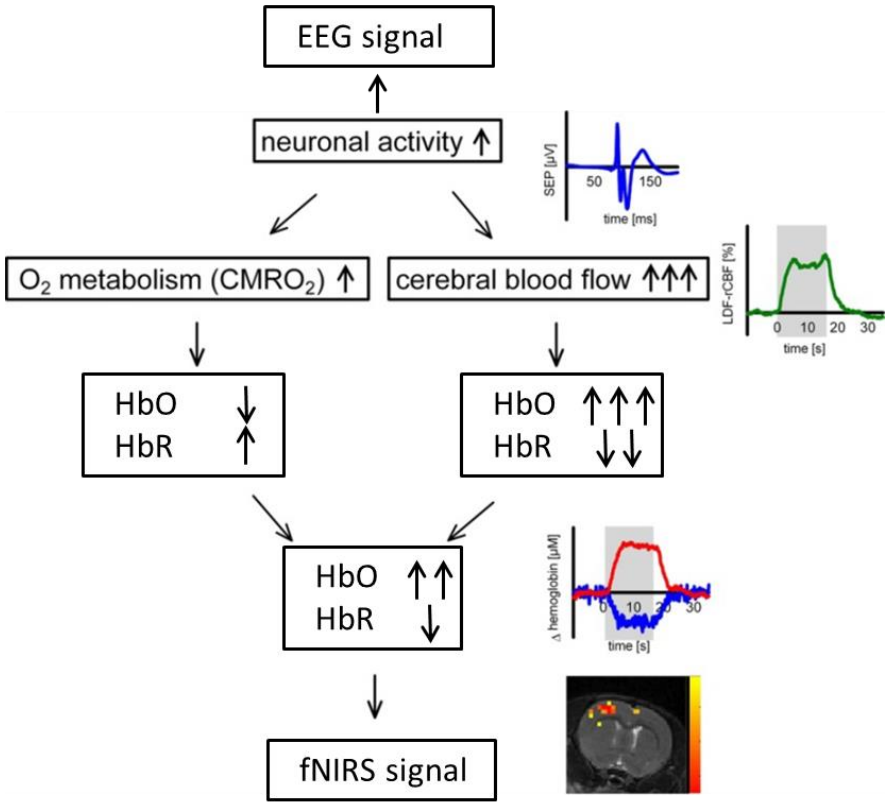

Figure 1-4. The schematic of neurovascular coupling [22].

1.6 Multimodal fNIRS-EEG Studies in Human

The integration of the fNIRS and EEG provides complementary information about electrical and metabolic-hemodynamic activity of the brain activity without causing electro-optical interference, which has led to increasing investigations of the benefits of integrated EEG and fNIRS in a number of studies [21, 23, 24]. In the last decade, numerous papers have been published on simultaneous recordings of fNIRS and EEG, mainly focusing on both nonclinical and clinical topics.

In terms of nonclinical applications, three main areas have been extensively explored using integrated fNIRS and EEG: brain computer interface (BCI), neurovascular coupling, and the investigation of healthy brain functions. In general, BCIs allow users to control computers or external devices based directly on the modulation of brain activity. The active investigations of the benefits of hybrid EEG-fNIRS BCI have been conducted and validated on healthy populations in a number of BCI studies recently [23-25]. Specifically, by combining features derived from two modalities, these multimodal fNIRS-EEG BCIs have shown enhanced classification accuracy over single modality in a variety of tasks, including mental arithmetic (MA), motor imagery and execution [26-29]. A special direction of combined fNIRS-EEG was proposed by Khan et al., wherein two commands (“forward” and “backward”) were decoded by EEG signals from the prefrontal area and other two commands (“left” and ”right”) were decoded by the fNIRS siganls from the motor area [30]. High classification accuracies were reported for the four different control signals using the multimodal fNIRS-EEG features. Apart from the feature fusion, a few studies have attempted to optimize the computational cost and the complexity of the hybrid BCIs, mainly by reducing the

number of electrodes/optodes. Previous work has suggested different approaches for this aim by selecting the most representative channels or signal components for classification, including bundled optode- based approaches [31], channel averaging approaches [32], and general linear model-guided [29].

Regional neural activity is typically accompanied by electrical activity generation and concurrent metabolic variation. Simultaneous fNIRS-EEG recording are highly suited for neurovascular coupling investigation both in a data-driven approach or, if the coupling is assumed known, for better neural activity estimation. Specifically, neurovascular coupling can be assessed using different experimental settings, including resting-state and external stimulation. In terms of resting-state neurovascular coupling, Keles et al., collected data with a customized whole-head fNIRS-EEG cap and focused on the spectral-EEG effects on neurovascular coupling [33]. They found a delayed alpha activity (8 to 16 Hz) modulation of hemodynamic response in posterior areas and a strong beta activity (16 to 32 Hz) modulation of hemodynamic response that might be driven by the alpha-beta coupling in EEG. In addition to the resting-state analysis on time series, neurovascular coupling can also be explored with specific task. Li et al., collected concurrent EEG and fNIRS data during a motor execution task and performed an EEG-informed fNIRS general linear model (GLM) analysis with the assumption that EEG temporal variation may be highly correlated with the hemodynamic response induced by the motor task [34]. Their results showed that the EEG-derived information, particularly the alpha and beta components, could better capture the strength of neural activity at single trial task and thus enhance the performance of fNIRS GLM analysis when compared with the standalone fNIRS method. Thus, this study demonstrates the

inherent correlation between two modalities, and provides new insight for investigating the neurovascular coupling.

A large part of combined fNIRS-EEG studies have focused on the characterization of brain functions. Within this field of application, the complementary properties of fNIRS and EEG have led to extensive investigations of the spatiotemporal hemodynamic and electrical evolution of brain activity associated with a variety of functions, including language, auditory response, motor intention, working memory, and emotions [35-38]. Ehlis et al., conducted simultaneous fNIRS-EEG measurements on a group of healthy subjects to assess cortical correlates of auditory sensory gating in humans [35]. The combination of electrophysiological information and hemodynamic response revealed a positive correlation between the amount of sensory gating and the strength of the hemodynamic response in the left prefrontal and temporal cortices, which strengthened the hypothesis of a possible inhibitory influence of the prefrontal cortex on primary auditory ones. The multimodal fNIRS-EEG integration can also be employed to study the brain response induced by another modality, such as electrical stimulation or magnetic stimulation. Takeuchi et al., investigated hemodynamic responses and neural activity relationships in the somatosensory cortices of healthy adults during electrical stimulation of the right median nerve [38]. The fNIRS signal showed increased HbO concentration at the contralateral primary somatosensory region during stimulation, followed by responses that spread to more posterior and ipsilateral somatosensory areas. Besides, the EEG signal indicated that positive somatosensory evoked potentials (SEPs) peaking at 22-ms latency (P22) were recorded from the contralateral somatosensory area. fNIRS and EEG topographical maps of hemodynamic

responses and current source density of P22 were significantly correlated. Overall, these findings demonstrate that the multimodal fNIRS-EEG holds excellent flexibility and great potential in a variety of applications.

Clinical studies using multimodal fNIRS-EEG can be categorized into three main areas: developmental disorders of newborn/child, neurorehabilitation and psychiatry. Due to its noninvasiveness and high portability, the multimodal fNIRS-EEG is a potentially suited technique for continuous monitoring of the neurological functioning in critically ill preterm and full-term infants. For instance, concurrent fNIRS-EEG recordings have been utilized to characterize brain function alterations in infants in a previous study. It turned out that in patients with neurological damage such as seizures, transient hemodynamic events can be observed accordingly [39]. Such findings indicates that the multimodal fNIRS-EEG approach may give new insights into the brain functioning in preterm infants, which could identify potentially vulnerable conditions after birth and better understand the required treatments. In addition, concurrent fNIRS-EEG recordings are particularly suited for studying brain disorders in children without causing major restraint and discomfort. Numerous evidences have indicated that multimodal fNIRS-EEG can be applied to monitor and relieve the developmental disorders in children at preschool and primary school age. Zennifa et al., applied concurrent fNIRS-EEG recording to monitor the unrestrained cognitive state of children with mental retardation [40]. Marx et al., took a further step by employing the multimodal approach to the treatment of children with attention-deficit-hyperactivity disorder (ADHD) in a neurofeedback design. In this pilot study, HbO in the prefrontal cortex of children with ADHD was measured and used as feedback. FNIRS-based

neurofeedback was compared with the EEG (slow cortical potentials) and feedback from EMG signals. The author claimed that ADHD symptoms decreased significantly 4 weeks and 6 months after the fNIRS and EEG or EMG training according to different metrics [41].

Neurorehabilitation is a fundamental part in neurological disease such as stroke and Alzheimer's disease (AD). Concurrent fNIRS-EEG monitoring of brain activity during post-injury recovery can be of great help in providing brain function alterations without restricting the patient movement. Concurrent fNIRS-EEG recording has been applied for rehabilitation purposes, either for monitoring functional recovery and/or providing advanced rehabilitation training that rely on the previously described BCIs. In terms of brain function monitoring, Li et al., developed a multimodal fNIRS-EEG brain imaging algorithm by using the spatial prior derived from the fNIRS signals to enhance the EEG source localization result. They then employed this technique to study the brain network alteration in mild AD patients and identified key brain regions that are typically altered by cognitive decline in mild AD stage [21]. On the other hand, concurrent fNIRS-EEG has also been employed as a BCI training system for post-stroke motor recovery. BCI for stroke motor recovery generally provides intensive training that requires patient's intention to move the paretic limb with the contingent sensory feedback of the paretic limb movement guided by assistive devices. It has been demonstrated in previous study that BCI training was able to significantly improve motor performance in stroke patients with severe paresis compared to control group [42].

The applications of utilizing multimodal fNIRS-EEG to investigate psychiatric disorders have increased dramatically in recent years, mainly including bipolar disorder,

schizophrenia, and game addiction. fNIRS studies on bipolar patients have reported altered fNIRS responses during cognition task compared with those of patients with major depressive disorder or healthy subjects. And EEG also identified altered electrical activities that are always related to deficits of frontal activity and frontotemporal-parietal connectivity [43]. The combination of fNIRS and EEG could therefore reveal more comprehensive information associated with bipolar disorder. Following this, similar analysis pipeline have been widely adapted and employed to understand the neurophysiological mechanisms underlying different psychiatric disorders, such as schizophrenia [44] and game addiction [45]. Apparently, fNIRS and EEG offer distinct but correlated physical and physiological information, advancing their flexible and lightweight integration in multiple brain research fields.

1.7 Summary

This chapter introduces the basic concepts of the brain functional activation and the fundamental of two noninvasive brain imaging techniques -- the fNIRS and EEG. We then discuss the limitations of single-modality technique, the neurovascular coupling phenomenon of the brain, and provide a brief literature summary of employing multimodal brain imaging technique to investigate the cortical activity associated with healthy brain as well various brain disorders. The remaining of this thesis focuses primarily on concurrent EEG-fNIRS studies, specifically the experimental validation of their complementary properties and the integration analysis between EEG and fNIRS data. In particular, Chapter 2 implements an fNIRS-guided EEG channel selection method for enhancing the classification performance of a brain computer interface (BCI)

system. Chapter 3 describes a novel EEG-informed fNIRS analysis to validate the complementary properties of EEG and fNIRS. In Chapter 4 and Chapter 5, we develop an fNIRS-informed EEG source localization approach to investigate the cortical activity with high spatiotemporal resolution and describe how this approach can be used to characterize the cortical reorganization associated with Alzheimer's disease and stroke.

Chapter 2 – Enhancing Performance of a Hybrid EEG − fNIRS BCI System using fNIRS-Guided Channel Selection

2.1 Abstract

Brain-Computer Interface (BCI) techniques hold a great promise for neuroprosthetic applications. A desirable BCI system should be portable, minimally invasive, and feature high classification accuracy and efficiency. As two commonly used noninvasive brain imaging modalities, Electroencephalography (EEG) and functional near-infrared spectroscopy (fNIRS) BCI system have often been incorporated in the development of hybrid BCI systems, largely due to their complimentary properties. In this chapter, we aim to investigate whether fNIRS-guided channel selection can be used to enhance the accuracy and efficiency of a hybrid EEG-fNIRS BCI system. Eleven healthy volunteers were recruited and underwent simultaneous EEG-fNIRS recording during a motor execution task that included left and right hand movements. Singular EEG and fNIRS channels corresponding to the motor cortices of each hemisphere were selected via general linear model analysis of the fNIRS signal. Early temporal information was extracted from the EEG channel (0-1s) along with initial hemodynamic dip information from fNIRS (0-2s) for classification using a support vector machine (SVM). Results demonstrated a lofty classification accuracy using a minimal number of channels and features derived from early temporal information. In conclusion, a hybrid EEG-fNIRS BCI system can achieve higher classification accuracy (91.02%±4.08%) and efficiency by integrating their complimentary properties, compared to using EEG (85.64%±7.4%) or fNIRS alone (85.55%±10.72%).

2.2 Introduction

Brain-Computer Interface (BCI) systems, which use cortical activity to control external devices, have shown promising potential for multiple applications [46]. One of the main focuses of current BCI-related research is increasing the efficiency of real-time reactions while using a convenient setup that minimizes the burden on the user. Considering factors like setup cost and time resolution is therefore essential when choosing measurement modalities for a BCI study. BCI systems can be either invasive or noninvasive [47-49], though noninvasive BCIs are usually preferable since they incur neither the expenses nor safety risks of electrode implantation.

Over the past few decades, different noninvasive methods, including Electroencephalography (EEG) [50-52], functional Near-Infrared Spectroscopy (fNIRS) [30, 53-55], functional Magnetic Resonance Imaging (fMRI) [56, 57], and Magnetoencephalography (MEG) [58], have been extensively explored. Each modality has its own strengths and limitations, so it falls to the experimenter to select an appropriate method with high efficiency and low cost. Current practice then shows that EEG and fNIRS are considered the leading non-invasive BCI modalities due to their modest costs and practicality [59-61].

In recent decades, the complimentary individual properties of EEG and fNIRS have led to active investigations of the benefits of integrated EEG and fNIRS in a number of BCI studies [23-25]. In general, integrated EEG-fNIRS approaches offer various benefits over single-modality methods by capitalizing on their individual strengths; EEG provides favorable temporal resolution (about 0.05 s), while fNIRS offers better spatial resolution (about 5mm) and is robust to noise [17, 18]. Secondarily, EEG and

fNIRS signals are associated with different aspects of cortical activity, providing a built-in validation for identified activity. Measurements obtained from each of these two modalities thereby provide complementary information and can be used to enhance the performance of BCIs.

In hybrid EEG-fNIRS BCI applications, the main challenge is how to improve the classification accuracy while reducing the complexity of system and improving response time [62-64]. Since Fazli et al., [24] showed that BCI performance in a binary motor task can be enhanced by incorporating EEG features with those derived from the fNIRS signals, hybrid EEG-fNIRS BCIs have become a major research focus. These multimodal BCIs have shown enhanced classification accuracy in a variety of tasks, including mental arithmetic (MA), hand rotations, and movements [26-28]. However, some methodological limitations remain unsolved. For example, most hybrid EEG-fNIRS systems have relied on principle component analysis (PCA) or common spatial pattern (CSP) methods to transform the original data and select the components with largest discriminability between the two target classes [65, 66]. As a result, multiple channels – usually all available channels from both hemispheres – are required to perform feature extraction, classifier training, and classifier testing. This dramatically increases both computational and systemic costs and reduces the stability of the system setup. Furthermore, the purpose of integrating EEG and fNIRS in a BCI study should be to achieve a true multimodal integration that accentuates the favorable properties of each individual approach [67]. In particular, the spatial information of fNIRS could be further exploited to enhance hybrid EEG-fNIRS studies. Unfortunately, most hybrid BCIs simply process the signals separately and combine two groups of features for

classification. Finally, although high classification accuracy has been achieved [68], the temporally slow hemodynamic response and wide time window used for feature extraction remain major issues associated with the use of fNIRS for BCI applications [62].

In this study, we aimed to perform a binary classification of left and right hand movements in a hybrid EEG-fNIRS BCI system using signals obtained from the motor cortex. A fNIRS-guided channel selection criterion based on the general linear model (GLM) was proposed. The early information from the selected EEG channels was extracted using a short time window (0-1s) while the initial dip (0-2s) of the hemodynamic response was captured from the selected fNIRS channels. To our knowledge, this is the first hybrid EEG-fNIRS-based BCI study to take advantage of the spatial information of fNIRS for channel selection and apply the early temporal information of both modalities to enhance the transfer rate of the system while maintaining a decent performance.

2.3 Materials and Methods

2.3.1 Participants

Eleven healthy, right-handed subjects (n=11, male, 25.5±3.2 years) participated in this experiment. The experiment was approved by the local ethics committee (Guangdong Provincial Work Injury Rehabilitation Center, China), and performed in accordance with the Declaration of Helsinki. Each subject was fully informed about the purpose of the research and provided written, informed consent prior to the start of the experiment. No participants had any history of neurological or psychiatric disorders or

disease. No participants had any previous experience with the experimental task and all were naive to the BCI.

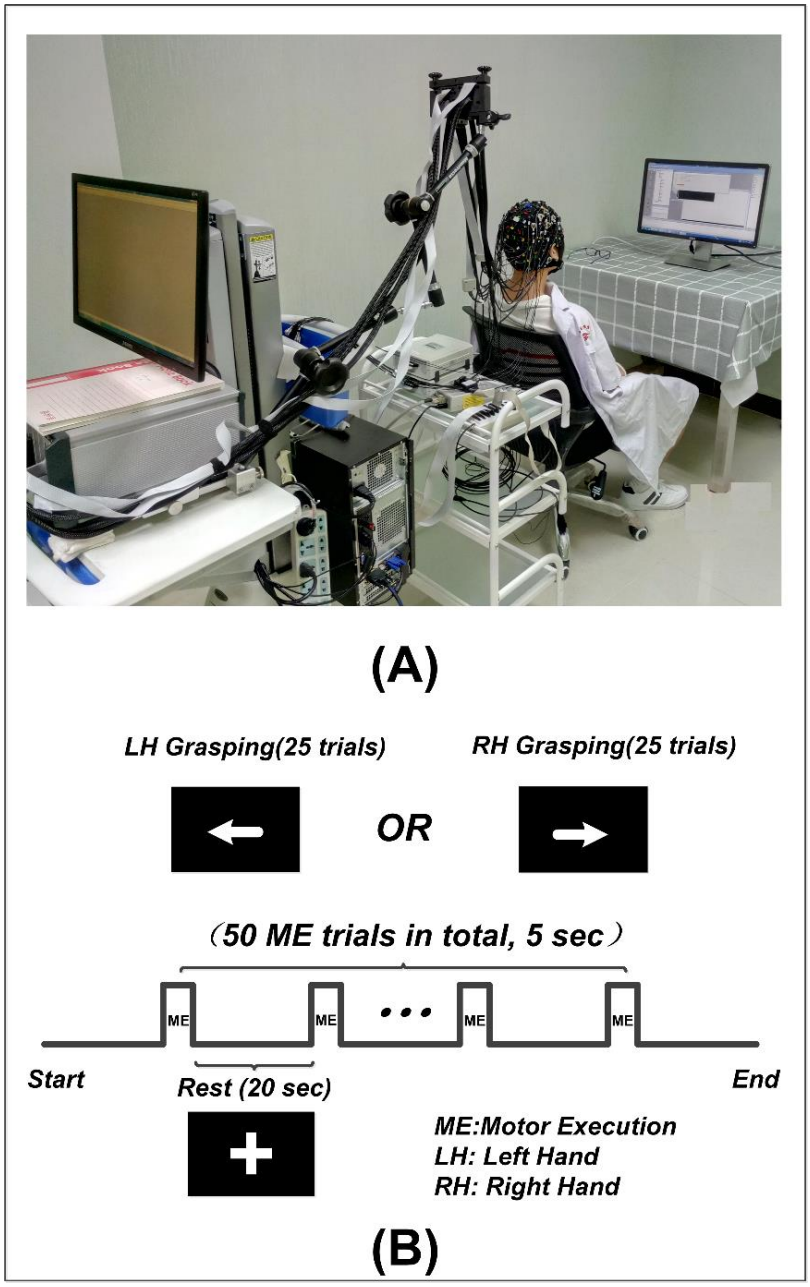

Figure 2-1. The experiment setup. (A) The environment of concurrent EEG-fNIRS measurement. (B) The paradigm used in the experiment.

2.3.2 Study protocol

The experiment was performed in a confined room to reduce any environmental disturbances. During the experiment, subjects were seated in a comfortable chair and asked to remain still and relaxed. Subjects received visual instruction through a screen placed 1m in front of their eyes (Figure 2-1A). The motor execution paradigm used in the experiment consisted of 50 randomized trials of left and right hand grasping tasks (25 trials for each hand movement). Each trial started with 20 seconds of rest, indicated by a "+" symbol, followed by 5 seconds of motor execution, in which an arrow was shown pointing either left or right, as shown in Figure 2-1B. Subjects were asked to squeeze a rubber ball with the corresponding hand for the entire duration that the arrow stimulus was shown.

A concurrent EEG and fNIRS measurement setup was employed in this study. EEG signals were recorded at 500 Hz using a BrainAmp DC EEG recording system (Brain Products GmbH, Germany). Sixteen EEG electrodes were placed on the scalp over the left and right motor cortices (FFT7h, FFC5h, FFC3h, FFT8h, FFC6h, FFC4h, FTT7h, FCC5h, FCC3h, FTT8h, FCC6h, FCC4h, CCP5h, CCP3h, CCP4h, and CCP6h). Two EEG electrodes were attached on both mastoids, the average of their signals was used as re-reference signal in preprocessing raw EEG data. FNIRS signals were recorded simultaneously using a NIRScout system (NIRx Medizintechnik GmbH, Germany) with 12 sources and 12 detectors. The inter-optode distance was 3 cm and a total of 34 fNIRS channels were equidistantly distributed throughout the motor cortex areas. The wavelengths used for HbO and HbR detection were 760 nm and 850 nm, respectively.

The fNIRS signals were acquired at a sampling rate of 7.81 Hz. A schematic illustration of the location of EEG electrodes and fNIRS channels is shown in Figure 2-2.

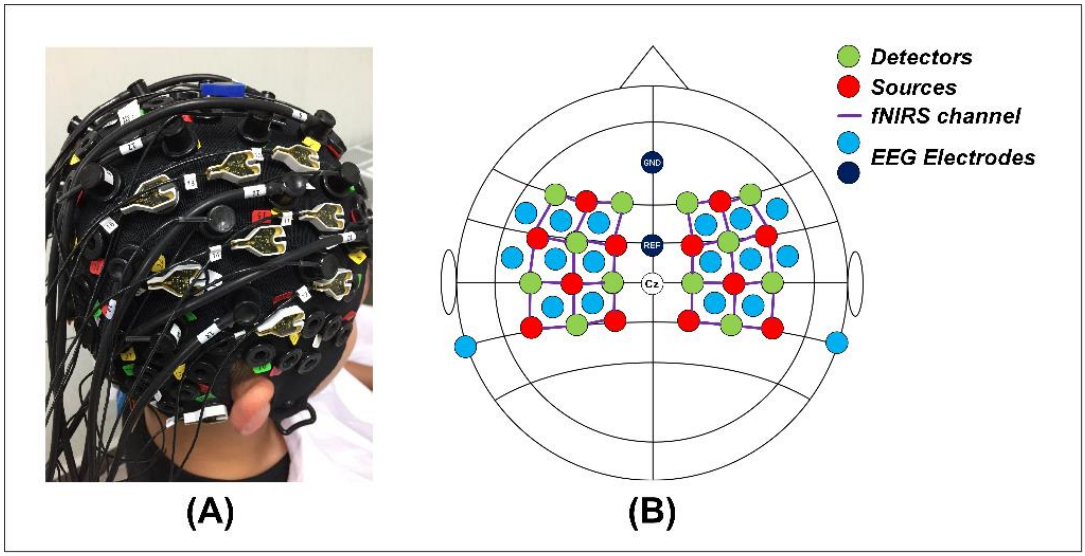

Figure 2-2. (A) Real photo of a subject wearing the cap completely mounted with EEG electrodes, fNIRS sources and detectors. (B) The configuration of the EEG electrodes and fNIRS optodes on the cap.

2.3.3 Data preprocessing

Raw EEG signals of all channels were first re-referenced by subtracting the average of two EEG channels on both mastoids. Since the valuable EEG information related to motor function is usually related to frequencies below 40 Hz [15], raw EEG signals were first down-sampled to 250 Hz and filtered from 1 to 45 Hz using a 3rd order Butterworth band-pass filter. Single-trial EEG data was segmented from 2s prior to the onset of movement instruction (baseline: -2-0s) to 5s after the onset (execution: 0-5s), resulting in 25 segmented trials for each hand movement. Baseline correction was performed by subtracting the mean value of individual baseline interval from its corresponding segmented trial.

To process the fNIRS signal, the concentration changes of hemoglobin (HbO and HbR) were computed using the Modified Beer-Lambert Law (the differential path length factors for the higher (850 nm) and lower (760 nm) wavelengths were 6.38 and 7.15, respectively) [12]. A 4th order Butterworth band-pass filter was applied from 0.01-0.2 Hz to remove artifacts, including cardiac interference (0.8 Hz) and respiration (0.2-0.3 Hz) [69]. In addition, spline interpolation was performed to remove any motion artifact contamination from the fNIRS signal [70]. Single trial fNIRS data was segmented from 5s prior to the onset of movement instruction (baseline: -5-0s) to 20s after the onset (execution: 0-20s), creating fNIRS trials that directly correspond to those obtained through EEG segmentation. The mean value of each baseline signal was subtracted from associated execution task.

2.3.4 Channel selection and feature extraction

Before features can be extracted, it is essential that appropriate channels are selected if a BCI system is to achieve favorable accuracy with minimal complexity. Previous work has suggested different approaches for selecting the most representative channels or signal components for classification, including common spatial patterns [66], bundled-optode-based approaches [31], and channel-averaging approaches [32]. A main goal of this paper is to use the spatial information from fNIRS to identify the single fNIRS channel and EEG channel on each hemisphere that yields the most significant differences between the binary motor tasks, which will enable increased classification accuracy with as few channels as possible. Here, the general linear model (GLM), a well-known and widely used method that fits the expected hemodynamic response to

the measured fNIRS signal, was applied to show the channels that yield the largest contrast between the two classes [71].

Both HbO and HbR concentration changes reflect changes in the hemodynamic response, though it has been suggested that HbO is a more sensitive indicator in fNIRS studies [72]. Therefore, HbO was adopted in the GLM analysis of the present study. The GLM model is given by

$$\boldsymbol{Y} = \boldsymbol{X\beta} + \boldsymbol{\varepsilon}, \tag{2-1}$$

where Y is an N × M matrix of measured data (where N denotes the number of data points and M denotes the number of fNIRS channels), X is an N × L design matrix (where L denotes the number of the conditions, including the tasks and any term that is considered as a source related to the variance of the data). β is a L × M matrix of regression coefficients to be estimated where L is associated with the number of the conditions and the value of β reflects the magnitude of the condition-evoked brain response. Finally, ε is an N × M matrix of residual error. In this present study, β is a 3 × M matrix assigned with three conditions, where the first row indicates the left hand movement, the second row indicates the right hand movement, and the third row is a constant term on all channels.

The regression coefficient β and the residual error ε can be tested through a one-sample t-test to identify the channels with t-values that represent a significant contrast between the two motor execution tasks. This t value is calculated by

$$\boldsymbol{t} = \frac{\boldsymbol{c^T * \beta}}{\sqrt{\boldsymbol{\varepsilon^2 c^T (X^T X)^{-1} c}}}, \tag{2-2}$$

where c is the contrast vector, which determines the contrast between specific conditions.

In our study, the following criterion was used to select the EEG channel and fNIRS channel of interest. First, the regression coefficient β of each individual fNIRS channel was estimated through the GLM, from which a group of channels with t-values that represent a significant contrast between the two motor execution tasks were selected as candidate channels. For each hemisphere, an fNIRS channel that yielded the highest t-value among those candidate channels was selected. One EEG channel, which was adjacent to the chosen fNIRS channel, was selected for classification. Therefore, the two EEG channels were selected according to the two fNIRS channels with the greatest discriminatory potential.

In order to extract the features associated with early temporal information, EEG data from 0-1s (0s denoting the onset of the stimuli) was segmented out from the selected channels, resulting in a 1s-long time window of EEG data with 250 points for each trial. The discrete wavelet transform (DWT) was then employed to decompose the segmented single trial EEG data [73], DWT is a technique that decomposes time series data of each selected EEG channel into a number of layers. In each layer the signal is filtered with a quadrature mirror filter (a low-pass filter and a high-pass filter). The output of each layer is a series of detail coefficients (from the high-pass filter) and approximation coefficients (from the low-pass filter). In this study we assumed that the wavelet approximation coefficients from the output of the last DWT layer contained the main power of the event-related oscillation in brain activity [74], which can be used for the discrimination of left and right hand movements. Here, the segmented signals of the

selected EEG channels were decomposed with a 4-layer ‘Symlet’ wavelet, resulting in 22 approximation coefficients for each trial. Then all approximation coefficients of the selected EEG channels were combined into a 44-dimensional EEG feature set (22-dimensional × 2 channels) for the single trial classification of the left and right hand movements.

The peak information from the HbO and HbR signals has been widely used in many fNIRS-based BCI studies [62]. However, the inherent delay of the hemodynamic response impedes the efficiency of a real-time fNIRS-based BCI application.

The hemodynamic feature of interest in the current study is known as the initial dip – a metabolically-linked phenomenon wherein HbO concentration decreases slightly or HbR concentration increases slightly 0 – 2s after the presentation of stimuli[75]. This fluctuation is considered to be the early and rapid metabolism of blood-borne oxygen by the responding population of neurons, occurring before the main activity-coupled vascular response. Though the initial dip has a relatively low amplitude, Zafar et al., have shown that detecting and classifying the initial dips is feasible with fNIRS [76]. As a result of their rapid evolution in the face of stimuli the initial dip information was extracted for classification in this study.

Prior to the extraction of initial dip information, principal component analysis (PCA) was performed to further remove any artifacts remaining in the preprocessed fNIRS signal. In this manner, the N-trial fNIRS data set from the selected channel was transformed into N linearly uncorrelated components known as principal components, ordered by the amount of variance of the original data that each component accounts for. The application of PCA to filter the multi-trial fNIRS data within a channel assumes

that the event-evoked hemodynamic response is the main component across all trials. This means that the hemodynamic response provides the dominant contribution to the variance of the fNIRS data and implies that the first several principal components will be similarly linked to the expected event-evoked hemodynamic response.

The PCA filtration is given by

$$\boldsymbol{Y} = \boldsymbol{E} * \boldsymbol{X}, \tag{2-3}$$

where X is the N × M data matrix (in which N denotes the data points of each trial and M denotes the number of trials), E is the eigenvector matrix with the dimensions N × N, and Y is the N × M matrix consisting of the N uncorrelated principal components. By keeping the first R components with the largest variances and removing the remaining components, the original data X can be reconstructed by

$$\boldsymbol{X_{recon}} = \boldsymbol{Y_{new}} * \boldsymbol{E_{new}^{T}}, \tag{2-4}$$

where X_{recon} is the N × M filtered data, E_{new} is the new eigenvector matrix with dimension M × R, and Y_{new} is the N × R matrix consisting of the R uncorrelated principal components.

In our study, all trials of each hand movement were filtered by PCA with the first component accounting for approximately 70% of the variance of the data set. Then the mean values of the HbO and HbR fluctuations within the 0 – 2s interval were computed for each trial, resulting in a 4-dimensional fNIRS feature set (2 mean values (HbO + HbR) × 2 channels) for the single trial classification of the left and right hand movements.

2.3.5 Classification

Prior to the classification, we constructed three different feature sets: EEG-only feature set, fNIRS-only feature set, and a hybrid feature set (EEG + fNIRS). The EEG-only feature set contained 44 approximation coefficients obtained from the selected EEG channels for each trial, while the fNIRS-only feature set contained 4 hemodynamic features (mean values of HbO and HbR of the two selected fNIRS channels) for each trial. Then all single trial features in both modalities were respectively normalized and rescaled between 0 and 1. The hybrid feature set was formed as a 48- dimensional feature vector for each trial, which contained the normalized EEG features (44 dimensional) and fNIRS features (4 dimensional). In summary, the dimensions of hybrid feature vectors were 48 features × 25 trials for either a left or right hand movements.

A support vector machine (SVM) was applied to perform the classification of the two-hand motor execution for each individual subject. The goal of SVM is to construct a hyper-plane that maximize the margins between the classes by minimizing the cost function [77]. In this study a SVM toolbox named “LIBSVM” was employed to train the SVM classifier and perform the prediction [78]. In particular, a Radial Basis Function (RBF) kernel which works under both linear and nonlinear situations was applied with default parameters (penalty parameter $C = 1$, $\gamma = 1/\text{number of features}$). As the obtained feature set was small (25 trials in total for each motor task), the Leave-One-Out cross-validation (LOOCV) method was utilized by randomly selecting one trial as a testing set and using the remaining 24 trials as the training set to train a classifier for prediction until all trials were tested. The classification accuracy for each

subject was calculated as the ratio between the number of correct predictions and the total number of predictions. Classification was performed separately using three kinds of feature sets for comparison; an EEG-only feature set, an fNIRS-only feature set, and a hybrid feature set (EEG + fNIRS). A flowchart is presented in Figure 2-3 to describe the study design.

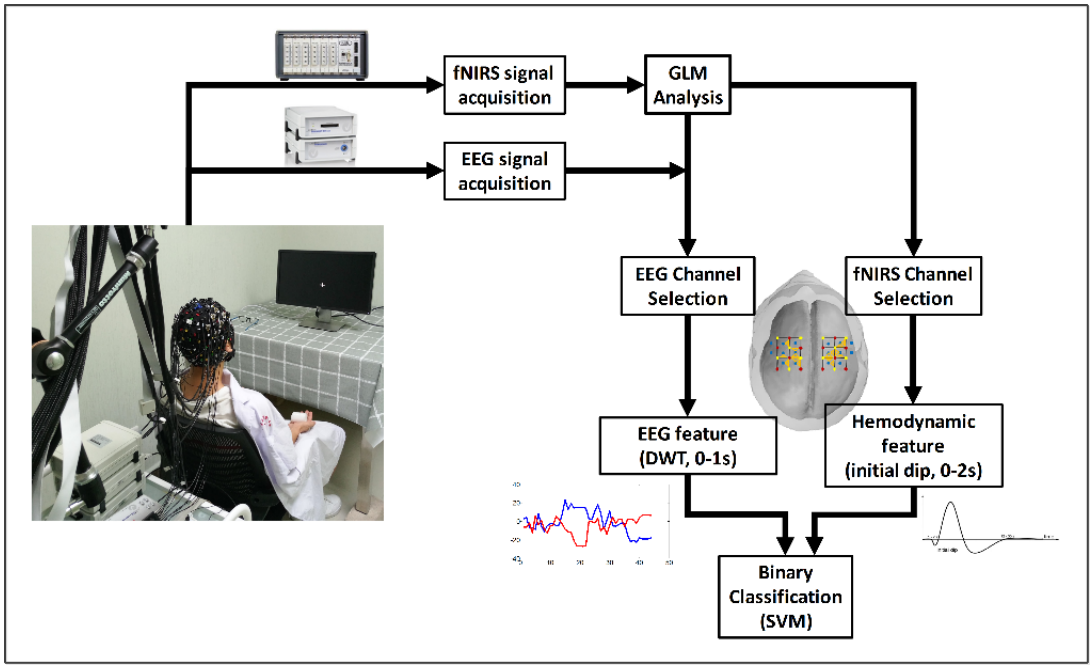

Figure 2-3. The flow chart of the study.

2.4 Results

Figure 2-4A shows a summarized mapping of the EEG and fNIRS channels selected from each subject for classification based on the GLM results. Each triangle indicates an EEG-fNIRS pair of selected channels. The number in the orange triangle represents the number of subjects whose selected channel is located at the given area, as shown in Figure 2-4B.

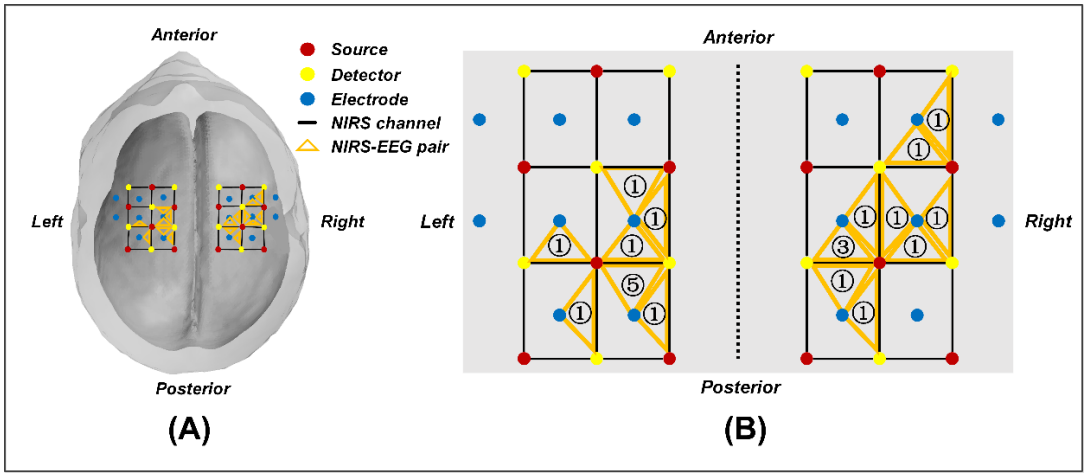

Figure 2-4. (A) Group-wise location summary of the selected EEG and fNIRS channels for all subjects. (B) Zoom-in view of the group-wise summarized location.

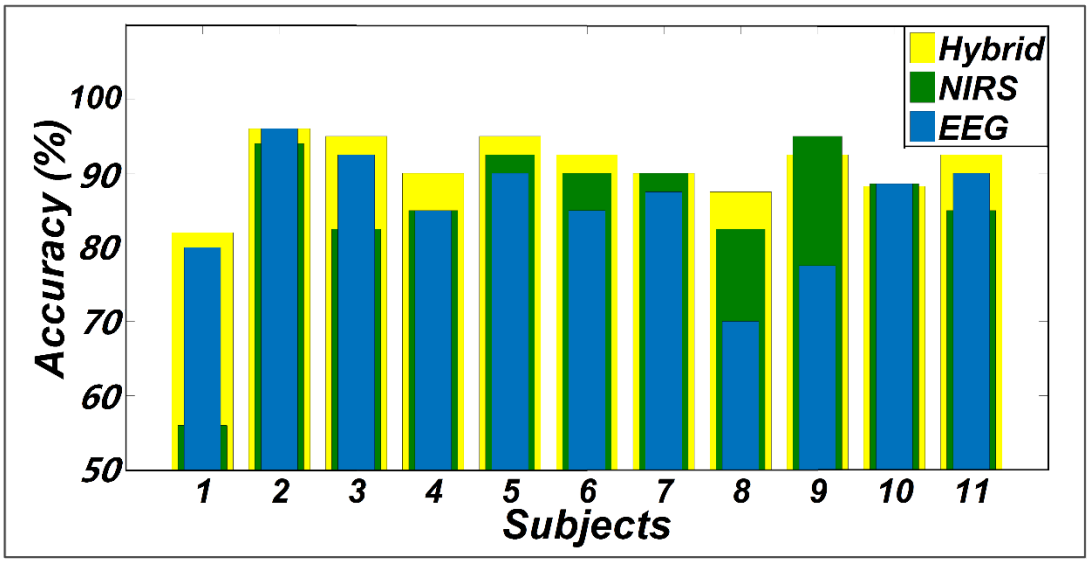

Figure 2-5. Classification accuracies of two hand movements obtained from three feature sets (EEG+fNIRS, EEG-only and fNIRS-only).

One goal of our study was to comparatively evaluate the classification reliability of the features extracted from EEG, fNIRS, and EEG + fNIRS based on the results of the GLM. To do this, we performed a single-trial classification of the left vs. right motor execution task. Classification accuracies obtained from each subject by the three different feature sets can be seen in Table 2-1. A classification accuracy of 100% would

indicate that the two motor tasks are perfectly separable, while a classification accuracy of 50% would represent the poor performance of a random classifier in the context of the binary classification task. Figure 2-5 shows the histogram plot of all classification results, with the overall classification accuracies of all three feature sets exceeding 85%. Specifically, the average accuracy of the EEG-only feature set (85.64%±7.4%) slightly outperformed the fNIRS-only feature set (85.55%±10.72%). The best performance, however, was achieved from with the hybrid EEG-fNIRS feature set (91.02%±4.08%), providing an improvement in the classification accuracy and minimizing the standard deviation. To examine how significantly the hybrid feature set outperformed the single modality, paired t-test was applied to test the classification results obtained by the three different feature sets. Prior to the paired t-test, the W/S test was firstly performed to test the normality of the obtained classification accuracies, which is the prerequisite of paired t-test analysis [79]. The result revealed that all the accuracies were normally distributed at a significance level of 0.05 (q_{EEG} = 3.5124, q_{fNIRS} = 3.6365, q_{Hybrid} = 3.4275, $q_{critical}$ = [2.74 3.80]). The statistical results of paired t-test are shown in Figure 2-6. It can be observed that the classification performance based on the hybrid feature set significantly improved on classification based on EEG-only features (P=0.0123) and classification based on fNIRS-only features (p=0.0457) as well.

Table 2-1. Summary of SVM classification accuracies for feature sets of NIRS-only (HbO + HbR), EEG-only and hybrid (EEG + fNIRS).

Subject No.	Accuracy (%)		
	EEG	fNIRS	EEG+fNIRS
1	80.0	56.0	82.0
2	96.0	94.0	96.0
3	92.5	82.5	95.0
4	85.0	85.0	90.0
5	90.0	92.5	95.0
6	85.0	90.0	92.5
7	87.5	90.0	90.0
8	70.0	82.5	87.5
9	77.5	95.0	92.5
10	88.6	88.6	88.2
11	90.0	85.0	92.5
Mean (%)	85.64	85.55	91.02
Std. (%)	7.40	10.72	4.08

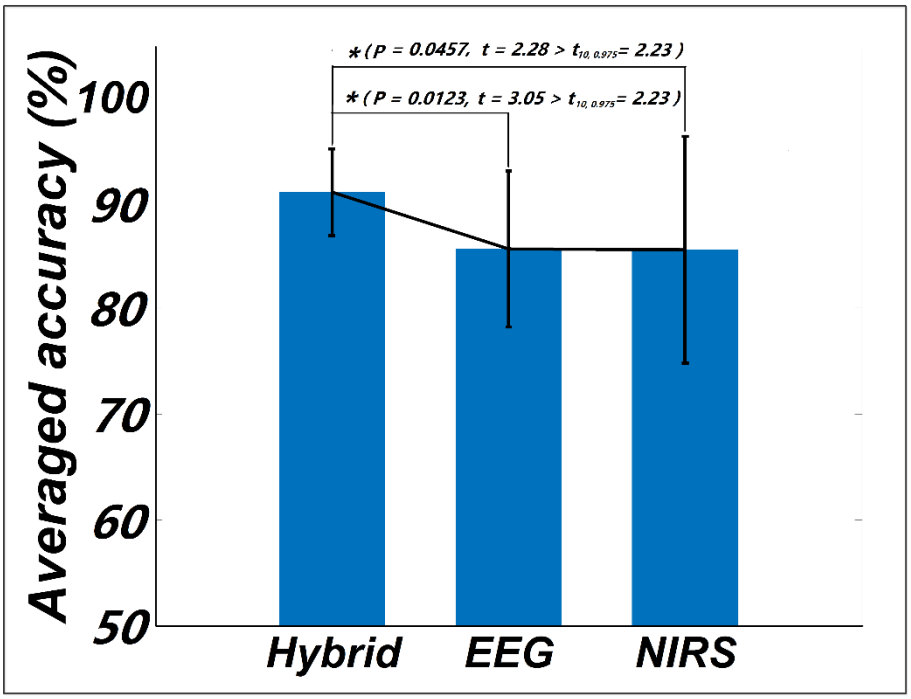

Figure 2-6. Statistical plot of the classification accuracies obtained from the three feature sets, respectively.

2.5 Discussion and Conclusion

Multi-modal imaging has been reported to improve classification accuracy over unimodal methods [24]. In this chapter, we attempted to achieve the highly accurate and computationally efficient classification of a binary motor execution task using a hybrid BCI design. This was performed through the selection of singular hemispheric EEG and fNIRS channels and the application of rapidly-evolving temporal features from both modalities. The results indicated that the multi-modal fNIRS-EEG approach significantly improved the performance over that of unimodal alone, yielding an average accuracy of 91.02%±4.08% and proving the suitability of the hybrid approach for binary motor execution tasks.

Channel selection plays a crucial role in the design and application of a BCI system, especially with respect to the number and the location of the selected channels. For the classification of motor execution tasks, it is quite common to utilize multiple channels from the C3 and C4 areas [23, 24]. These methods, however, might not be able to minimize the variation from subject to subject, as identical channels may align with different brain regions. Although recent studies have investigated the efficiency of different channel selection criteria [31, 32, 66], few efforts have been made to optimize the number and location of these channels. A previous fNIRS study proposed a selection criterion based on high t-value channels from the auditory cortex during the classification of four sound categories [80]. This method, however, still relied on multiple channels with no noticeable improvement in performance. In this study, we only made use of single EEG and fNIRS channels from each hemisphere with the highest t-value based on the GLM results, for classification. Here we attempted to

capitalize on the spatial information from fNIRS, a valuable advantage of fNIRS technology, to ensure that the most effective channels were chosen for feature extraction and classification. As such we might be able to reduce the complexity of a BCI system and minimize the burden on the user. Our results demonstrated that it is feasible to take advantage of the high spatial resolution offered by fNIRS to select channels for classification, to therefore reduce the channel number and the complexity of the BCI system while maintaining desirable performance.

In addition to the classification performance, the proposed channel selection criterion applied the spatial information from fNIRS to the selection of both the EEG and fNIRS channels, establishing a connection between the two modalities rather than performing the separated channel selection performed in previous studies [23, 24, 59]. The reliability of this proposed method was validated by the favorable classification performance shown in Figure 2-5, where all of the average classification accuracies using the three different feature sets exceeded 85%. It is noteworthy that, while all selected channels were located within the motor cortex, the exact channel of interest varied by subject (Figure 2-4). This shows that the proposed channel selection method was able to identify appropriate, subject-specific channels according to the GLM results, minimizing any error from potential variation in channel positions. The mapping results therefore emphasize the importance of selecting customized channels from each individual subject instead of simply choosing motor-related channels – like C3 or C4 – for motor task classification.

It should be noted that, while unimodal classification may have been poor in specific subject, the hybrid combination revealed the potential to stabilize the classification

performance with a higher mean accuracy and smaller standard deviation (Figure 2-6, Table 2-1). Apparently, the inclusion of the different information measured by EEG and fNIRS is beneficial to the robustness of the BCI. On the other hand, EEG-based BCIs have been reported to yield superior temporal results in real-time BCI applications [17]. Recently, fNIRS-based BCIs have also been developed that show favorable classification rates by using different combinations of features and various classifiers [62]. These fNIRS-based BCIs, however, are not yet viable as an alternative to EEG-based BCIs; the most reliable feature of fNIRS is the HbO peak information, which shows a long delay in the response to stimuli [62]. In this study, we aimed to enhance the response efficiency of a hybrid system while maintaining favorable accuracy. This was performed by focusing on the initial dip of the hemodynamic response, which has been proven to be a potential feature for fNIRS-based BCI application[64]. Generally it is difficult to detect the initial dip due to its short duration and high sensitivity to low frequency artifact (e.g., Mayer wave). In order to obtain a clean initial dip in single-trial fNIRS signal, a PCA-based algorithm was employed to extract the main component, which was considered the true hemodynamic response associated with the motor execution task. In the present study, we selected the first principal component, which accounted for over 70% of the total variance of the original signal. Results showed that this was sufficient to achieve a high classification accuracy. In particular, the lofty classification accuracies obtained by the fNIRS-only classifier (85.55%±10.72%) as well as from hybrid classifier (91.02%±4.08%) demonstrated the effectiveness of the initial dip in discriminating the binary motor tasks. By applying a 0–2s time window to the fNIRS signal, it was observed that the addition of fNIRS features significantly

enhanced the performance of the EEG-based BCI without significantly increasing the time delay, demonstrating the advantage of a hybrid EEG-fNIRS system and showing that early temporal features can be used to create a faster and more stable BCI system, which overcomes the problem in Fazli's study [24].

One limitation of our study lies in the configuration of the EEG electrodes and fNIRS optodes, where the EEG electrodes were surrounded by the fNIRS channels, as shown in Figure 2-2. Although we chose EEG electrodes that were close to the selected fNIRS channels, placing the EEG electrodes on the surface pathways of the fNIRS channels may optimize the channel configuration and enhance the physiological consistency between the EEG and fNIRS channels. This problem may be addressed by using a customized cap in the future.

2.6 Summary

In this chapter, an fNIRS-guided hybrid EEG-fNIRS configuration for binary motor task classification was proposed. Singular EEG and fNIRS channels were selected from the motor cortex of each hemisphere based on fNIRS-informed prior information. The high accuracy and efficiency of classification results are encouraging and suggest the integrated EEG-fNIRS strategy developed in this study as a promising approach to develop a high-performance BCI system. More importantly, from the view of fNIRS-guided analysis, this chapter validate our hypothesis that there is certainly complementary information offered by EEG and fNIRS to study the brain activity.

Chapter 3 ─ Enhancing fNIRS Analysis Using EEG Rhythmic Signatures: an EEG-informed fNIRS Analysis Study

3.1 Abstract

Neurovascular coupling represents the relationship between changes in neuronal activity and cerebral hemodynamics. Concurrent EEG and fNIRS recording and integration analysis has emerged as a promising multi-modal neuroimaging approach to study the neurovascular coupling as it provides complementary properties with regard to high temporal and moderate spatial resolution of brain activity. In this chapter we developed an EEG-informed-fNIRS analysis framework to investigate the neuro-correlate between neuronal activity and cerebral hemodynamics by identifying specific EEG rhythmic modulations which contribute to the improvement of the fNIRS-based general linear model (GLM) analysis. Specifically, frequency-specific regressors derived from EEG were used to construct design matrices to guide the GLM analysis of the fNIRS signals collected during a hand grasp task. Our results showed that the EEG-informed fNIRS GLM analysis, especially the alpha and beta band, revealed significantly higher sensitivity and specificity in localizing the task-evoked regions compared to the canonical boxcar model, demonstrating the strong correlations between hemodynamic response and EEG rhythmic modulations. Results also indicated that analysis based on the deoxygenated hemoglobin (HbR) signal slightly outperformed the oxygenated hemoglobin (HbO)-based analysis. The findings in our study not only validate the feasibility of enhancing fNIRS GLM analysis using simultaneously

recorded EEG signals, but also provide a new perspective to study the neurovascular coupling of brain activity.

3.2 Introduction

Neuronal activity occurs within a localized brain region is usually accompanied with vascular response to meet the increased demand of glucose and oxygen. This well-regulated system in the brain is called neurovascular coupling, which can be altered by brain disorders [81]. To date, modern neuroimaging techniques, such as EEG and fMRI, have been widely used to investigate the relationship between neuronal activity and cerebral hemodynamics [10, 82, 83]. EEG is by far the most widely used neuroimaging technique to measure the neuronal electrical activity. It is well-accepted that EEG signals originate from the mixture of propagating electric potential fluctuations, mainly reflecting the postsynaptic activity of a mass of cortical pyramidal cells [84]. Particularly, rhythmic EEG activities can be modulated by external stimuli, such as cognitive, motor and visual tasks, resulting in the so-called event-related potentials (ERPs) [85]. On the contrary, fMRI comprises one of the primary methods to indirectly observe the neuronal activity by detecting Blood Oxygen Level Dependent (BOLD) contrast that identifies regions with significantly different concentrations of oxygenated blood induced [86]. This serves as an indirect measure of underlying neuronal activity—the high metabolic demand of active brain regions requires an influx of oxygen-rich blood, increasing the intensity of voxels where activity can be observed [81, 87].

Taking the advantages of EEG and fMRI, the relationship between neuronal activity and hemodynamic response has been actively investigated recently. Emerging

evidences have shown that BOLD fluctuations correlated positively with trial-by-trial fluctuations in EEG gamma band and negatively with the frequency at alpha and beta band during a visual attention task [88]. In addition, simultaneous EEG-fMRI recording during a hand grip task has revealed a strong correlation between the BOLD fluctuations and the task-evoked EEG oscillations, especially the alpha and beta band [89]. However, fMRI is typically limited by the high sensitivity to body-motion artifacts, a lack of portability and high costs, rendering it less compatible with EEG when investigating brain activity under realistic situations such as motor execution task [90].

As a noninvasive optical imaging technique, fNIRS also measures the concentration change of oxygenated hemoglobin (HbO) and deoxygenated hemoglobin (HbR) associated with brain activity through a spatially distributed set of optodes (emitters and detectors) placed on the scalp [12]. Compared to fMRI, fNIRS offers better tolerance to motion artifacts, higher temporal resolution and high portability for long-term, noninvasive monitoring [10, 91, 92]. As they rely on similar cerebrovascular dynamics, the results obtained by fNIRS have been proven to be roughly analogous to those of fMRI while maintain moderate spatial resolution [93, 94], making this technique more appropriate for practical applications, such as investigating motor function and social communication [29, 95, 96].

The good compatibility and complimentary properties of EEG and fNIRS have led to growing investigations of integrated EEG and fNIRS analyses in a number of studies on neurovascular coupling [33, 97, 98]. For instance, Croce et al., demonstrated the feasibility of enhancing both the electrical and hemodynamic activity reconstruction through combined EEG and fNIRS measurements in a simulation study [99]. In human

study, Khan et al., have shown the feasibility of detecting an early fNIRS response using EEG signal as a marker [100]. Zich et al., have shown a strong correlation between the EEG-evoked potential at 8-30 Hz and the modulations of hemodynamic response during a motor imagery task [101]. More specific evidence was reported in a recent simultaneous EEG-fNIRS study, wherein an increase in HbO was accompanied by a decrease in HbR concentration and a decrease in amplitudes of alpha and beta EEG rhythms during a motor task [97]. Most of the aforementioned studies, however, typically focused on the superficial correlation between the task-evoked EEG oscillations and fNIRS signals and failed to take into account the inherent relationship between two modalities [97, 100-103]. There is clearly a need to further explore the relationship between neuronal activity and the hemodynamic response.

In typical fMRI / fNIRS data analysis, the BOLD signal or the fNIRS signal is commonly regressed via a general linear model (GLM) constructed by convolving the canonical hemodynamic response function (HRF) with a boxcar function representing the temporal profile of the experimental paradigm to identify cortical regions activated by specific stimuli [10, 104, 105]. To explore the neurovascular coupling, several recent integrated EEG-fMRI analysis studies employed the EEG-derived frequency-specific features as a replacement of the canonical boxcar function to characterize the correlation between EEG and the BOLD signal [88, 89]. In light of these previous works, in this chapter we presented an EEG-informed-fNIRS analysis framework to investigate the inherent neuro-correlate between EEG and fNIRS signals by understanding how EEG frequency-specific oscillations selectively contribute to the hemodynamic response measured by fNIRS during a motor execution task. In particular, modulations of several

representative EEG rhythms which are reported to be highly correlated with hemodynamic response, including alpha, beta and gamma band, were employed to construct various EEG-informed models to improve the performance of GLM analysis. We hypothesized that the EEG frequency-specific models are able to enhance the fNIRS GLM estimation compare to canonical boxcar model, providing new perspective to investigate the neurovascular coupling using simultaneous EEG and fNIRS measurement.

3.3 Materials and Methods

3.3.1 Participants

Ten healthy, right-handed subjects (n=10, male, 28.5±3.1 years) participated in this experiment. All participants were healthy subjects with no history of neurological or psychiatric disorders or disease. The experiment was approved by the local ethic committee, and performed in accordance with the latest Declaration of Helsinki. Each subject was fully informed about the purpose of the research and provided written, informed consent prior to the start of the experiment. No participants had any previous experience with the experimental task and are all were naive to the used techniques.

3.3.2 Experiment and data acquisition

In this study motor execution paradigm was employed and performed in an isolated room to reduce environmental disturbances. During the experiment, subjects were seated in a comfortable chair and asked to remain still and relaxed. Subjects received visual instruction through a screen placed 1m in front of their eyes. The motor execution paradigm consisted of 40 randomized trials of left and right hand grasp tasks (20 trials

for each hand movement). Each trial started with a 8-second motor execution task, indicated by an arrow pointing either left or right, followed by 17 seconds of rest period, indicated by a "+" symbol in a black background (Figure 3-1A). During the motor execution period, subjects were asked to naturally squeeze a rubber ball with the corresponding hand.

A concurrent EEG and fNIRS measurement setup was employed in this study. EEG signals were recorded at 500 Hz using an EEG recording system (Brain Products GmbH, Germany). Thirty-two EEG electrodes were placed on the scalp according to the 10-20 international EEG system. FNIRS signals were recorded simultaneously at 3.91 Hz using a continuous-wave NIRS imaging system (NIRScout, NIRx Medizintechnik GmbH, Germany). The wavelengths used for the detection of the concentration changes oxy- and deoxy- hemoglobin were 760 nm and 850 nm. A total of 45 fNIRS channels with 3 cm inter-optode distance were distributed over the entire motor area and other areas. A schematic illustration of the location of EEG electrodes and fNIRS channels is shown in Figure 3-1B. To identify the cortical regions associated with the fNIRS channels, a template of brain model obtained from the MNI305 space was used as a common brain model for all subjects. Then each fNIRS channel was normally projected to the cortical surface, following the method described in [106]. The DKT40 atlas was chosen in this study to define 68 functional regions of interest (ROIs) using automatic anatomical labeling [107]. The full projection of all fNIRS channels on cortical surface was shown in Figure 3-1C.

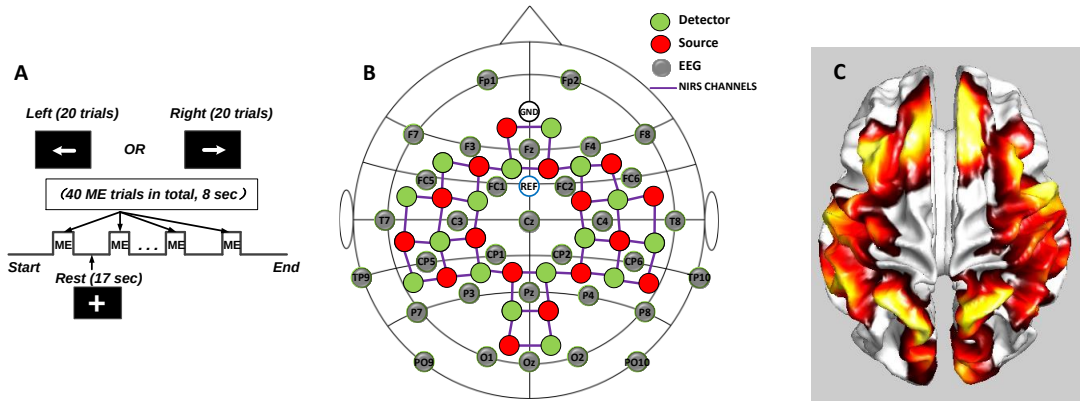

Figure 3-1. (A) The motor execution (ME) paradigm; (B) Locations of EEG electrodes and fNIRS optodes; (C) The cortical regions associated with the fNIRS channels.

3.3.3 EEG and fNIRS data preprocessing

EEG preprocessing was performed using BrainVision Analyzer 2.0 software (Brain Products, Germany). The collected EEG data was first filtered from 0.5 Hz to 45 Hz by a 4th order Butterworth band-pass filter, with an extra 4th order Butterworth notch filter at 50 Hz to remove any residual powerline noise. Ocular artifact removal was then performed for each subject using independent component analysis (ICA) and the number of removed IC components was 3 and no more than 5 on average. Data was then re-referenced to the average of two EEG channels on both mastoids (TP9 and TP10). We then extracted the alpha (8 - 13 Hz), beta (14 - 25 Hz) and gamma band (26-45 Hz) from the preprocessed EEG signals by a 4th order Butterworth band-pass filters. Single-trial EEG data was segmented from 2s prior to the onset of movement instruction (baseline: -2s–0s) to 10s after the onset (execution: 0s–8s), resulting in 20 segmented trials for each hand movement and each EEG frequency band (alpha, beta and gamma). Baseline correction was performed by subtracting the mean value of individual baseline interval from its corresponding segmented trial.

The raw fNIRS signals were first converted to optical density data, after which the concentration changes of hemoglobin (HbO and HbR) were computed based on the Modified Beer-Lambert Law (the differential path length factors for the higher (850 nm) and lower (760 nm) wavelengths were 6.38 and 7.15, respectively) [12, 108]. The resulted time courses of HbO and HbR signals were then analyzed to identify task-evoked cerebral regions by GLM analysis.

3.3.4 GLM analysis based on Autoregressive- Iteratively Reweighted Least Squares (AR-IRLS)

The GLM is a well-known and widely used method that fits the expected hemodynamic response to the measured fNIRS signal and identifies the channels that highly correlate with the specific stimuli through statistical evaluation [109]. Briefly, for measured fNIRS signal $\boldsymbol{Y}$ in a channel, the first-level GLM model is given by

$$\boldsymbol{Y} = \boldsymbol{X}\boldsymbol{\beta} + \boldsymbol{\varepsilon}, \tag{3-1}$$

where $\boldsymbol{X}$ is the design matrix, $\boldsymbol{\beta}$ is the regression coefficients to be estimated and $\boldsymbol{\varepsilon}$ is the error term. In the case of a block design experiment, $\boldsymbol{X}$ is commonly given by a convolution matrix of the canonical hemodynamic response and boxcar functions describing the latency and duration of the stimulus. Particularly, columns of $\boldsymbol{X}$ are regressors that usually represent conditions or tasks in the experiment and additional nuisance terms that account for the systemic physiology or motion artifacts [110].

The estimated regression coefficient $\boldsymbol{\beta}$ and the error $\boldsymbol{\varepsilon}$ can be tested through *t*-test to identify the channels that represent a significant contrast between different tasks (e.g. left vs. rest or left vs. right). The t-test is calculated by

$$\boldsymbol{t} = \frac{\boldsymbol{c^T * \beta}}{\sqrt{\boldsymbol{c^T cov(\beta) c}}}, \tag{3-2}$$

where $\boldsymbol{cov(\beta)}$ is the covariance matrix of $\boldsymbol{\beta}$, $\boldsymbol{c}$ is the contrast vector, which determines the contrast between specific conditions.

As reported in literature, however, serial correlations and motion artifacts represent two major sources of confounding noise in fNIRS that can reduce the performance of conventional GLM analysis and increase the false positive rates of detecting the true task-activated regions [111]. Therefore, in this study we adopted the AR-IRLS algorithm to enhance the performance of GLM analysis. The detail of the AR-IRLS can be found in reference [111]. Briefly, the first step of AR-IRLS is to significantly reduce the serial correlations in fNIRS signals by filtering the original channel-wise fNIRS signals with a series of autoregressive (AR) filters $\boldsymbol{F}$. Equation (3-1) is rewritten as

$$\boldsymbol{FY = FX\beta + F\varepsilon.} \tag{3-3}$$

After the correction of serial correlations in fNIRS measurements, the iteratively reweighted least squares (IRLS) is employed to deal with the outliers caused by motion artifacts during the experiment. In this approach, the influence of each sample point is weighted based on the value of the residual in Equation (3-3), which can be rewritten as

$$\boldsymbol{WFY = WFX\beta + WF\varepsilon,} \tag{3-4}$$

where $\boldsymbol{W}$ is diagonal matrix of weights iteratively calculated based on the error in Equation (3-3) by a specific weighting function. The solution of Equation (3-4) is obtained using robust weighted regression and given as

$$\boldsymbol{\beta = (X^T F^T W F X)^{-1} X^T F^T W F y.} \tag{3-5}$$

After the estimation of the coefficients $\boldsymbol{\beta}$, *t*-test can be performed to identify the channels that represent a significant contrast between different tasks based on Equation (3-2). In addition, the second-level analysis can also be performed based on the firs-level models to obtain group-wise activation pattern using a fixed effect model, in which the task is treated as fixed effect. Group level *t*-test can be subsequently done to obtain different group-level response to the motor tasks. In this study the first-level AR-IRLS-based GLM analysis and second-level group analysis were performed using default parameters setting in NIRS Brain AnalyzIR Toolbox [112].

3.3.5 EEG-derived Regressor for fNIRS GLM Analysis

It is known that the amplitude oscillations of EEG signals can be modulated by specific stimulus, which is defined as event related potential (ERP) [85]. In this study we extracted the frequency-specific ERP from the EEG signals as regressors to modify the design matrix in the GLM analysis of fNIRS signals, as the $\boldsymbol{X}$ shown in Equation (3-1). At first, we selected only the channels expected to be involved in the motor execution task for the extraction of EEG-based regressors. Specifically, in our case channels located at motor area on left (FC5, FC1, C3, CP5, CP1) and right (FC2, FC6, C4, CP2, CP6) hemisphere were selected as representative channels for right and left hand movement, respectively.

For each movement, the representative channels were first averaged to obtain 20 averaged trials. The time-varying power of each trial was then computed by squaring the amplitude of each sample point. The peak and corresponding latency were searched within the first 2 seconds of the time-varying power of each trial (0-2s) starting from the task onset since it has been shown that the motor task-evoked ERP occurs rapidly

after the task onset [113]. The same processing was applied to all three EEG frequency components (alpha, beta and gamma). The obtained peaks and latencies were then employed to construct EEG-derived design matrices to replace the canonical boxcar design for GLM analysis of fNIRS signals. Overall, we constructed three EEG-derived design matrices (alpha/beta/gamma) and one canonical design matrix for the first-level and second-level fNIRS GLM analyses for each hemoglobin type (HbO / HbR).

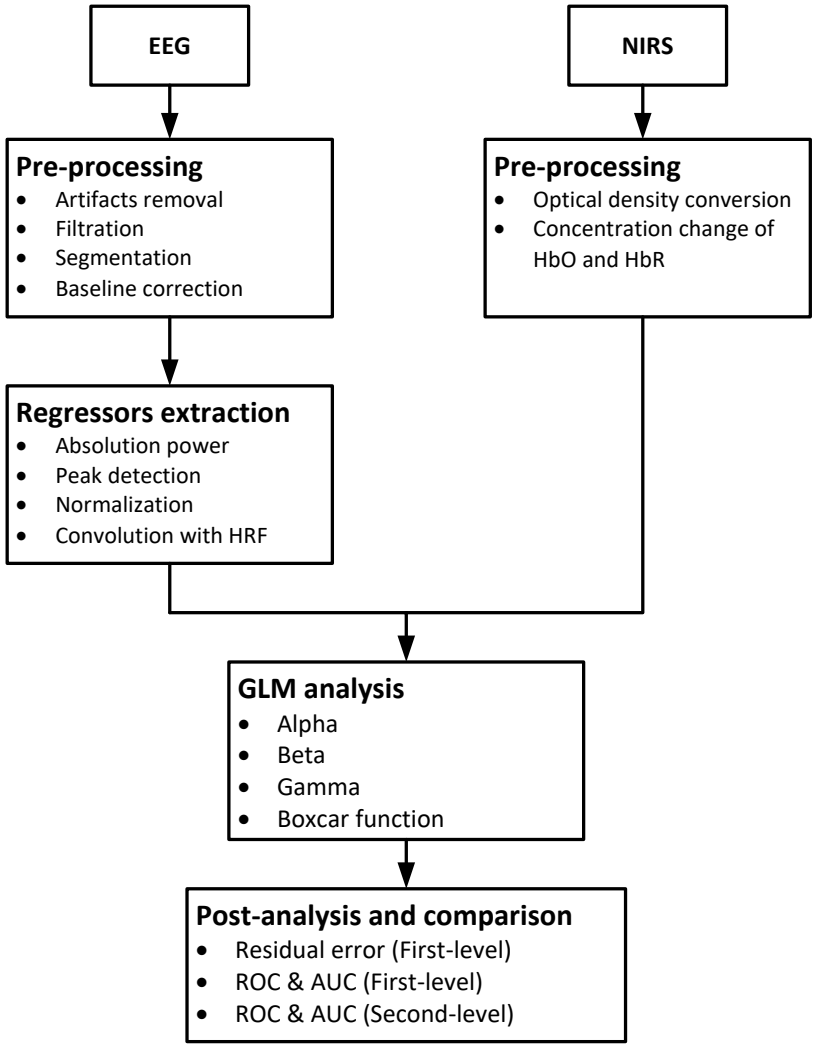

Figure 3-2. The schematic of the EEG-informed fNIRS GLM analysis framework.

In order to validate the feasibility of EEG-informed fNIRS GLM analysis during the motor task, we proposed two metrics to quantitatively evaluate the performance of GLM analyses with respect to various design matrices. The first metric was defined as the mean residual error (MRE) of the regression model in Equation (3-4). MRE indicated the goodness of fitting between the expected model and the actual measured data. A smaller MRE would therefore represent a better fitting of the linear model. The second metric was the area under the curve (AUC) of Receiver operating characteristic (ROC) of the model, which has been widely used to evaluate the performance of the GLM in previous fNIRS studies [112, 114]. In this study, we generated the ROC for each model and each subject by varying the p-value threshold for task-evoked activation from 0 to 1 and calculating the true positive rate (TPR, sensitivity) and false positive rate (FPR, 1-specificity). Specifically, the TPR was defined as the ratio between the number of the identified active channels at the target motor area and the total number of channels at target motor area. The FPR was defined as the ratio between the number of identified active channels at non-target motor area and the total number of all channels at non-target motor area. Referring to previous study [89], the target motor area was defined as the functional regions that are well known to be involved in motor execution, including primary motor cortex (M1-BA4), premotor cortex (PM-BA6), primary somatosensory cortex (S1-BAs1, 2 and 3), and supplementary motor area (SMA-BA6). In particular, we defined the left motor cortex as the target area for the right hand grasp task and the right motor cortex as the target area for the left hand grasp task. After the ROC was drawn, the AUC of ROC can be calculated to quantify the overall performance of each model. A higher AUC (from 0 to 1) indicates that the model has higher TPR and lower

FPR and therefore represents a better performance of the model. To compare the performance of different models, one-way repeated ANOVA test was employed to evaluate difference in these metrics among the EEG-informed models and the canonical boxcar model at single subject-level. Anderson-Darling-based normality test was performed on all data sets prior to the ANOVA analysis. Fisher's least significant difference (LSD) test was used as *post-hoc test* to assess difference between any GLM model pair. A flowchart is shown in Figure 3-2 to summarize the overall design of the study.

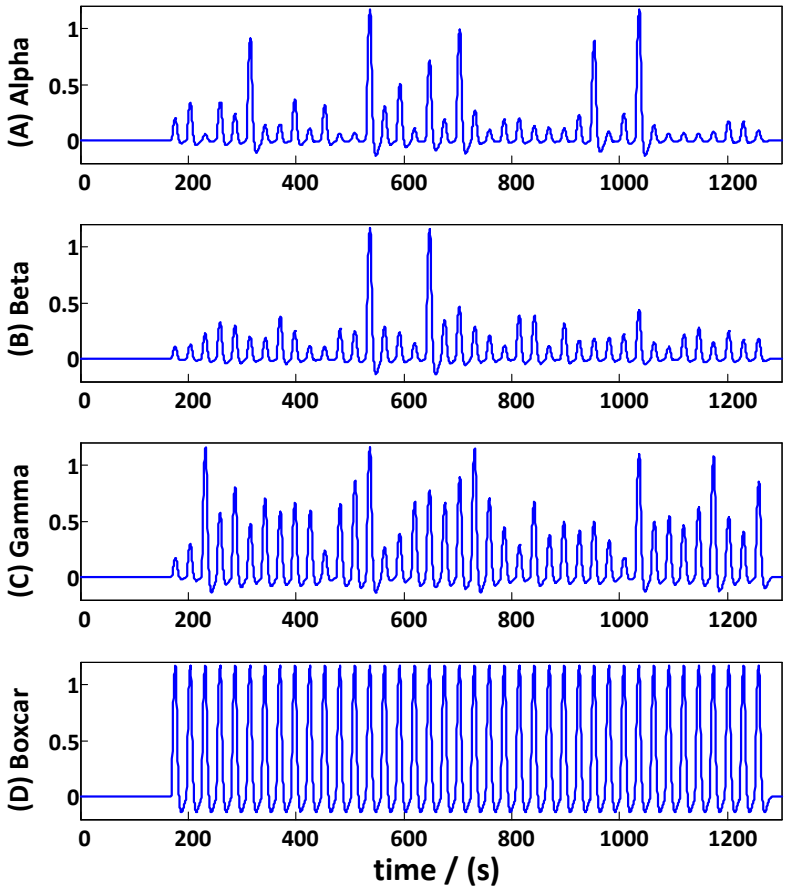

Figure 3-3. Design matrices generated by different EEG rhythmic modulations (A-C) and the conventional blocks (D).

3.4 Results

3.4.1 EEG-derived Design Matrix

The design matrices derived from different EEG frequency-specific responses and the canonical boxcar function are shown in Figure 3-3. Specifically, the main difference between the EEG-derived design matrices and the canonical design matrix lay in the onset and amplitude of each block, with apparent fluctuations in the EEG-derived design matrices compared to the canonical model. This seemed to be more realistic since it accounted for the inter-block variation during the experiment.

3.4.2 First-level GLM Analyses

At the first-level GLM analysis (multiple comparisons were corrected by False Discovery Rate (FDR), we first evaluated the performance of the EEG-informed models by the MRE obtained from the HbO and HbR signals, respectively. The one-way repeated ANOVA analysis showed a significant effect of model type on the MRE values ($F = 3.169$, $p = 0.006$). *Post-hoc* test between each two models further identified such differences among these models. As shown in Figure 3-4, for HbO signal there was no significant difference between any model pair, though the EEG-informed models presented slightly smaller residual errors compared to the canonical model at alpha and gamma band (Figure 3-4A). For HbR signal, significantly smaller MREs were identified at the alpha ($p = 0.029$) and beta ($p = 0.046$) model compared to the boxcar model, indicating better fittings in the corresponding EEG-informed models (Figure 3-4B). Additionally, we also compared the performance between HbO and HbR model regarding the same design matrix. Result suggested that GLM achieved significantly

smaller MRE when fitting the HbR signals based on the EEG-informed design matrices, including alpha (p = 0.007) and beta (p = 0.029).

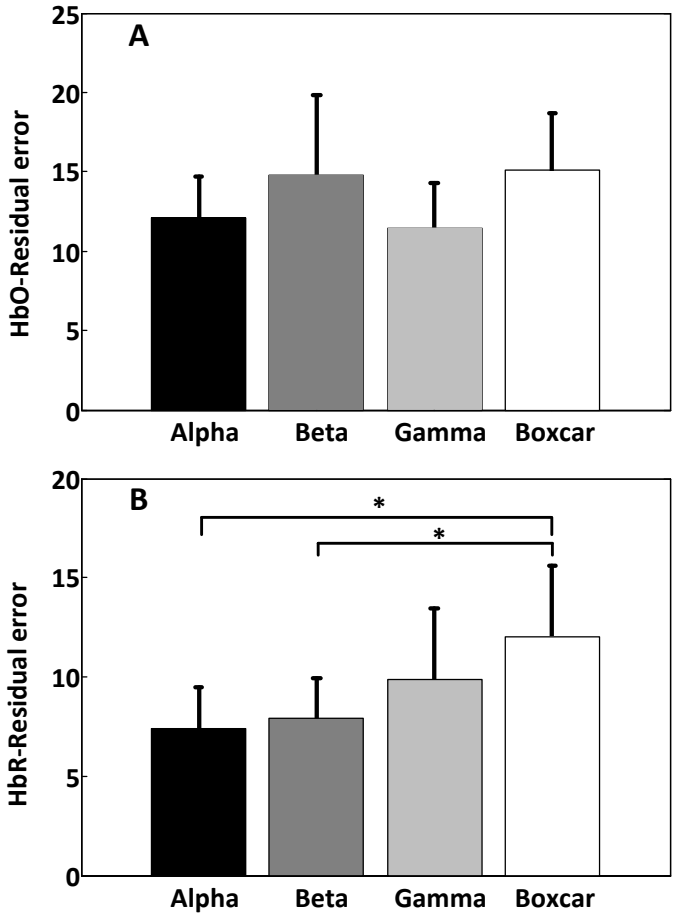

Figure 3-4. The residual errors (mean± standard error) of the GLM models fitted by different design matrices and hemoglobins (A: HbO; B: HbR).

Figure 3-5 shows the results of ROC analysis of all models. The one-way repeated ANOVA analysis indicated a significant effect of the model type (F = 2.601, p = 0.020) on the AUC values that represented the sensitivity and specificity of the model. The *post-hoc* test indicated that, in the case of HbO signal, alpha-based (p = 0.026) and beta-based (p = 0.005) model revealed significantly higher AUC compared to boxcar model (Figure 3-5A). For the HbR signal, alpha-based model achieved the highest AUC that was significantly higher than the gamma-based (p = 0.034) and boxcar (p = 0.038)

model (Figure 3-5B). Finally, when fitting the model using the same design matrix, no significant difference in the AUC values was found between HbO and HbR signal, though the HbR signal tended to achieved higher AUC (Figure 3-5). The statistical results of all comparisons are summarized in Table 3-1.

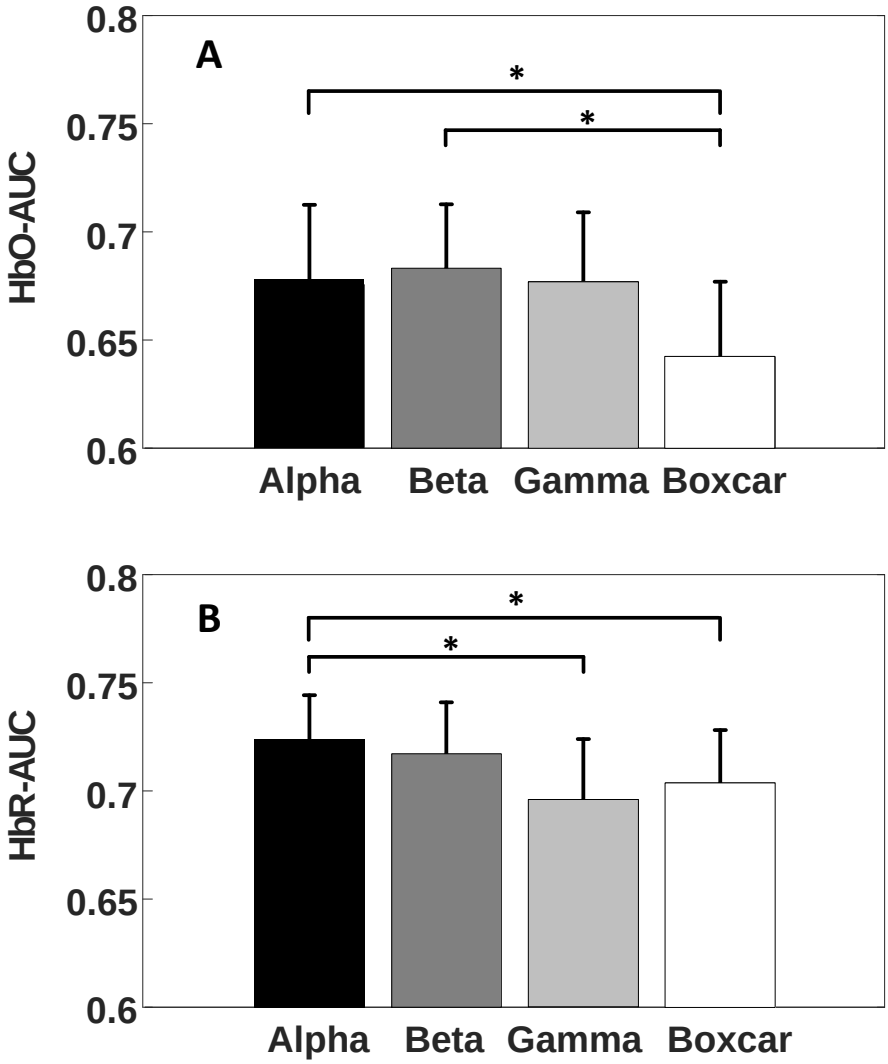

Figure 3-5. The AUC values (mean± standard error) of the GLM models fitted by different design matrices and hemoglobins (A: HbO; B: HbR).

Table 3-1. The statistical summary of the evaluation of different models at first level GLM analyses.

Comparison	p-values	
	MRE	AUC
HbO_Alpha -- HbO_Beta	0.178	0.326
HbO_Alpha -- HbO_Gamma	0.581	0.462
HbO_Alpha -- HbO_Boxcar	0.051	**0.026***
HbO_Beta -- HbO_Gamma	0.179	0.346
HbO_Beta -- HbO_Boxcar	0.462	**0.005***
HbO_Gamma -- HbO_Boxcar	0.105	0.061
HbR_Alpha -- HbR_Beta	0.175	0.170
HbR_Alpha -- HbR_Gamma	0.171	**0.034***
HbR_Alpha -- HbR_Boxcar	**0.029***	**0.038***
HbR_Beta -- HbR_Gamma	0.296	0.100
HbR_Beta -- HbR_Boxcar	**0.046***	0.061
HbR_Gamma -- HbR_Boxcar	0.327	0.263
HbO_Alpha -- HbR_Alpha	**0.007***	0.104
HbO_Beta -- HbR_Beta	**0.029***	0.141
HbO_Gamma -- HbR_Gamma	0.165	0.298
HbO_Boxcar -- HbR_Boxcar	0.147	0.077

3.4.3 Second-level GLM analyses

The second-level GLM analyses were performed by a fixed effect model for all first-level models to identify group-wise activation pattern associated with the motor task. Figure 3-6A shows the ROC plots of all models, wherein the models derived from various task-evoked EEG responses were comparable to the boxcar-fitted models for both HbO and HbR signal. Figure 3-6B shows the quantitative comparison between all models based on theirs AUC values. Specifically, all EEG-informed models, regardless of hemoglobin type (HbO/HbR), revealed slightly higher AUC values than the boxcar models in identifying the motor task-evoked activation ($AUC_{HbO\text{-}Alpha} = 0.823$, $AUC_{HbO\text{-}Beta} = 0.824$, $AUC_{HbO\text{-}Gamma} = 0.829$, $AUC_{HbO\text{-}Boxcar} = 0.811$, $AUC_{HbR\text{-}Alpha} = 0.812$, $AUC_{HbR\text{-}Beta} = 0.819$, $AUC_{HbR\text{-}Gamma} = 0.806$, $AUC_{HbR\text{-}Boxcar} = 0.787$). Further statistical test based on the method proposed by Hanley & McNeil indicated that there was no significant difference in the AUC values between any model pair [115].

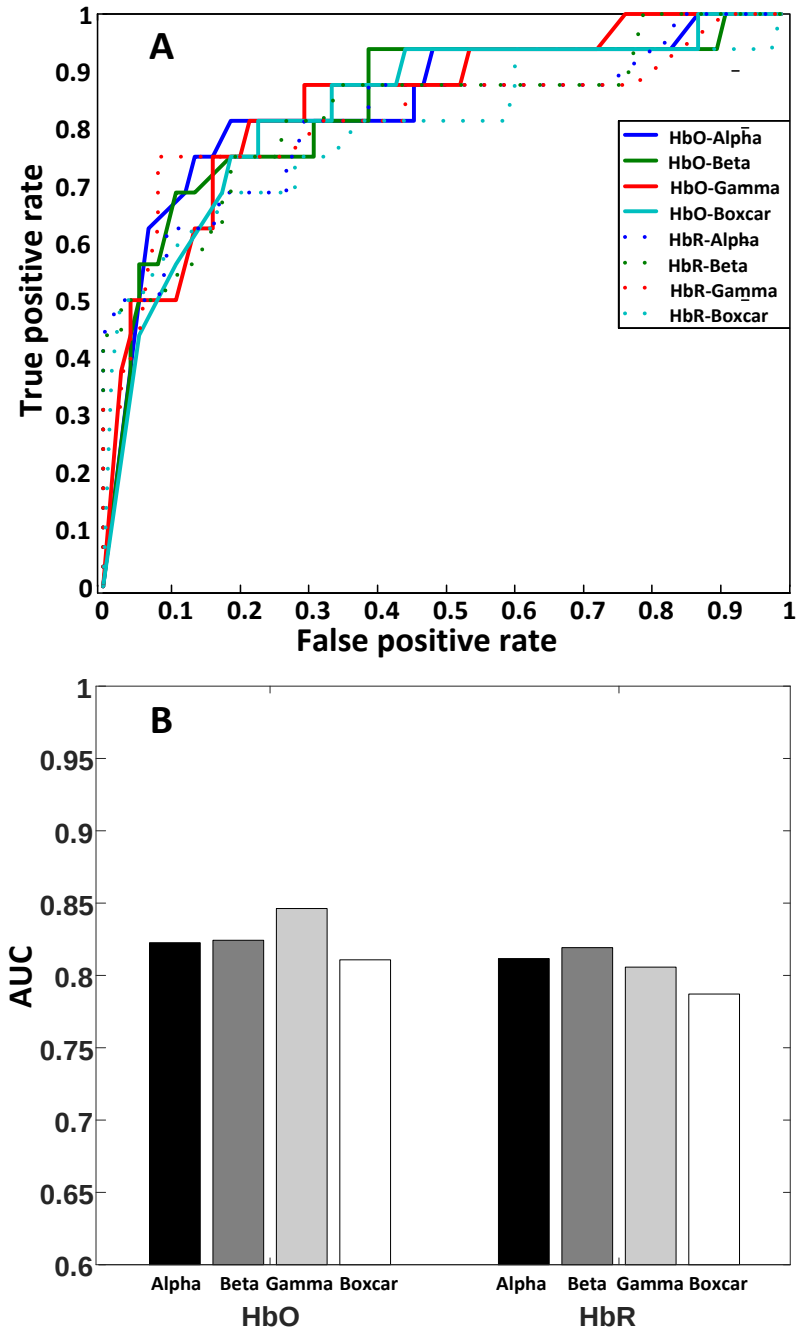

Figure 3-6. Performance summary of the second-level GLM analyses of all models.

In support to Figure 3-6, Figure 3-7 shows the group-level activation maps during left and right hand grasp task for different EEG-informed models and boxcar models, respectively. Overall, all EEG-informed models were able to identify comparable activation at the motor area (true positive rate) while to some extent reduce the

unexpected activation at non-motor area (false positive rate), demonstrating a more favorable performance achieved by the EEG-based models.

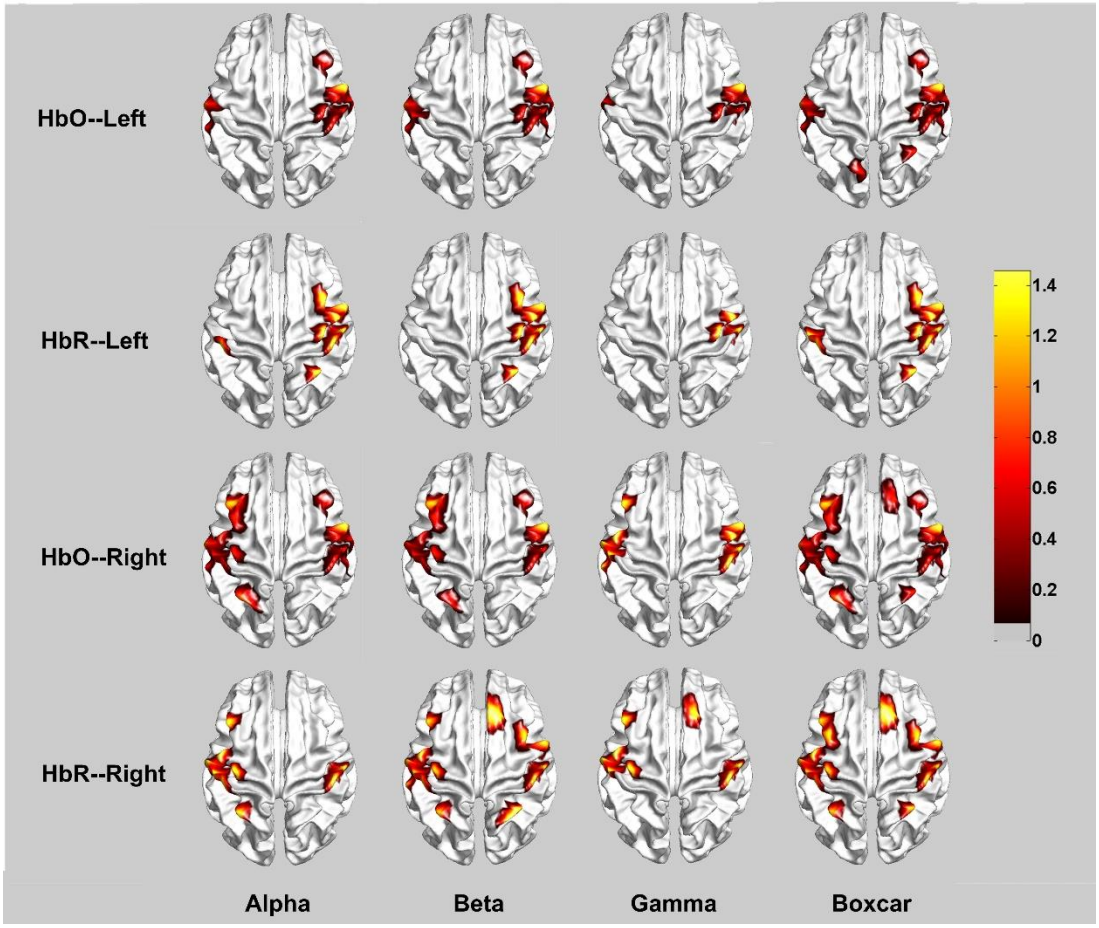

Figure 3-7. Group-level activation maps for the left and right hand grasp task estimated by EEG-informed models and canonical boxcar models, respectively.

3.5 Discussion

To explore the neurovascular coupling between neuronal activity and hemodynamic response, in this study we presented a framework to perform the EEG-informed fNIRS GLM analysis by incorporating the EEG rhythmic modulations in the GLM estimation during a motor execution task. Design matrices constructed by frequency-specific ERP (alpha, beta and gamma) were used for the EEG-informed fNIRS analysis as against the

canonical GLM analysis. Results not only supported our hypothesis that the EEG frequency-specific models were able to enhance the performance of fNIRS GLM analysis compared to the conventional boxcar model, but also provided a promising way to model and explore the neurovascular coupling using concurrent EEG and fNIRS recording.

Neurovascular coupling typically involves neuronal electrical activity and vascular interaction at the cellular level. A number of studies have employed concurrent EEG-fNIRS systems to investigate the correlation between the electrical scalp potential and the hemodynamic response signals [97, 102], demonstrating the feasibility to reveal the neurovascular coupling using EEG and fNIRS. With this in mind, in this study we took a further step to explore and utilize the inherent relationship between EEG and fNIRS signals to enhance the performance of fNIRS GLM analysis during a motor execution task. At the best of our knowledge, our results showed for the first time that considering the task-evoked EEG response improved the ability of the fNIRS signals to capture the brain activation induced by the motor task. It is noteworthy that the EEG-informed models, as assessed by the proposed metrics, significantly outperformed the canonical model in localizing the motor-evoked regions (Figure 3-4 − Figure 3-7). Referring to the previous EEG-informed fMRI study that reported worst result relative to canonical model during similar motor execution task [89], our study provides preliminary evidence that EEG-fNIRS measurement may be more appropriate to characterize specific task-evoked pattern in the brain. In particular, based on the GLM results (Figure 3-4 − Figure 3-7 and Table 3-1), models derived from the alpha and beta rhythmic modulations demonstrated more favorable performance including small mean residual

error and high sensitivity/specificity among all models, which were highly correlated with the hemodynamic response during the motor task and turned out to be the most relevant EEG rhythms in characterizing the neurovascular coupling phenomenon. This result aligns with the findings reported in various EEG-based motor execution studies, where the fluctuations of alpha and beta band stand as the robust biomarkers during hand movements [85, 116, 117].

It is typically more preferable in most studies to perform GLM analysis based on HbO signal, mainly because the HbO signal generally presents a series of peaks in a block design experiment that could be regarded as response to the experimental task. However, it remains to be determined which type of hemoglobin is more suitable for measuring cortical activation [14, 118]. In this work, we evaluated the performance of various design matrices for both HbO and HbR signal. Interestingly, result suggested that GLM analysis based on HbR signal achieved smaller residual error and higher AUC at first-level, which slightly outperformed the results obtain from HbO signal (Figure 3-4 − Figure 3-7 and Table 3-1). This finding is consistent with a previous EEG-fNIRS study that EEG-informed fNIRS analysis achieved better performance in localizing the seizure zones by using the HbR signal [119]. It is possible that HbR response reflects better the underlying neuronal phenomena than HbO response, especially since HbO is more prone to artifacts raised by extracerebral physiological signal that could interfere with the accurate estimation of the task-evoked response in the brain. More investigations should be done to address this concern in the future.

Despite the better performance achieved by the EEG-informed fNIRS GLM analysis, one noticeable issue is some channels at non-motor area were unexpectedly identified

as active after statistical test (Figure 3-7). This could be attributed to physiological noise that acts as confounders in the fNIRS measurement. As noted in previous literature, systemic artifacts such as blood flow in scalp composes a large portion of the measured fNIRS signals, leading to high false positive rate in fNIRS analysis [120]. Although in this work we employed the AR-IRLS algorithm to alleviate the serial correlations artifact, the performance of GLM may be still subject to the residual physiological noise that violates common statistical assumptions of the independence of repeated measurements over time. We expected that newly-proposed approaches, such as the short-separation technique [121], could be applied in future study to dramatically suppress such artifacts.

Understanding the neurovascular coupling between neuronal activity and hemodynamic response plays a crucial role in improving the interpretability and value of neuroimaging data. In this work we purely attempted to model the relationship between motor task-evoked EEG response and fNIRS signals by applying the ERP fluctuations of EEG signals at motor area as regressors to the fNIRS GLM analysis. This approach took the advantage of previous findings that the amplitude oscillations at specific EEG frequency bands are well-modulated by classical motor tasks, such as hand grasping and finger tapping [116, 117, 122]. Another representative study of EEG-informed fNIRS analysis was done by Nguyen and his colleagues, where the apparent onsets and amplitudes of epileptic spikes were marked by EEG traces and convolved with the HRF for GLM analysis [119]. Despite the above typical EEG-derived features, however, the optimal features to model the relationship between EEG and fNIRS signals during uncommon motor task or other non-motor tasks, are nowadays an open topic and

remains to be further investigated. We expect this work to be extensively explored by studying other types of EEG-linked features, and other types of task-based activations.

While the present study provides promising results regarding the EEG-informed fNIRS analysis, there are several limitations that should be acknowledged. First, the designed locations of EEG and fNIRS channels here were configured based on a generic head model. Although the generic model still features a realistic anatomy, the lack of subject-specificity blinds the current method to identify the exact cortical area of channels for each individual. Considering this, it would be useful for future research to obtain anatomical MRI for the subjects, which can be used to customize the head model and optimize the GLM analysis. Second, instead of providing a whole-head coverage, in this study we only covered key regions of the brain due to a limited number of optodes, which may limit the spatial information obtained by the GLM. It is therefore suggested that future research utilize a setup with full coverage when possible.

3.6 Summary

In this chapter, an EEG-informed fNIRS analysis framework was developed to enhance the performance of fNIRS GLM estimation during a motor execution task and to investigate how different EEG rhythmic modulations are independently related to changes in the hemodynamic response. Our results demonstrated that the EEG-derived models, especially derived from the alpha and beta band, achieved more favorable performance in capturing the motor task-evoked activation in the brain compared to the canonical boxcar model. Taken together, through Chapter 2 and Chapter 3, we have

experimentally validated the inherent correlation between neuronal activity and hemodynamic response from views of fNIRS-guided and EEG-guided, respectively.

Chapter 4 – Dynamic Cortical Connectivity Alterations Associated with Alzheimer's Disease: an fNIRS-Informed EEG Source Imaging Study

4.1 Abstract

With the neurovascular coupling being validated in our previous chapters, in this chapter we take a further step by presenting an integrated fNIRS-EEG analysis to demonstrate the feasibility of employing multimodal neuroimaging technique to characterize the cortical reorganization induced by brain disorders. Emerging evidence indicates that cognitive deficits in Alzheimer's disease (AD) are associated with disruptions in brain network. Exploring alterations in the AD brain network is therefore of great importance for understanding and treating the disease. In this chapter, we develop an fNIRS – informed EEG source imaging approach to explore dynamic, regional alterations in the AD-linked brain network. FNIRS and EEG data were simultaneously recorded from 14 participants (8 healthy controls and 6 patients with mild AD) during a digit verbal span task (DVST). FNIRS-based spatial constraints were used as priors for EEG source localization. Graph-based indices were then calculated from the reconstructed EEG sources to assess regional differences between the groups. Results show that patients with mild AD revealed weaker and suppressed cortical connectivity in the high alpha band and in beta band to the orbitofrontal and parietal regions. AD-induced brain networks, compared to the networks of age-matched healthy controls, were mainly characterized by lower degree, clustering coefficient at the frontal pole and medial orbitofrontal across all frequency ranges. Additionally, the AD group

also consistently showed higher index values for these graph-based indices at the superior temporal sulcus. These findings not only validate the feasibility of utilizing the proposed integrated EEG-fNIRS analysis to better understand the spatiotemporal dynamics of brain activity, but also contribute to the development of network-based approaches for understanding the mechanisms that underlie the progression of AD.

4.2 Introduction

Alzheimer's disease (AD) is an irreversible, chronic neurodegenerative brain disease that is typically characterized by progressive impairment of cognitive functions, including a marked degradation of memory [123]. In recent years, AD has been considered the most common form of dementia, afflicting about 5.7 million people in United States [124]. AD is physiologically characterized by the pathological presence of amyloid-beta (Aβ) and hyperphosphorylated tau proteins, as well as significant neurodegeneration and deficits within neurotransmitter systems [125, 126]. These alterations often lead to abnormal cortical activity and connectivity that can be detected by noninvasive measurement techniques, such as EEG, fMRI, and fNIRS.

EEG presents a number of advantages when exploring neural activity: it is non-invasive, inexpensive, clinically available, and features a very high temporal resolution (millisecond-level) [29]. By applying connectivity analyses to source-localized EEG signals, AD-linked alterations in regional connectivity have been identified [127-129]. In particular, several studies have reported abnormal functional connectivity in the alpha and beta band signals of AD patients [127, 128]. Separately, Kabbara et al., have showed that AD networks are characterized by lower global information processing and higher

local information processing than those of healthy, age-matched controls [128]. Results also revealed a significant positive correlation between global efficiency, average clustering coefficient and vulnerability in AD network and corresponding Mini-Mental State Examination (MMSE) scores, which supports the feasibility of using EEG-based connectivity analyses to monitor the different stages of AD, or even preclinical AD [130].

A common technical challenge for EEG source localization is the ill-posed nature of the "inverse problem"; the number of variables that give rise to EEG signals vastly outnumbers the available measurements [84]. Conventional source imaging analysis typically makes use of a pseudo-inversion to alleviate this issue [131]. This solution, however, relies on a maximized likelihood estimation and consequently suffers from complex calculation and spatial imprecision. Attempts have therefore been made to overcome this challenge by combining EEG data with the results from other neuroimaging modalities, such as functional magnetic resonance imaging (fMRI) [90]. In general, traditional fMRI/EEG integration approaches, based on Wiener filtration or Bayesian methods [132-135], use an fMRI-derived BOLD activation map as spatial prior information to constrain the source space for EEG localization. Mathematically, these constraints are imposed as a part of the source covariance matrix, wherein fMRI-active EEG sources are maintained while fMRI-inactive EEG sources are penalized [136-138]. This produces source localization results with increased spatial precision and reduced error. Beyond this, we have also developed a Dynamic Brain Transition Network (DBTN) approach, which uses time-variant fMRI spatial constraints to optimize fMRI-EEG integration based on a hierarchical Bayesian model [90].

FMRI-EEG integration approaches achieve highly specific, accurate results. Unfortunately, fMRI techniques face some inherent limitations; fMRI is costly to perform, highly sensitivity to body-motion artifacts, and requires rigorous experimental design [139]. These factors make fMRI data difficult to obtain and raise the potential for erroneous results or artifacts, limiting the clinical diagnostic potential of EEG-fMRI. To overcome these issues, physicians and researchers may opt to use functional near-infrared spectroscopy (fNIRS) as supplement to EEG source localization. Functional near-infrared spectroscopy is a noninvasive optical imaging technique that typically utilizes two distinct wavelengths (between 600 and 1000 nm) to measure the changes in cortical oxy- and deoxy-hemoglobin concentrations that are coupled with neuronal metabolic activity [12]. As they rely on similar cerebrovascular dynamics, the results obtained by fNIRS are roughly analogous to those of fMRI [10, 91], though fNIRS systems are portable and more resilient to motion artifacts. Furthermore, a recent study has tested and validated the use of fNIRS data as a spatial constraint to guide EEG source localization, achieving comparable results to fMRI-constrained EEG [140].

In this chapter, a dynamic cortical connectivity mapping technique, based on an integrative analysis of concurrently recorded EEG and fNIRS signals, was developed and employed to identify the cortical network changes associated with AD. Specifically, concurrent EEG and fNIRS data were collected from both healthy controls and patients with mild AD (mAD) during a cognitive task. EEG source imaging was then performed using spatial priors derived from fNIRS information, and the reconstructed time-courses of cortical activity were used to generate connectivity networks for mild AD patients and healthy controls. Finally, the resultant networks were compared to identify AD-

linked differences in cortical processing. It is hypothesized that the manifestation of AD, even at early stages, alters the neural circuitry of the brain when engaged in cognitive tasks, leading to “network biomarker” that can be identified using the proposed fNIRS-constraint EEG source localization technique [128]

4.3 Materials and Methods

4.3.1 Participants

Fourteen subjects were recruited as a part of this experiment, including six right-handed patients with mild AD (mAD, 72.5±7.34 years, 2M/4F) that were recruited from a local hospital and eight right-handed healthy volunteers (HC, 62.75±8.21 years, 6M/2F) that were recruited from the local community. Subjects were matched for age and gender, and had no history of cerebrovascular lesions or psychiatric disorders. No subject had previous experience with the experimental task. The mental state of each subject was examined using the Mini-Mental State Examination (MMSE), which is a 30-point questionnaire that provides a quantitative measure of cognitive status or impairment [141], and scores were recorded. The experiment was approved by the Research Ethics Board of Nanjing Ruihaibo Medical Rehabilitation Center and performed in accordance with the Declaration of Helsinki. Each subject was fully informed of the research purpose and methods, and provided written, informed consent prior to the start of the experiment.

4.3.2 Study protocol

A digit verbal span task was employed in this study, as shown in Figure 4-1A. The task session consisted of 30 blocks, with each block broken down into 4× 10-second

sections. Subjects first underwent an 10-second encoding task, in which they were asked to memorize a number sequence that displayed on a computer monitor 1.5 meters in front of them (Figure 4-1B). After encoding task, the number disappeared from the screen and the subjects were asked to stay relaxed for 10-second. This was followed by the 10-second "retrieval" task, wherein subjects were instructed to verbally recall the memorized number and results were recorded. The final 10 seconds in each block were set aside as a rest period. To remind the subjects of the beginning of tasks, a 1000 Hz-pure tone with 60dB SPL-intensity was presented 1-second before each encoding and retrieval task and lasted for 100 ms through a small speaker placed beside the monitor. The background of the screen was set to green to make the subjects, especially the AD patients feel comfortable and relaxed during the experiment [142]. Number sequences varied in length from 4 to 6 digits (each ranging from 1 to 9), and number lengths were varied every 10 blocks without replacement. All 30 sequences were unique and presented randomly to minimize subject-expectancy effects. Prior to the beginning of the experiment, subjects were seated in a comfortable chair and asked to relax for 3 minutes with eyes closed, during which baseline fNIRS signals were collected. To help the participants get familiar with the experimental procedures, each participant was allowed to practice the task for about 10 minutes before beginning the experiment.

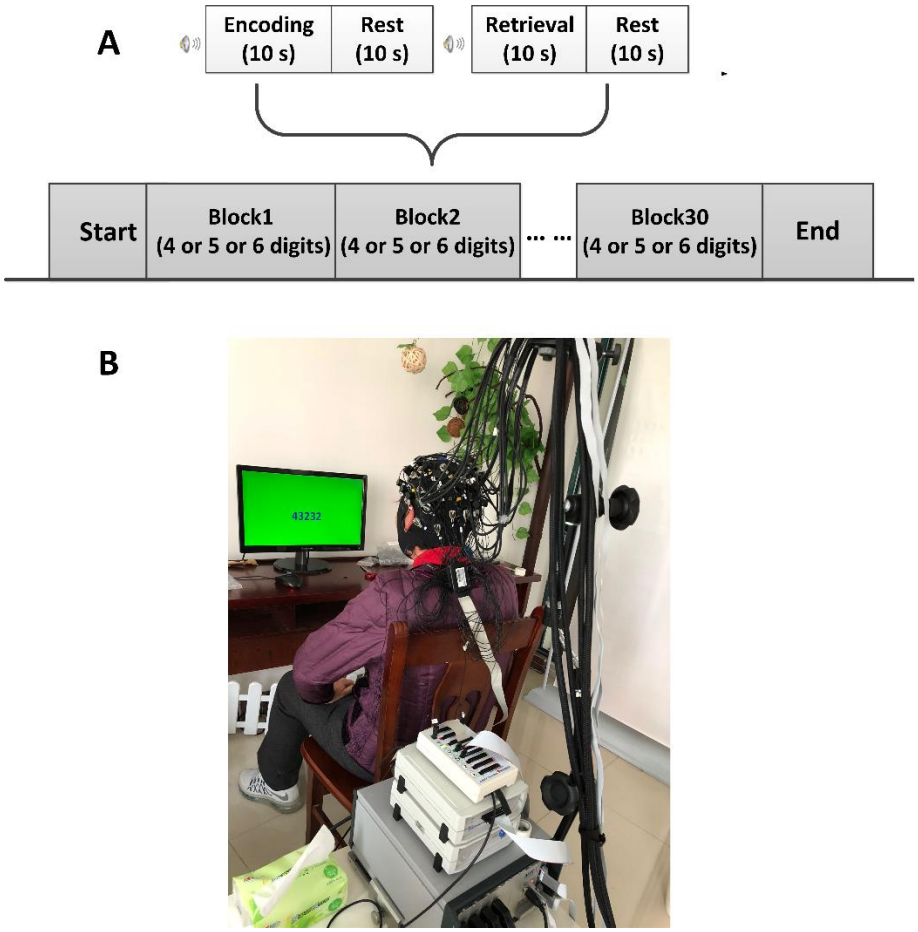

Figure 4-1. Experimental design. (A) The digit verbal span task used in this study. (B) Illustration of experimental environment.

4.3.3 Data acquisition and pre-processing

A concurrent EEG and fNIRS measurement setup was employed in this study. EEG data was collected using a BrainAmp DC EEG recording system (Brain Products GmbH, Germany). Electrode placement followed the international 10-20 convention for a 32-channel cap and signals were recorded at a sampling rate of 500 Hz.

A multi-channel NIRScout system (NIRx Medizintechnik GmbH, Germany) was used to measure the fNIRS signals at a sampling rate of 3.91 Hz. The inter-optode distance was fixed at 3 cm and a total of 46 measurement channels were distributed

throughout the bilateral frontal and parietal cortices, according to the international 10-20 EEG placement system. The onset of each task was simultaneously recorded by the EEG amplifiers and fNIRS acquisition system, which was used for synchronizing two modalities during the data analysis. A schematic illustration of the EEG and fNIRS channel locations is provided in Figure 4-2.

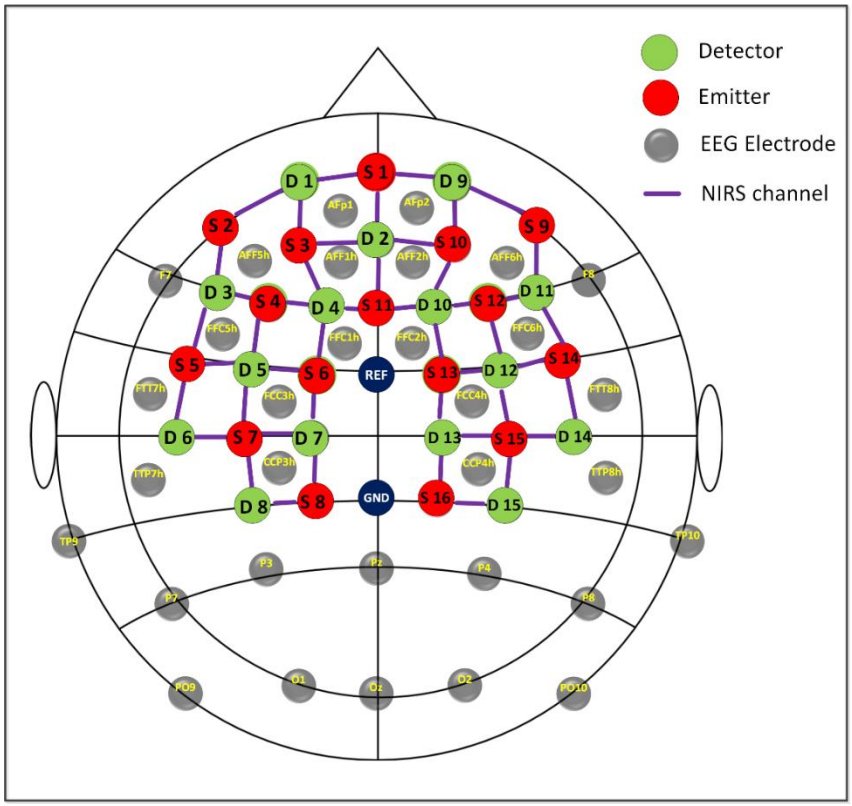

Figure 4-2. The configuration of EEG electrodes and fNIRS optodes.

In this study, considering the EEG signal would be affected by the muscle movement when the subject is speaking in the retrieval task [143], only the EEG and fNIRS signals recorded during the encoding task were used for analysis. EEG preprocessing was performed using BrainVision Analyzer 2.0 software (Brain Products, Germany). Data was first filtered from 0.5 Hz to 50 Hz, with an extra notch filter at 50 Hz to remove any residual powerline noise. Ocular artifact removal was then performed for each subject

using independent component analysis (ICA) and the number of removed IC components was 3 and no more than 5 on average. Data was then re-referenced to a common-average reference and baseline correction was performed for each trial. Next, EEG data was segmented to form epochs that began 2 seconds before the onset of the encoding stage and ended 5 seconds after. Finally, artifact removal and trial rejection were performed through manual inspection. On average, fewer than 10% of the total number of trials were rejected per subject.

Every fNIRS channel was manually inspected and trials with large spikes were considered "noisy" and excluded from further analysis. On average, fewer than 10% of the total trials were rejected per subject. To process the fNIRS signals, a 4th order Butterworth band-pass filter, with cut-off frequencies of 0.01 - 0.2 Hz, was applied to remove artifacts such as cardiac interference (0.8 Hz) and respiration (0.2–0.3 Hz) [69]. The concentration changes of oxy- and deoxy-hemoglobin ([HbO] and [HbR]) were computed according to the Modified Beer-Lambert Law (nirsLAB, NIRx Medizintechnik GmbH, Germany) [12]. For each channel, fNIRS signal was baseline-corrected by subtracting the mean value of the resting-state signal from the signal during the active task. FNIRS signals from the encoding task period were then segmented from the onset of the task to 20 seconds afterwards.

4.3.4 fNIRS-informed EEG Source Imaging Analysis

a) The forward problem

In this study, a template brain model obtained from the MNI305 space was used as a common brain model for all subjects. The full segmentation and surface reconstruction of the MNI305 MRI volume was performed using the Freesurfer image analysis suite

(publicly available at: http://surfer.nmr.mgh.harvard.edu/), resulting in the generation of a high-definition cortical layer and the brain, skull, and scalp boundary surfaces. These surfaces were then used to construct a three-compartment Boundary Element Method (BEM) model, with appropriate conductivity values assigned to each compartment using the MNE software [144]. The high-density cortical layer mesh was downsampled to ~16,000 vertices per hemisphere and used as the source space, such that each vertex location corresponded to a dipole source oriented perpendicular to the surface. A lead-field matrix G was then computed via a forward calculation using the cortical source space, the 3-layer BEM model. EEG and fNIRS electrode positions were digitized and co-registered to the fiducial points on the template brain.

b) fNIRS spatial priors

The classical General Linear Model (GLM) [145-147] was employed for the statistical analysis of preprocessed fNIRS data for each individual subject, and maps of significantly activated channels were obtained by contrasting the encoding task and baseline. Correction for multiple comparisons was performed using a cluster-based method [148] to limit the Family-wise error rate (FWER) to a maximum of 0.05. Channels with values in the fNIRS map above the p-value threshold ($p_{\text{-corrected}} > 0.05$) were deemed insignificant and omitted, ensuring that only statistically significant voxels were used as constraints for the subsequent source imaging routine.

The fNIRS scalp activation map was normally projected and interpolated onto the cortical layer. Briefly, this procedure began by assigning the location of each fNIRS channel (defined as the mid-point between the emitter and detector) on the scalp layer. Next, the fNIRS scalp locations were normally projected onto the cortical layer,

following the method described in [106]. Finally, the fNIRS activation value at each channel was applied and interpolated to the sources on the cortical layer using method described in [38].

In this study, individual fNIRS activation maps were divided into multiple sub-maps based on clusters of neighboring locations and cortical functional regions, allowing for greater spatial flexibility when applying the fNIRS information as a constraint. Specifically, active voxels were grouped into multiple sub-sets using a connected-component labeling technique (the Dulmage-Mendelsohn decomposition algorithm [149]). Subsequently, each cortical patch was divided into smaller patches based on a predefined brain atlas to ensure that individual regions did not cover multiple functional brain regions. The DKT40 atlas was chosen in this protocol to define 68 functional regions of interest (ROIs) using automatic anatomical labeling [107], which were used for source localization and connectivity analyses.

c) EEG source imaging analysis

A spatiotemporal fNIRS-constrained EEG source imaging approach was presented here, wherein each EEG epoch was analyzed using a sliding-window approach. Very briefly, the linear mapping between sensor space and source space is described as

$$\begin{aligned} Y &= GJ + \varepsilon, \\ \varepsilon &\sim \mathcal{N}(0, C), \\ J &\sim \mathcal{N}(0, R), \end{aligned} \tag{4-1}$$

where $Y(t_{window}) \in \mathbb{R}^{m \times d}$ represents the windowed EEG signals consisting of m channels and d measurement samples, $G \in \mathbb{R}^{m \times s}$ represents the lead field matrix, and

$J(t_{window}) \in \mathbb{R}^{s \times d}$ represents the unknown source activity of s dipole sources in the source space for the corresponding time window. ε represents the noise component in the sensor space with its noise covariance matrix C, and R represents the source covariance matrix. The current density J can then be reconstructed according to the equation

$$J = RG^T(GRG^T + \lambda^C)^{-1}Y, \tag{4-2}$$

where the regularization parameter, λ^C, represents the trade-off between model accuracy and complexity, which is traditionally determined using the L-curve method [150]. The source covariance matrix R represents prior knowledge about the distribution of J. Following the framework for spatiotemporal fMRI-constrained EEG source imaging, R assumes the form of a weighted sum of multiple spatial priors, in which each prior is constructed as a sub-map of the fNIRS activation pattern given by

$$R = \sum_{i=1}^{N} \lambda_i^R Q_i. \tag{4-3}$$

R is defined as the sum of N covariance components weighted by an unknown hyperparameter λ^R. Each covariance component, $Q_i = q_i q_i^T$, is formed from a subset q_i of the fNIRS map as explained above. The hyperparameters λ^R are estimated for each EEG window $Y(t_{window})$ using a Restricted Maximum Likelihood algorithm (see more details in [90]) and the corresponding current density J (t_{window}) is determined (Equation 4-2). In this study, the EEG time window was selected to be 200 ms long, with a 50% overlap, designed to provide a temporal resolution suited to the study of evoked response potentials. A time-course of cortical activity for each brain ROI was extracted by averaging the voxel activity within the region.

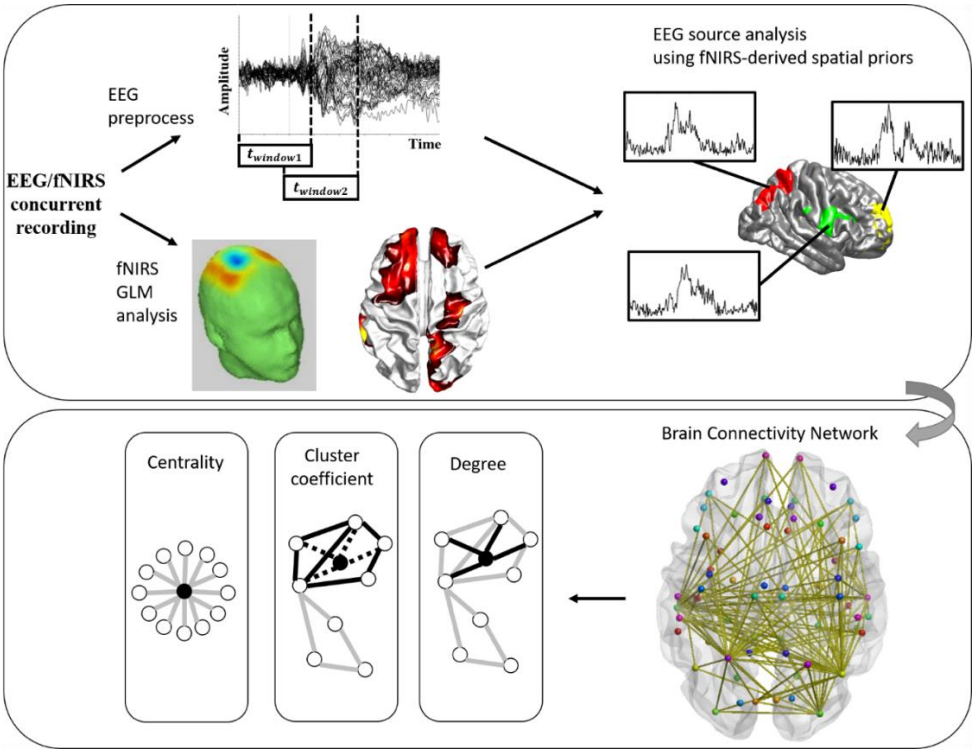

Figure 4-3. The overall schematic for EEG source analysis guided by fNRIS spatial priors and subsequent brain connectivity analysis.

4.3.5 Functional connectivity analysis

The interaction between any pair-wise set of brain regions can be characterized by the Phase Lag Index (PLI) [151]. In general, PLI measures the difference between the instantaneous phases of two time-series – this case, the activation time-course of the two ROIs. Weighted PLI extends the concept of PLI by weighting phase differences based on the magnitude of their lag [152]. The instantaneous phase of each time-series for every time point is computed by performing a Hilbert transform and isolating the resultant phase component. Given the instantaneous phase difference between the activities of two ROIs, $\Delta\Phi$, the wPLI is computed as

$$wPLI = \left| < \frac{|\sin(\Delta\Phi)|}{\sin(\Delta\Phi)} > \right|. \quad (4\text{-}4)$$

In graph-theory terms, each ROI forms a “node” within the graph and the wPLI values calculated between each pair of nodes form the “edges”. Following this approach, a weighted undirected graph was constructed from the obtained wPLI interaction matrix [153].

4.3.6 Graph-theory analysis

Based on the obtained weighted, undirected node-edge graph, several graph-theory measures were adopted to characterize the brain connectivity networks in healthy and mild AD patients. The metrics used in this study included degree, clustering coefficient, and centrality index. In general, the degree metric for a particular ROI reflects the number of connections that link the target ROI to the rest of the network. Clustering coefficient represents the ratio of connections that exist between a node and its nearest neighbors to the maximum number of possible connections. This serves as a summary of the local interactions between a particular ROI and its neighboring ROIs. Finally, the centrality index, called betweenness centrality, measures the number of “shortest paths” between the other node pairs that pass through a target node. Cortically, this indicates how influential the target region is as a hub within the brain network. Prior to the calculation of all graph measures, the weighted, undirected node-edge graph for each subject was thresholded by setting the 60% of the weakest edges as 0 to remove trivial connections. All graph measures were then computed using the Brain Connectivity Toolbox [154]. Figure 4-3 illustrates the analysis process described above.

Finally, to quantify the differences between healthy and AD networks in terms of graph-theory measures, including frequency and regional measures of degree, clustering

coefficient, and centrality, statistical tests were performed using the Mann Whitney U Test also known as Rank-Sum Wilcoxon test.

4.4 Results

4.4.1 Demographic, behavior and clinical rating scores

The demographic information for all subjects, including age, gender, education, MMSE scores and performance in the cognitive task, are summarized in Table 4-1. There were no significant difference between healthy controls and MAD patients in terms of age ($p = 0.072$), gender ($p = 0.119$), education ($p = 0.9$). However, the patient group showed significantly lower scores on the MMSE ($p < 0.001$) and performed poorer in the digital verbal span task ($p = 0.014$) relative to healthy controls.

Table 4-1. The demographic information of all subjects. The "*" indicated a significant difference between two groups. The "+" indicated the result was obtained via Chi-square test.

Characteristic	HC (n=8)	Mild AD (n=6)	*p*-value
Ages (years)	62.75±8.21	72.5±7.34	0.072
Gender (M/F)	6M/2F	2M/4F	0.119^{+}
MMSE	28.1±1.1	19.7±3.0	**< 0.001***
Education (years)	11±2.51	11.17±2.79	0.9
Performance	30	24±5.97	**0.014***

4.4.2 EEG response to cognition task

The grand-averaged EEG response to the encoding task in each channel was done by averaging all trials over all subjects in each group and shown in Figure 4-4. Traces of EEG activity are presented for the frontal region (channel AFF1 and AFF2), parietal region (channel Pz), and the occipital region (channel O1 and O2).

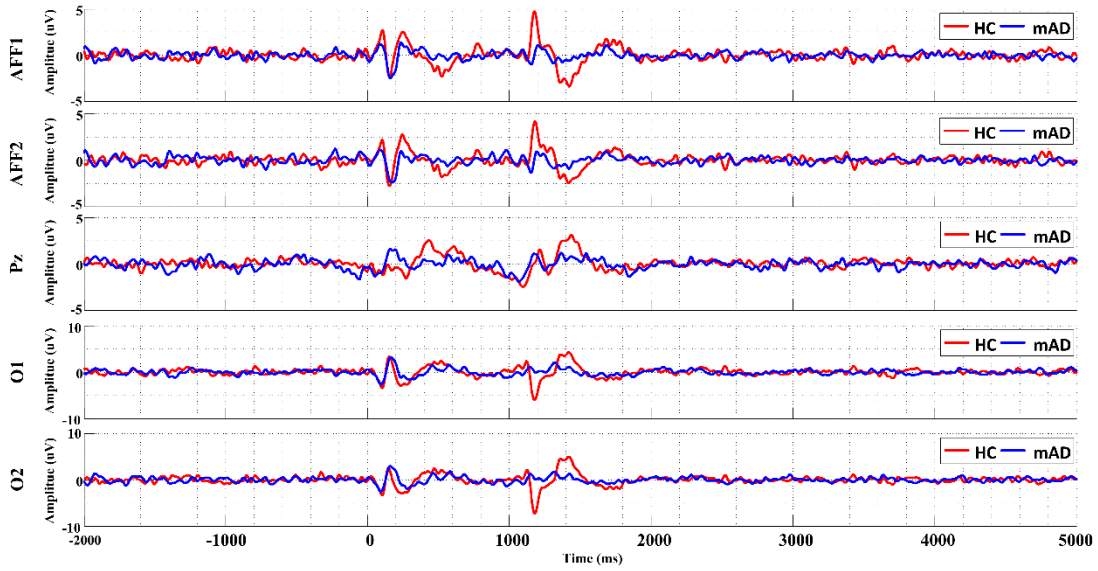

Figure 4-4. EEG grand-average results for the HC group (red) and mAD group (blue), at the frontal channels (AFF1 and AFF2), parietal channel (Pz), and occipital channels (O1 and O2).

For both HC and mAD groups, brain responses to the auditory alert stimuli (t = 0 ms) were observed at around 200ms. Minimal differences were observed between the responses of the two groups at this stage. Drastic differences started emerged ~1100ms after the onset of the encoding task (t = 1100 ms), when the HC group showed a peak in activity at the frontal and occipital regions that was reduced in or absent from the mAD group. We performed two sample *t*-tests to assess the difference between two groups in terms of the mean amplitude of auditory-evoked response (0 - 400 ms) and mean amplitude of task-evoked response (1000-2000 ms). The results indicated that, for all selected channels, there was no significant difference in auditory responses ($p_{corrected} > 0.05$) but significant difference in task-evoked response between two groups ($p_{corrected} < 0.05$).

4.4.3 Current source analysis guided by fNIRS priors

Figure 4-5 shows the topographies of EEG signals and the corresponding fNIRS activation maps of a representative healthy subject and an AD patient obtained through GLM analysis and displayed on the cortical surface after undergoing the projection and interpolation procedure. It could be seen that the activation patterns obtained by two modalities were similar in healthy subject and patient. Specifically, the activation pattern of the HC showed an increase in activity at the frontal regions of the brain, and higher bilateral symmetry than that of the AD patient. Commonly activated regions included the bilateral premotor cortex, the orbitofrontal cortex, frontal pole, precentral gyrus and occipital lobe. In general, differences between the activated cortical regions of the healthy and AD brains pertained more to the frontal regions (frontal pole, orbital frontal).

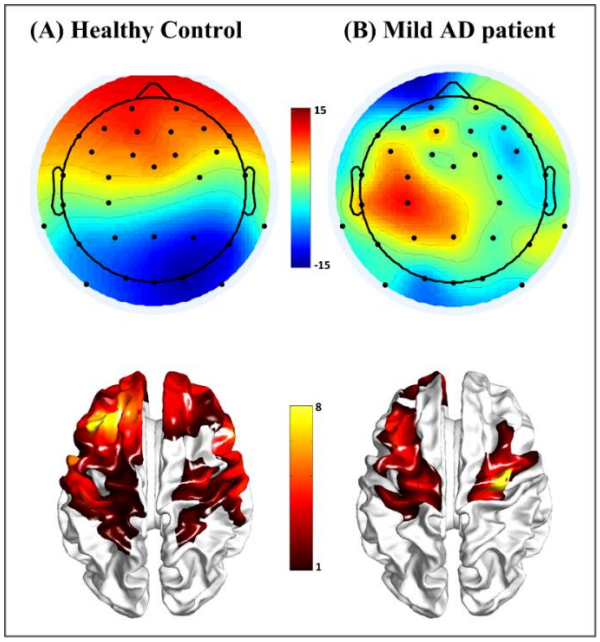

Figure 4-5. Representative EEG topographies (1300 ms) and fNIRS activation maps for the healthy subject (A) and mild AD patient (B) during the encoding task. Color scheme represents the t-statistic ($p_{corrected} < 0.05$).

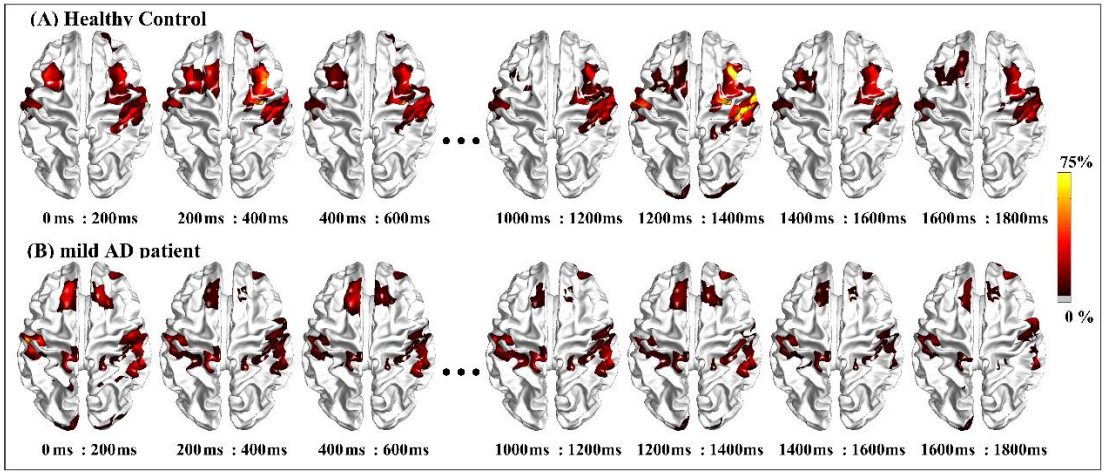

Figure 4-6. Source current activity for a (A) healthy control and (B) mild AD patient associated with the encoding task, averaged for every 200ms time-step.

The spatiotemporal patterns of cortical activity associated with the memory-encoding task are depicted in Figure 4-6. Overall, the activation pattern showed high similarity between the HC and AD patient groups. Major differences were observed at the activity of the frontal regions from 400 ms to 600 ms, 1200 ms to 1400 ms, and 1400 ms to 1600 ms. The detailed time-courses of cortical activity at the 68 regions of interest were used as a basis for subsequent brain connectivity analysis.

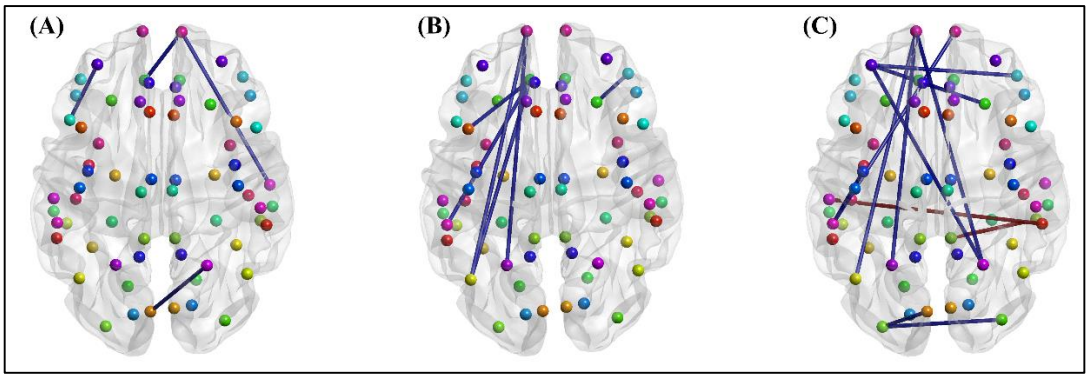

Figure 4-7. Differences in brain connectivity structure between the HC and mAD groups (puncorrected < 0.05), reflected by wPLI measures in the low alpha band (A), high alpha band (B) and beta band (C).

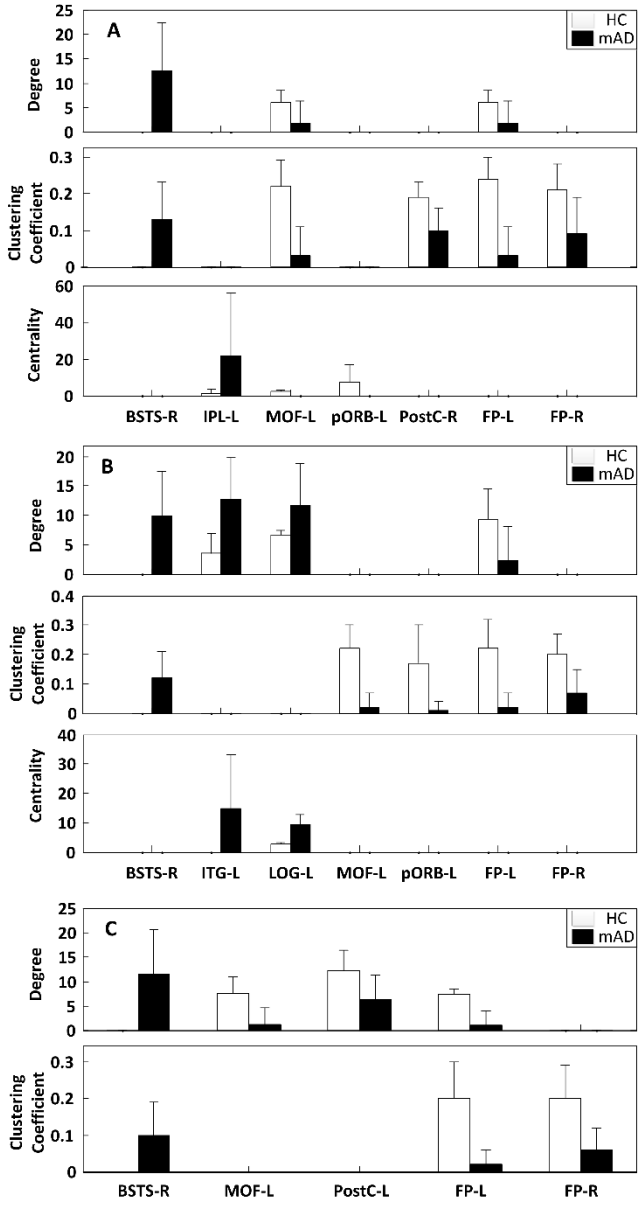

Figure 4-8. Regional graph theory measures for the connectivity networks of the HC (blue) and mAD groups (orange). Only regions revealed significant difference between two groups are shown for low alpha band (A), high alpha band (B) and beta band (C)

4.4.4 Connectivity and graph theory analysis

The connectivity analysis for each subject yielded a weighted undirected graph, and two-tailed t-testing was performed to identify which regional connections (edges) were different between the HC and mAD groups. Figure 4-7 shows the significant differences

in connectivity structure across all frequency bands between both groups. The mAD group consistently showed weaker cortical connectivity to the orbitofrontal and parietal regions. Specifically, weaker connections in the low alpha (8-10 Hz) and high alpha (10-13 Hz) frequency range (Figure 4-7A and B) included: parietal ↔ frontal-pole, parietal ↔ orbital-frontal, and frontal ↔ superior-temporal. Connectivity within the beta frequency range (13-30 Hz) showed greater suppression in the mAD group than in the HC group, particularly in the case of inter-hemispheric interactions (Figure 4-7C). Specific alterations in the beta range included: parietal ↔ frontal-pole, bilateral occipital lobes, and bilateral orbitofrontal lobes. Noticeably, the mAD group exhibited a bilateral interaction between left and right temporal regions that was significantly stronger than that observed in the HC group. Considering the results across frequency bands, it appears that inter-hemispheric connections were more likely to be weakened in AD patients.

Graph theory was then applied to provide quantitative measure of the revealed network properties. Figure 4-8 show the degree, clustering coefficient, and centrality indices for the brain regions that showed statistically significant differences ($p_{uncorrected} < 0.05$) between the HC and mAD groups, particularly at frontopolar, orbitofrontal and temporal regions. Due to the small sample size and large number of nodes in this study, we didn't perform multiple comparison correction after the Mann Whitney U Test. As the results indicate, the HC group showed significantly higher index values for degree and clustering coefficient at the frontal pole (FP), medial-orbitofrontal (MOF), and postcentral (PostC) cortices, which were consistent across all frequency ranges. In contrast, the mAD group showed higher degree and clustering coefficient at the superior

temporal sulcus (BSTS) across all frequency bands. Significant difference in centrality between two groups was only seen in alpha band, with HC group revealed higher centrality at medial-orbitofrontal (MOF) and pars orbitalis (pORB) in low alpha band and lower index values at inferior parietal (IPL), inferior temporal (ITG) and lateral occipital (LOG) areas in high alpha band. Interestingly, the regional differences regarding graph measures between two groups were more prominent in the left hemisphere (Figure 4-8).

4.5 Discussion

Alzheimer's disease, as a form of dementia, presents with a number of cognitive symptoms that disrupt daily life. AD-linked impairments can be complex in nature and typically show progressive deterioration over the course of the disease. While the exact mechanisms that give rise to AD symptoms remain largely unknown, new imaging approaches have advanced our ability to noninvasively detect cortical activity and connections. The research presented here has sought to show the feasibility of EEG-fNIRS integrated imaging to explore cortical dynamics and potential neural biomarkers in AD. By capitalizing on the temporal resolution of EEG and spatial resolution of fNIRS, cortical functional connectivity was investigated in the low alpha, high alpha and beta frequency ranges. Secondary analysis was performed based on the principles of graph theory, which allowed regional network properties to be numerically quantified. Specific interest was paid to the measures of degree, clustering coefficient, and centrality, and results were compared to the networks derived from healthy subjects. The body of results presented here then provides both insight into the functional changes

that accompany AD onset and evidence that regional graph-based measures are markedly changed in mild AD.

To perform a full, in-depth investigation of cortical dynamics, it was first necessary to simultaneously collect data from both EEG and fNIRS. Examination of the EEG results revealed two primary peaks of interest; one occurring at ~200-300 ms and a second arising at ~1100ms (Figure 4-4). Based on the experimental paradigm, it is believed that the first peak constitutes an auditory evoked potential, with possible P300 components, while the late peak is believed to represent cognitive task-related potential. Directly comparing how these peaks manifested in the HC and mAD groups presented a noteworthy contrast – the amplitude of the task-based peak (1100 ms) was greatly reduced in AD patients, while the amplitude of the auditory evoked potential (~300 ms) remained largely the same. This indicates that stereotypical, stimulus-linked ERPs are resilient to AD-linked cognitive deficits, while signals linked to encoding stimulus are diminished. These findings align with previous studies that have reported significantly reductions in the signal amplitude of MCI/AD patients when compared to healthy controls in cognitive tasks [155, 156], exhibiting the functional differences that accompany cognition impairment. In addition to superficial EEG signals, the reconstructed EEG source current activity, with spatial constraint from fNIRS signals, further uncovered a convincing spatiotemporal patterns of cortical activity associated with the memory-encoding task between healthy controls and AD patients. As demonstrated in Figure 4-6, compared to healthy controls, AD patients revealed an altered distribution that featured more activity along the central sulcus and frontal area. The result presented here generally aligns with previous studies that identified activity

in the middle frontal gyrus, dorsal lateral prefrontal cortex (DLPFC) and inferior parietal cortex during digit verbal span task [157, 158], validating the ability of the proposed fNIRS-EEG integration approach to characterize the spatiotemporal dynamics of AD-linked brain network.

Having effectively completed unimodal analyses, the fNIRS-informed EEG source imaging analysis framework was adapted and applied to investigate cortical dynamics and connectivity. Weighted phase lag index (wPLI) values were calculated between the time courses at each pair of ROIs, with results effectively indicating the different brain networks between groups. On the whole, the mAD group showed reduced functional connectivity when compared to their healthy counterparts (Figure 4-7). The most apparent network alterations were observed in the high alpha and beta bands, with the low alpha connectivity map showing relatively fewer alterations (Figure 4-7). Furthermore, changes showed that marked lateralization-significantly reduced connections were observed more often in the left hemisphere than right in high alpha and beta bands (Figure 4-7B, 4-7C). In particular, the left frontal pole and orbitofrontal cortices appeared to show major reduced connections. The importance of these cortical regions has been suggested by previous literature as well [159-161]. For example, Johnson reported a significant positive correlation between atrophy and activation in left frontal area in AD patients, which may account for the cognition decline of AD patients [161]. Reductions in the bilateral connections of AD patients, such as the connections between the left and right frontal cortices in the beta band (Figure 4-7C), provide additional evidence that hemispheric integration is reduced in AD cohort. Similar findings of hemispheric asymmetrical connectivity patterns were also

previously reported [128, 162]. Finally, results from the AD patients found a pair of significantly increased wPLI values in the beta band. These increases were associated with the right temporal lobe and connected with the left temporal and right parietal areas, indicating that AD-linked cognitive impairments do not simply inhibit the global connectivity network. The unique nature of this connection may make it a specific point of interest as a potential biomarker. Previous studies have further identified two marked patterns of cortical properties in AD; temporal lobe atrophy and a reduction in the temporal and occipito-temporal beta power and mean frequency [163-165]. As wPLI characterizes the synchronization between regions (and stability thereof), it is reasonable to conclude that the relatively symmetrical degradation of the temporal lobe and the coincident reduction of beta frequency in AD may contribute to an increase in apparent wPLI values. With this in mind, monitoring the wPLI values between the temporal lobes or temporal-parietal lobes may provide advanced warning of the characteristic changes in AD. Furthermore, it should the noted that the interhemispheric nature of these interactions minimizes the chance for crosstalk and volume conduction, making the potential biomarker more resilient and accurate.

The direct measurement of wPLI provides a very detailed perspective of which cortical regions interact during the cognitive task and how these interactions vary in patients with AD. Unfortunately, the large amount of data from pure connectivity results makes it difficult to identify specific, meaningful differences between HC and the AD group. As a result, we applied graph theoretical measures to the identified connectivity structures and generated descriptive summary statistics for the identified networks, easing discrimination and highlighting potential biomarkers for diagnosis of AD. It

should be noticed that small-worldness, computed from clustering coefficient and shortest path length of the network, is recently proposed to characterize global properties (high segregation and integration) of a brain network [166-168] and has been well-explored by previous AD studies using multiple neuroimaging techniques, such as fMRI and EEG [169, 170]. However, this fNIRS-EEG integration study solely focused on regional analysis using node-based measures to identify regional alterations in particular regions associated with AD, providing more regional information of the brain network compared to the global property conveyed by small-worldness. Node-based measures, including degree, clustering coefficient, and centrality were used as a part of this study, and each exhibited significant differences between the HC and AD groups across frequency ranges, as indicated in Figure 4-8. Degree, which indicates the number of connections within a region, showed significant differences in a number of regions, particularly in the right superior temporal sulcus (BSTS-R, low alpha, high alpha and beta bands), left medial orbitofrontal (MOF-L, low alpha and beta bands), and left frontal pole (FP-L, low alpha, high alpha and beta bands) regions. Clustering coefficient showed a greater number of significant differences in all frequency ranges, particularly in the bilateral frontal pole (FP-L and FP-R) and right superior temporal sulcus (BSTS-R). Frequency-specific differences in clustering coefficient were found in the left medial orbitofrontal (MOF-L, low alpha and high alpha), right postcentral (PostC-R) and left pars orbitalis (pORB-L, beta) regions. Finally, centrality showed the most lateralized significance, including differences in the left inferior parietal, medial orbitofrontal, pars orbitalis, inferior temporal and lateral occipital areas within alpha band. Notably, centrality in the low and high alpha bands appeared to be increased in parietal, occipital,

and temporal locations, areas that did not show significance in any other comparisons. These results indicate the potential of EEG-fNIRS-based neural biomarkers for the early characterization of AD, with regional indices appearing to be particularly impacted by cognitive decline. In particular, the left frontopolar regions showed significant decreases for degree and clustering coefficient in each frequency band, highlighting it as a particular region with discriminatory potential. On the contrary, the right superior temporal sulcus showed significant increases for these two measures in the each frequency band, making them potential markers of interest as well. These results reinforce the findings that can be observed from synchronization index (such as wPLI) measurements alone [171, 172] and evidence a fundamental shift in network structure as hubs of activity transition from frontal to temporal locations over the course of AD onset. While these studies have focused largely on AD-linked changes within the default mode network, the present feasibility study has focused on cortical networks activated during a memory-based task. Considering that memory deficit is a defining characteristic of AD and that the prefrontal cortices are heavily implicated in memory processing, the regional alterations observed here are considered reasonable and evince the capability of integrated EEG-fNIRS approach in the detection of task-induced network changes.

Though this research has effectively used EEG-fNIRS to uncover potentially impactful dynamics of activity, there are several limitations that should be acknowledged. First, the source localization here was performed using a generic head template with default electrode locations. Although the generic model still features a realistic anatomy, the lack of subject-specificity blinds the current method to individual

differences in anatomy or cap setup. Considering this, it would be useful for future research to obtain anatomical MRI for the subject, which can be used to customize the model and forward calculation. Second, the fNIRS setup for this study was not able to provide full coverage due to a limited number of optodes. To minimize the effect of insufficient coverage, the cap setup here was designed to cover key regions of interest, and the proposed fNIRS-EEG integration approach was previously demonstrated to be highly robust against "false-positive prior" (i.e. active regions in fNIRS but not in EEG) and "missing prior" (i.e. missing regions from fNIRS activation map but active in EEG) as described in detailed in [140]. However, we acknowledge that gaps in coverage may still limit the prior information of fNIRS and reduce source localization accuracy, it is therefore suggested that future research utilize a setup with full coverage when possible. Finally, this study focused solely on evaluating the feasibility of utilizing fNIRS-EEG integration approach to explore dynamic alterations in the AD-linked brain network compared to healthy population. The preliminary results, though achieved based on the limited sample size, are believed to have provided sufficient evidence to support our feasibility evaluation. When attempting early detection of AD, however, it will be important to differentiate between each of these pathological conditions, including MCI or preclinical stage of AD that contribute to the development of AD. It will then be necessary to expand subject base and population in the future if true, defining neural biomarkers are to be obtained.

4.6 Summary

The complimentary properties and easy application of EEG and fNIRS has led to a significant research focus on their multimodal combination. In this chapter we presents a feasibility study for the integration of EEG and fNIRS, using a spatiotemporally accurate integration method to explore the alterations of AD networks compared to healthy controls. Following this approach, variations in regional connectivity were assessed and used to uncover frequency-linked differences between healthy controls and mild AD patients. Graph theory measures were then applied and a number of regional and frequency-specific features were identified. While more verifications will be necessary, this study has shown the potential for the inexpensive and portable assessment of possible AD neural biomarkers that are associated with brain connectivity network. With further research and definition, technique proposed in this study may advance the detection and treatment of AD, improving outcomes and reducing costs for both individuals and healthcare providers.

Chapter 5 ─ Longitudinally Assessing Brain Plasticity during Post-stroke Recovery using Concurrent fNIRS-EEG Recordings

5.1 Abstract

Persistent motor deficits are very common in post-stroke survivors and often lead to disability. Current clinical measures for profiling motor impairment and assessing post-stroke recovery are largely subjective and lack precision. Biomarkers indicating alterations in motor functions present as an essential tool for assessing and predicting post-stroke motor recovery and as such are of great clinical value. In this chapter, we apply multimodal neuroimaging technique to characterize the brain plasticity during post-stroke rehabilitation. EEG and fNIRS data were simultaneously recorded from nine healthy controls and eighteen stroke patients during a motor execution task. The proposed fNIRS-informed EEG source imaging technique was employed to estimate cortical neural activity and functional connectivity. Subsequently, graph theory analysis was performed to identify network features for monitoring and predicting motor function recovery during a four-week intervention. Results showed that the task-evoked strength at ipsilesional primary somatosensory cortex (S1) was significantly lower in stroke patients compared to healthy controls ($p < 0.001$). In addition, across the four-week course of rehabilitation intervention, the task-evoked strength at ipsilesional premotor cortex (PMC) ($R = 0.895$, $p = 0.006$) and the connectivity between bilateral primary motor cortices (M1) ($R = 0.9$, $p = 0.007$) increased in parallel with the improvement of motor function. Furthermore, a higher baseline (pre-intervention) strength at ipsilesional PMC was found associated with a better motor function recovery

(R = 0.768, p = 0.007), while a higher baseline connectivity between ipsilesional supplementary motor cortex (SMA)-M1 implied a worse motor function recovery (R = -0.745, p = 0.009). In conclusion, the established multimodal EEG/fNIRS neuroimaging technique demonstrates a great potential for monitoring and predicting post-stroke motor recovery in a longitudinal manner.

5.2 Introduction

Stroke is the major cause of motor impairment, leading to motor deficits at acute stage and most stroke survivors are left with residual motor deficits throughout their life [173]. Over the past decades, effort has been taken to understand the neural mechanisms of motor recovery following stroke and enhance the efficacy of rehabilitation therapy. Emerging evidences have shown that cortical reorganization accompanies the restoration of motor function after stroke [174, 175], yet how well post-stroke rehabilitation can benefit from this functional alteration has not been completely determined. Therefore, it is important to identify biomarkers that could precisely characterize the pattern of motor recovery and maximize the therapeutic effect during post-stroke therapy.

Cortical reorganization during post-stroke therapy is generally associated with altered regional excitability as well as aberrant connection between relevant function areas [175-178]. Advanced non-invasive neuroimaging techniques, including EEG and fMRI, have been widely applied to explore the dynamic alteration of cortical excitability and connectivity after stroke and shown great potential for understanding the relationship between dysfunctional brain network and motor deficit [8, 179-181]. For

example, resting-state fMRI studies have shown that interhemispheric connectivity between bilateral primary motor cortex is positively correlated with the motor improvement of stroke patients and can predict better upper limb motor gains across longitudinal rehabilitation [177, 182-184]. Additionally, Cheng et al., explored the task-evoked brain network property using graph theory analysis during a motor task and found that network-derived indices are capable of predicting motor function restoration [179]. In contrast to fMRI, EEG presents a number of advantages over fMRI for exploring the stroke-linked neuronal activity: it is highly-portable, inexpensive, and features a very high temporal resolution[15]. By applying connectivity analyses to EEG signals, the modulations of regional connectivity following stroke have been identified in previous studies [8, 181]. Overall, these findings suggest that measures of cortical motor excitability and connectivity may serve as good biomarkers for characterizing the cortical reorganization after stroke.

However, one challenge of EEG is the volume conduction problem; a single electrode on the scalp picks up activity from multitude sources (cortical activity, subcortical activity, external noise, etc.), which results in a difficulty in accurately localizing the source activity and spuriously affects phase-synchronization indices used in EEG connectivity analyses [152, 185]. EEG source localization has therefore been developed to overcome the limitation of surface EEG in characterizing the brain activity [186]. Typically, this approach relies on the surface EEG signals and the anatomical structure and physiological properties of the brain to estimate sources within the brain, which allows us to more accurately localize the regions associated with specific function [187, 188]. A common challenge for EEG source localization is the ill-posed “inverse

problem"; the number of sources that give rise to EEG signals vastly outnumbers the available measurements, making it impossible to localize the measured scalp EEG activity to the actual current-generating source within the brain with absolute certainty [189, 190]. Therefore, attempts have been made to overcome this challenge by combining EEG data with the results from other neuroimaging modalities, such as fMRI. Prior studies have shown that, using high spatial prior information acquired by fMRI, people are able to estimate brain activity with high spatiotemporal resolution in both computer simulations and real experiments involving visual and motor tasks [90, 191-193]. However, fMRI is typically limited by the high sensitivity to motion artifacts, poor portability, and high costs, rendering it less appropriate for investigating brain activity related to human motor control in realistic situations (e.g., in sitting or standing positions) [139].

One alternative solution for overcoming this limitation is to use the portable fNIRS as a supplement to EEG source localization. Our previous study has demonstrated the possibility of utilizing the fNIRS constrained-EEG source localization to investigate the dynamic cortical connectivity associated with Alzheimer's disease [21]. These evidences support that connectivity analysis based on integrated fNIRS-EEG source localization could be applied to characterize the stroke-linked cortical reorganization for the longitudinal assessment of post-stroke motor recovery.

With this in mind, this chapter aims to characterize the cortical reorganization during post-stroke rehabilitation using our novel fNIRS-informed EEG source imaging algorithm. Specifically, fNIRS and EEG data were simultaneously collected from healthy controls and stroke patients during a motor task. Spatial priors related to the

motor task were extracted from the fNIRS signals to enhance the performance of the EEG source imaging, from which the time-courses of cortical activity were reconstructed and used for the functional connectivity analysis for all subjects. We hypothesized that brain network within motor regions would be associated with individual motor function. It was expected that network-based biomarkers were able to assess and predict motor improvement after rehabilitation intervention.

5.3 Materials and Methods

5.3.1 Participants

Eighteen stroke patients with hemiparesis (11 Males/ 7 Females, age: 58.67 ± 10.26 years) were recruited from Guangdong Provincial Work Injury Rehabilitation Center, and nine age-matched, healthy subjects (HC, 6 Males / 3 Females, age: 44.44 ± 16.63 years) were recruited as a control group in this study. All participants are right-handed, age and gender-matched. The experimental protocol was approved by the ethics committee of the Guangdong Provincial Work Injury Rehabilitation Center. Participants gave written informed consent according to the Declaration of Helsinki.

The inclusion criteria for stroke patients were as follows: (1) stroke that occurred 1–6 months prior to the first assessment; (2) age between 18-70 years; and (3) able to follow instructions and to consent (Mini Mental State Exam score > 27). The exclusion criteria included: (1) deficits in communication or attention that would interfere with the experiment participation; (2) contraindication to magnetic resonance imaging (MRI) scanning; and (3) other diseases that would substantially affect the function of upper extremity.

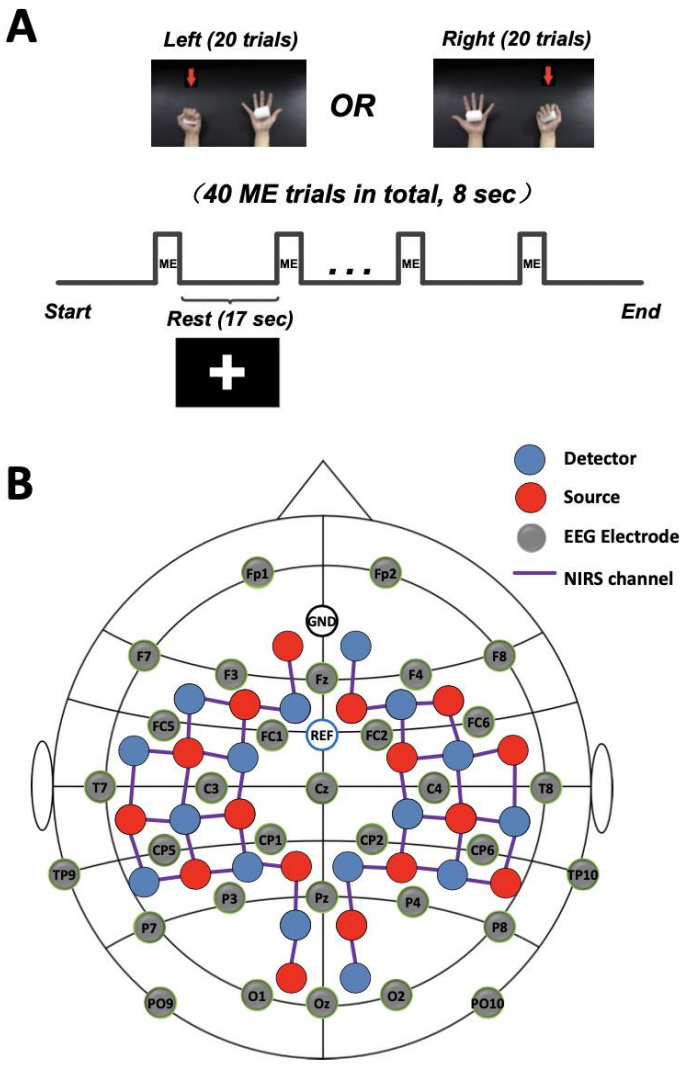

Figure 5-1. Experimental design. (A) The experimental motor execution (ME) task used in the study. "+" symbol indicated the resting period. (B) The channel locations of EEG and fNIRS.

5.3.2 Study protocol

All patients underwent a 4-week conventional rehabilitation intervention in the hospital. The intervention included standard physical training, occupational therapy and massage for 6 hours per day, 5 days per week. Prior to the beginning of intervention, all patients underwent a baseline assessment of upper extremity function by Fugl-Meyer

Assessment rating scale (FM-UL, normal = 66) and participated in a concurrent EEG-fNIRS recording (pre-intervention). At the end of the rehabilitation intervention, 7 of the 18 patients participated in the second concurrent EEG-fNIRS recording and assessment of motor function (post-intervention). All motor function assessments were performed by an experienced therapist from the Department of Rehabilitation Medicine in the participating hospital.

During the experiment, Subjects received visual instruction through a monitor placed in front of them. A motor execution (ME) paradigm consisted of 40 randomized trials of left and right hand clench task (20 trials for each hand) was adopted. Each trial started with a 8-second ME task, indicated by an short video showing a left/right open-close hand, followed by 17 seconds of a resting period, indicated by a "+" symbol in a black background (Figure 5-1A). During the ME period, subjects were asked to naturally squeeze a sponge ball with the corresponding hand. In particular, patients were required to try their best to squeeze the rubber without causing any shaking of their bodies when performing hand clenching using their affected hands.

A concurrent EEG and fNIRS measurement setup was employed to collect the EEG signal and hemodynamic response signal (Figure 5-1B). Specifically, thirty-two EEG electrodes were placed on the scalp, and EEG signals were measured using an EEG recording system (Brain Products GmbH, Germany) at 500 Hz sampling rate. At the same time, a total of 40 fNIRS channels were positioned over the main brain regions, including the motor cortex, frontal cortex, temporal cortex and occipital cortex. FNIRS signals were recorded simultaneously using a continuous-wave NIRS imaging system (NIRScout, NIRx Medizintechnik GmbH, Germany) at 3.91 Hz sampling rate.

5.3.3 Data preprocessing

The raw EEG signals were first filtered by a notch filter at 50 Hz to remove powerline noise and then a 4th order Butterworth bandpass filter (0.5 Hz--45 Hz). Eye movement artifact was then removed using independent component analysis. Data were re-referenced by subtracting the average of all channels from each channel. After that, EEG data were segmented to multiple trials that began 2000ms before the task onset and ended 8000ms after, and baseline correction was performed for each trial. Finally, we manually inspected and excluded any trial with artifact.

For the fNIRS signals, a 4th order Butterworth band-pass filter (0.01--0.5 Hz) was applied first to eliminate artifacts such as cardiac interference (0.8 Hz). After that, motion artifacts were removed from the fNIRS signals using a wavelet-based method [194]. The concentration changes of the HbO and HbR were then computed according to the Modified Beer-Lambert Law [10]. The obtained signals were manually inspected for every channel, wherein noisy trials were excluded from further analysis. Similar to the method in our previous study [21], the General Linear Model (GLM) was employed to obtain the activated channels significantly induced by each hand movement, which would be used as spatial priors for the EEG source imaging.

Following the method described in Chapter 4, fNIRS-informed EEG source imaging was perform. A time-course of cortical activity for each brain ROI was reconstructed and extracted from each region, yielding 68 regional current source estimates for each subject.

5.3.4 Functional connectivity and graph theory analysis

To accurately characterize the brain plasticity after stroke, in this study we employed weighted phase lag index (wPLI) to assess the FC between brain regions and graph theory analysis to identify aberrant regional excitability caused by stroke. It should be noted that $wPLI$ is between 0 and 1, where 0 indicates no synchronization between two time series and 1 indicates a strong synchronization between two time series.

In this study, the reconstructed time series of each brain ROI was first filtered into different frequency bands, including theta (4-8 Hz), low alpha (8-10 Hz), high alpha (10-13 Hz) and beta (13-30 Hz). The wPLI between the time series of any ROI pair was then computed for each frequency band.

Graph theory was employed in this study to identify brain region with abnormal excitability after stroke. Specifically, we defined each ROI as a "node" and the wPLI between two nodes as the "edge" in a graph [154]. As such, based on the wPLI interaction matrix, a weighted undirected graph can be constructed for each frequency band and each subject [21]. Furthermore, a graph metric, termed as node strength, was applied to assess the excitability of each brain region. Specifically, the strength of a particular ROI is defined as the sum of weights of all edges connected to this ROI, which indicates the importance of ROI in the network [154]. In this study, we computed the strength of each ROI at all pre-defined frequency bands.

5.3.5 Multiple linear regression and statistical analysis

To identify the association between the FC indices and motor function of subjects, we performed bivariate analysis and multiple linear regression analysis in this study. Specifically, we focused on the strength of eight key brain regions that are essentially

involved in motor control system, including the primary motor cortex (M1), premotor cortex (PMC), primary somatosensory cortex (S1) and supplementary motor area (SMA) on both hemispheres. In addition, the connectivity between all eight regions, including 4 symmetrical connection between two hemispheres, 3 connections between M1 and other brain regions in the ipsilesional hemisphere, and 3 connections between M1 and other brain regions in the contralesional hemisphere, were also evaluated by testing the corresponding wPLI values. Overall there were 32 regional excitability index (assessed by strength, 8 regions × 4 bands) and 40 connectivity index (assessed by wPLI, 10 connections × 4 bands) to be analyzed. Note that the left hemisphere was defined as lesion side based on the motor deficit of patient group (Table 5-1), and the corresponding right hand task was analyzed. FC indices from patients with lesion in the right hemisphere were flipped across the midline for subsequent analyses [8].

We first investigated whether there was a significant difference in the FC indices between healthy controls and stroke patients using Wilcoxon rank sum test. Multiple linear regression was employed to document the linear relationship between the selected FC indices and the degree of motor impairment (FM-UL scores). Specifically, in the regression model, the independent variables were the selected FC indices among target regions, while the dependent variable was the FM-UL scores of all subjects.

The second analysis was to exam how the changes in FC (ΔFC) performed as a biomarker of improvement in motor function (ΔFM-UL) over the 4-week intervention in patients. The ΔFC of all 7 patients underwent two assessments were defined as the independent variables in the linear regression model, while the changes of FM-UL

scores between pre-intervention and post-intervention (ΔFM-UL) were defined as the dependent variable.

Table 5-1. The demographic information and clinical characters of all subjects.

Subject	Age (Years)	Gender	Affected hand	Days after stroke	Lesion location	FM-UL	
						Pre	Post
01	55	M	R	45	Left basal ganglia	12	/
02	66	F	R	89	Left pons	18	33
03	56	M	L	62	Right basal ganglia	56	60
04	36	M	R	75	Left basal ganglia	30	/
05	46	M	R	40	Left thalamus	53	/
06	37	M	R	84	Left coronal radiate	32	/
07	23	F	R	36	Left fronto-temporo-parietal	44	58
08	55	F	R	32	Left pons	56	/
09	51	F	L	44	Right basal ganglia	43	49
10	61	F	R	42	Left basal ganglia	14	/
11	47	M	R	72	Left basal ganglia	20	/
12	50	M	L	32	Right basal ganglia	11	13
13	36	M	R	99	Left basal ganglia	17	/
14	43	M	R	101	Left basal ganglia	18	20
15	63	F	R	52	Left pons	16	/
16	43	M	L	110	Right basal ganglia	22	27
17	54	F	R	43	Left basal ganglia	25	/
18	40	M	R	56	Left basal ganglia	61	/

Another analysis was to assess how well the baseline FC (pre-intervention) can predict the motor function gains (ΔFM-UL) after the 4-week intervention. We defined the baseline FC indices obtained from all 7 patients as the independent variables and the improvement of motor function (ΔFM-UL) after rehabilitation as the dependent variable. Importantly, prior to each individual multiple linear regression analysis, bivariate analysis was performed to test the correlation between each independent variable and dependent variable using Pearson's correlation. Similar to a previous study [8], a threshold relative to the absolute value of the maximal correlation coefficient ($>0.8\ R_{max}$) was required for the corresponding independent variables to be included in the regression model.

5.4 Results

5.4.1 Demographic and clinical behavioral data

Table 5-1 summarizes the demographic information and clinical behavioral scores of all patient subjects, including age, gender, site of the lesion, time of post-stroke and clinical assessment scores. Statistical analysis showed that there were no significant differences between healthy controls and stroke patients in terms of age ($p = 0.515$) and gender ($p = 0.609$). In addition, a significant improvement in the motor function (assessed by FM-UL scores) after the 4-week rehabilitation intervention was observed from seven patients who participated in the second evaluation (post-intervention vs. pre-intervention, $p = 0.017$).

5.4.2 Difference in functional connectivity between healthy and patient groups

The Wilcoxon rank sum test revealed that the baseline (pre-intervention) strength of ipsilesional S1 at theta band was significantly lower in stroke patients (n = 18) compared to healthy controls (n = 9) ($p_{corrected} < 0.001$, Figure 5-2A). We further examined the relationship between the significant FC index and the FM-UL scores of all patients. The linear regression analysis indicated that, when considering both pre- and post-intervention, there was only a mild positive but not significant correlation between the theta strength at the affected S1 and the degree of motor impairment of patients ($R = 0.254$, $p = 0.221$), as shown in Figure 5-2B.

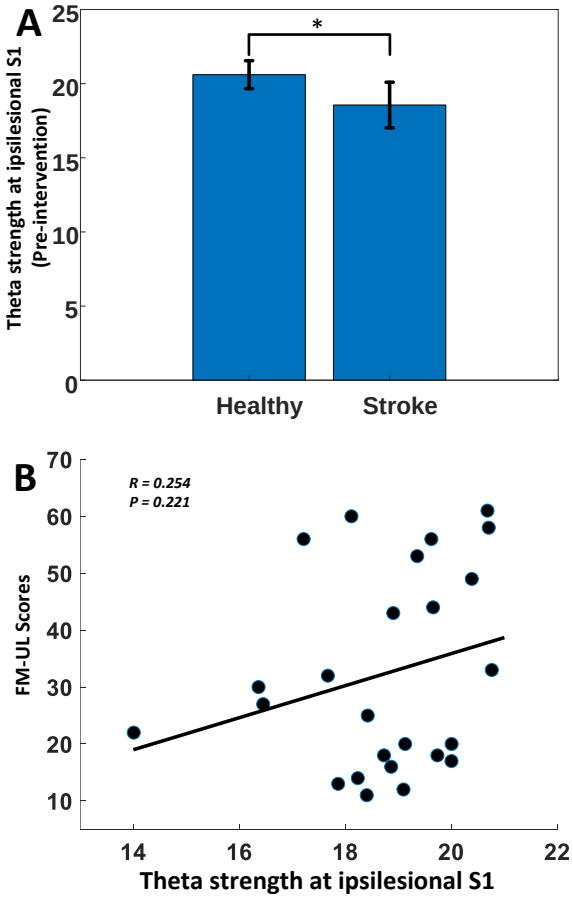

Figure 5-2. (A) Significant difference in theta strength (mean ± std) at ipsilesional S1 between healthy and patients at pre-intervention ($p < 0.001$). (B) Positive but not significant correlation between the strength of ipsilesional S1 at theta band and the degree

5.4.3 Correlation between changes of functional connectivity and improvement of motor impairment

A separate linear regression analysis was performed to evaluate the sensitivity of the change of FC (Δ FC) in monitoring the recovery of motor function (ΔFM-UL) in all seven patients who participated in the post-intervention evaluation. Results showed that there was a significantly positive correlation between the change in the high alpha connectivity of bilateral M1 areas and the improvement of motor impairment after the 4-week rehabilitation ($R = 0.900$, $p = 0.007$, Figure 5-3A). We also found that the

change in the task-evoked strength at ipsilesional PMC was positively correlated with the improvement of motor impairment at beta band (R = 0.895, p = 0.006, Figure 5-3B).

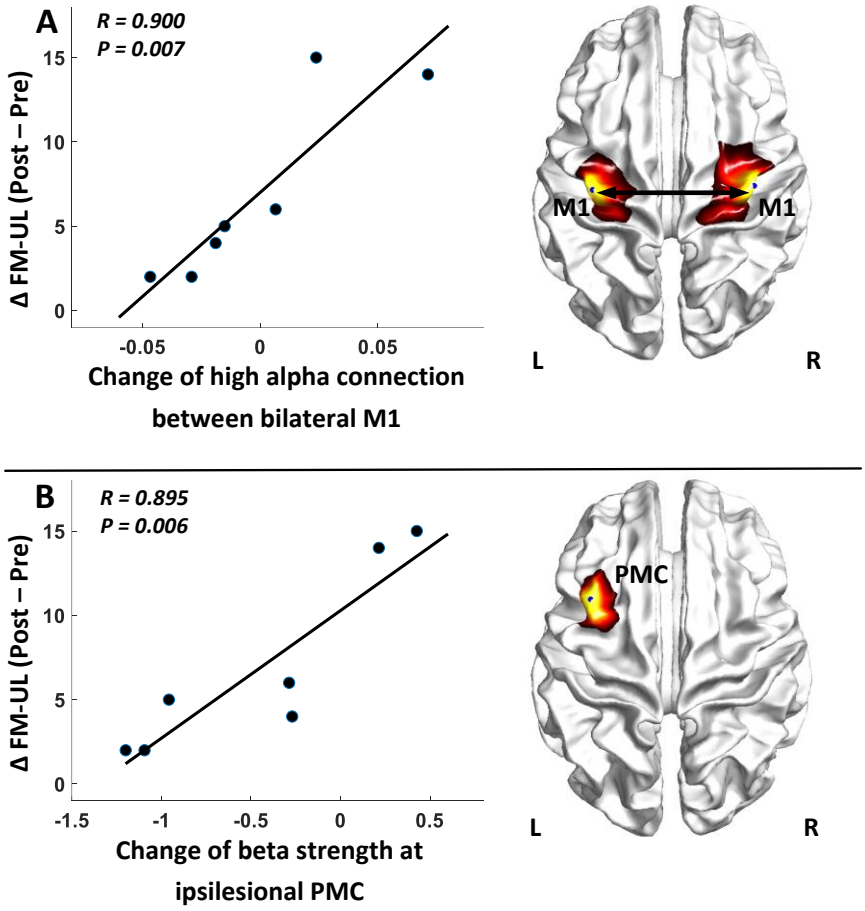

Figure 5-3. Correlation between the motor gains and changes of FC indices (A: change of connectivity between bilateral M1; B: change of the strength at ipsilesional PMC).

5.4.4 Baseline functional connectivity predicts motor improvement after intervention

To assess the feasibility of using FC indices as biomarkers to predict the motor gains after rehabilitation intervention, a linear regression model was fitted to correlate the baseline (pre-intervention) FC indices with the motor gains (ΔFM-UL) after the rehabilitation. The results showed that the higher baseline SMA-M1 connectivity at the affected hemisphere related to the worse motor gains after the training (R = -0.745, p =

0.009, Figure 5-4A), while greater motor gains were also predicted by higher baseline strength of the ipsilesional PMC at low alpha band (R = 0.768, p = 0.007, Figure 5-4B).

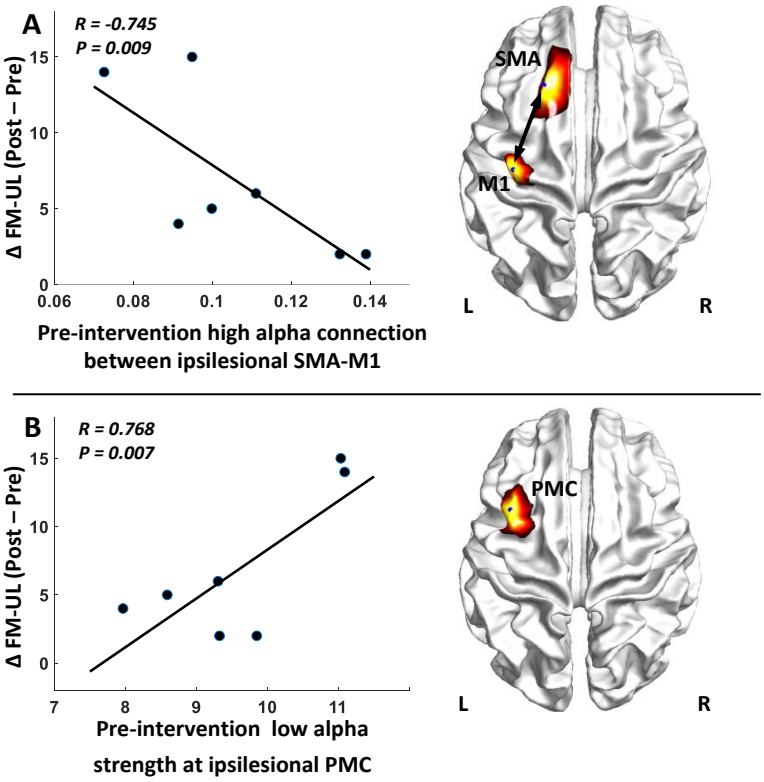

Figure 5-4. Correlation between the motor gains and the baseline (pre-intervention) functional connectivity measures (A: baseline connectivity between ipsilesional SMA-M1; B: baseline strength at ipsilesional PMC).

5.5 Discussion

The assessment and monitoring of motor function after stroke primarily rely on the inspection performed by physicians and therapists, which requires exhaustive testing sessions and introduces subjectivity and variability of the outcome. In addition, routine clinical examination lacks direct evidence that reflects the functional recovery of motor-related regions in the brain. Therefore, it is of great importance to explore useful biomarkers for insightful assessments of changes in brain motor function across a period

of therapy and an effective management of a rehabilitation program. Emerging evidence has suggested that a number of brain FC indices could serve as such potential biomarkers [8, 183, 184, 195]. However, the dominant technique to investigate brain network property, such as fMRI, is subject to multiple limitations, such as rigorous measurement restriction and high cost. While previous studies have demonstrated the feasibility of using surface EEG signal to characterize the alteration of FC following stroke, this approach suffers from the inherent volume conduction problem, making it difficult to localize the regional changes of the motor cortex during rehabilitation intervention. To address this challenge, this study presented an fNIRS-informed EEG source imaging approach to investigate the brain network alterations caused by stroke during a hand clenching task. The findings validated the feasibility of using the novel fNIRS-informed EEG source imaging approach to characterize the altered cortical excitability and connectivity caused by stroke, as well as to derive biomarkers for the assessment and prediction of motor function recovery in post-stroke rehabilitation.

Recent findings have suggested that there is a close association between the cortical excitability and upper extremity function in stroke patients [8, 196]. In the current study, using the cortical activation strength as an excitability measure, the ipsilesional PMC was identified as key region associated with the motor recovery. Specifically, the increment of beta strength at ipsilesional PMC was highly correlated with the motor function improvement across the 4-week intervention ($R = 0.895$, Figure 5-3B). Furthermore, the baseline (pre-intervention) strength of this region at low alpha band was also highly correlated with the motor improvement ($R = 0.768$, Figure 5-4B), accounting for a majority of the rehabilitation outcome after stroke. These results are

consistent with evidences reported in previous studies that better motor recovery is associated with increased task-evoked activation in ipsilesional PMC [197-199]. Similar findings were also reported in recent studies involved in resting state connectivity analysis [8]. Functionally, the role of PMC is critical in motor control and learning as it receives direct inputs from the dorsolateral prefrontal cortex and posterior parietal cortex, processes this information, and projects the output to M1 for movement execution [199]. In particular, emerging evidences have indicated that PMC is a vital part in grasping task, wherein mirror neurons within the PMC may play a potentially significant role in motor learning such as observational learning and imitation learning in our clenching task [200]. Furthermore, the predominant pattern of cortical reorganization following stroke rehabilitation, which mainly involved the increased activation of ipsilesional PMC, is also well-documented in a variety of studies [174, 199]. Taken together, these evidences support the findings in our study that the baseline and the change of activation strength at ipsilesional PMC were highly responsible for the major improvement of motor function across the intervention, demonstrating its important role in the post-stroke motor recovery.

Motor recovery was associated with the cortical reorganization that redistributes regional interactions throughout the whole motor network rather than a single region. Therefore, in this study, in addition to the investigation of the association between cortical excitability and motor function, we also attempted to identify biomarkers associated with cortical connectivity that can be used to characterize motor recovery after stroke. Interestingly, in this study we found that greater motor improvement after the intervention was predicted by lower baseline ipsilesional SMA-M1 connectivity

(Figure 5-4A), which could convey meaningful information. It has been demonstrated that, regardless of cortical or subcortical stroke, motor recovery could manifest brain plasticity at the cortical level, including M1, PMC and SMA [201]. According to previous studies, both M1 and secondary motor areas such as SMA have direct connections to the entire corticospinal tract (CST) that significantly correlated with the motor impairment after stroke [202]. It is possible that such a pathway from SMA to the spinal cord may at least strengthen to the motor recovery during post-stroke training. More specifically, the more disconnected between SMA and M1, the stronger the SMA can be recruited to compensate for the SMA-M1 deficiency. As such, it is possible that, when the functional connection between ipsilesional SMA and M1is heavily affected due to brain lesion, secondary motor areas such as SMA may contribute to post-stroke recovery by a stronger direct projection to the CST and partially taking over the functionality from the ipsilesional area, leading to better recovery of motor function after intervention (Figure 5-4A). However, it remains underdetermined whether the functional connectivity between SMA and CST is s more beneficial to the post-stroke recovery when connection between SMA and M1 is heavily affected after stroke. More evidence should be given to validate this hypothesis and the feasibility of employing such biomarkers to predict the motor recovery outcome before enrolling in an intervention program.

Another finding in the current study was that the change in the bilateral M1 connection at high alpha rhythm was positively correlated with the motor gains across the 4-week intervention (Figure 5-3A). Surprisingly, a larger increment of bilateral M1 connection was significantly associated with greater motor gains, whereas decreased

bilateral M1 connectivity was also correlated with mild motor gains after the intervention (Figure 5-3A). In fact, according to findings in our study and previous studies, the role of this particular connection during post-stroke motor recovery remains unknown. While some studies have found increased functional connectivity between bilateral M1 regions after intervention [184, 203], contradictory or non-significant results were also reported [8]. This discrepancy could be attributed to multiple reasons. For example, the clinical characteristics of patients recruited in these studies may vary sharply in terms of time after stroke-onset, stroke type and severity, which might induce a large variance in the bilateral M1 connectivity results. In addition, the contribution of the contralesional M1 to the motor recovery remains controversial. While activated contralesional M1 was reported to be more evidently correlated with a poorer outcome in the long-term stroke patients [204], recent studies have also argued that increased activation of contralesional M1 after stroke may be beneficial in some aspects of effectively recovered motor behavior [205, 206]. Taken these together, more evidences will be needed to determine the role of bilateral M1 connectivity in assessing the motor function recovery during post-stroke rehabilitation. Beyond this uncertainty of bilateral M1 connectivity, one particularly noteworthy finding in our study is that we were able to identify such discrepancy in explaining the motor recovery outcome (Figure 5-3A), demonstrating the high sensitivity of the proposed brain network analysis strategy and its potential value in investigating the brain plasticity after stroke.

While we found a significant difference in theta strength at the ipsilesional S1 between stroke and healthy group at pre-intervention, there was no significant linear correlation between this FC index and the FM-UL scores of patients (Figure 5-2). In

support of this finding, previous studies have demonstrated that significant FC indices found between healthy and patient groups were not deemed to act as effective biomarkers to characterize the motor function in the patient group [176, 203]. In fact, instead of simply focusing on the difference between healthy and patient groups, biomarkers associated with cortical excitability and connectivity among the patient group are more attractive and are expected to be capable of characterizing the motor recovery pattern of patients during rehabilitation intervention [196, 207]. As such, in current study, we not only presented consistent and strong correlations between the identified FC indices and motor gains (Figure 5-3), but also demonstrated the great potential of these biomarkers in predicting the motor recovery spanning the 4 weeks of intervention (Figure 5-4), which provided reliable and sensitive biomarkers for the investigation of cortical reorganization after stroke.

The current study has some limitations that raise consideration. First, the sample size is relatively small in this study. Also, patients recruited for only two visits may not be sufficient to draw a solid conclusion for a longitudinal study. In addition, the clinical characteristics of patients, such as lesion size, location and stroke subtype, are rather heterogeneous, which could have differential effects on behavioral and neurological outcomes. Finally, the EEG source imaging performed in this study relied on a general brain template, which might induce mild bias when estimating the cortical activity. It is expected that in future work MRI could be used to collect the anatomical information for each subject to optimize the proposed approach.

5.6 Summary

In this chapter we presented a high spatiotemporal fNIRS-informed EEG source imaging framework to characterize the alterations of cortical excitability and function connectivity following stroke. In summary, the results of functional connectivity and graph-based analyses suggested that the bilateral M1 connection and task-evoked strength of ipsilesional PMC have significant potential in assessing the motor recovery outcome across a 4-week intervention. In addition, we also found that the ipsilesional SMA-M1 connection and the task-evoked strength of ipsilesional PMC at the pre-intervention stage, were highly capable of predicting the motor recovery outcome. Therefore, the biomarkers derived from the proposed method may hold great potential in post-stroke rehabilitation assessment and expanding our understanding of cortical reorganization after stroke.

Chapter 6 ─ Conclusions and Suggestions for Future Research

6.1 Summary of this Dissertation

This dissertation provides a grand overview of noninvasive multimodal functional neuroimaging techniques including Electroencephalography (EEG) and functional Near-infrared Spectroscopy (fNIRS), as well as a validation of utilizing the multimodal neuroimaging approach to characterize the cortical reorganization associated with various brain disorders. In Chapter 1, we briefly introduces the basic concepts of the fundamental of two noninvasive brain imaging techniques. We then elaborate the benefit and the theoretical basis of using the multimodal brain imaging technique in comparison with single-modality technique.

The neurovascular coupling of the human brain that stands as the basis of combining EEG-fNIRS are experimentally validated in Chapter 2 and Chapter 3. In particular, Chapter 2 implements an fNIRS-guided EEG channel selection method for enhancing the classification performance of a brain computer interface (BCI) system. This study, from the view of fNIRS-guided analysis, validates our hypothesis that there is certainly complementary information offered by EEG and fNIRS to study the brain activity. Subsequently, Chapter 3 introduces a novel EEG-informed fNIRS analysis to investigate the physiological correlation between the EEG and fNIRS signals. This study, from the view of EEG-guided, experimentally validates the inherent correlation between neuronal activity and hemodynamic response.

Leveraging the high spatial resolution of fNIRS and high temporal resolution of EEG, we then explore feasible approaches to study the human brain dynamics related to

various clinically-seen brain disorders. In Chapter 4, we develop an fNIRS-informed EEG source localization approach to investigate the brain network alterations induced by Alzheimer's disease. In Chapter 5 we also demonstrate how the proposed fNIRS-informed EEG source localization approach can be used to characterize the brain plasticity during longitudinal post-stroke rehabilitation. The obtained results and findings presented in Chapter 4 and 5 further highlight the versatility and usefulness of this powerful multimodal EEG/fNIRS integration method in uncovering the functional activity within the brain.

6.2 Suggestions for Future Research

The underlying network interactions of the brain is of a highly dynamic nature, in both resting state and task-engaging state. While the fNIRS-informed EEG source imaging approach presented in this dissertation allow for the imaging and investigation of cortical activity with good spatiotemporal resolution and accuracy, the brain connectivity analysis is still relying on the static reconstructed source current traces. More specifically, the cortical activity of the brain when engaging in a task is dynamic across the whole task duration and thus requires a more dynamic analysis on the signals. In this dissertation, however, the entire reconstructed time-courses of cortical activity of the brain engaging in a certain cognitive task are utilized for connectivity analysis, which result in a static connectivity map that only represents a single brain network associated with the entire task. Therefore, it is of great importance to look into the dynamic cortical activity during the task by constructing multiple brain networks in a time-varying manner.

Furthermore, apart from the fNIRS-informed EEG source imaging approach presented in this dissertation, there is a critical need to explore the feasibility of using EEG-informed fNIRS analysis to study brain activations related to multiple clinical scenarios. As we presented in Chapter 3, the time-sensitive property of the EEG signal provides rich information for the fNIRS GLM analysis as compared to the traditional block/event-related analysis methods. Specifically, we hypothesize that the EEG-informed fNIRS analysis could be beneficial to the bedside monitoring and localization of seizure by performing a time-varying GLM analysis on a portable EEG/fNIRS multimodal system. Such investigation could offer new options for those applications that are constrained by the limitations of fMRI.

References

[1] S. Herculano-Houzel, "The human brain in numbers: a linearly scaled-up primate brain," *Front Hum Neurosci*, vol. 3, p. 31, 2009.

[2] B. Pakkenberg *et al.*, "Aging and the human neocortex," *Exp Gerontol*, vol. 38, no. 1-2, pp. 95-9, Jan-Feb 2003.

[3] H. Berger, "Über das elektroenkephalogramm des menschen," *Archiv für psychiatrie und nervenkrankheiten*, vol. 87, no. 1, pp. 527-570, 1929.

[4] G. Buzsaki, C. A. Anastassiou, and C. Koch, "The origin of extracellular fields and currents--EEG, ECoG, LFP and spikes," *Nat Rev Neurosci*, vol. 13, no. 6, pp. 407-20, May 18 2012.

[5] D. L. Schomer and F. L. Da Silva, *Niedermeyer's electroencephalography: basic principles, clinical applications, and related fields*. Lippincott Williams & Wilkins, 2012.

[6] M. Brienza and O. Mecarelli, "Neurophysiological Basis of EEG," in *Clinical Electroencephalography*, O. Mecarelli, Ed. Cham: Springer International Publishing, 2019, pp. 9-21.

[7] D. A. Pizzagalli, "Electroencephalography and high-density electrophysiological source localization," *Handbook of psychophysiology*, vol. 3, pp. 56-84, 2007.

[8] J. Wu *et al.*, "Connectivity measures are robust biomarkers of cortical function and plasticity after stroke," (in English), *Brain*, vol. 138, pp. 2359-2369, Aug 1 2015.

[9] F. F. Jobsis, "Noninvasive, Infrared Monitoring of Cerebral and Myocardial Oxygen Sufficiency and Circulatory Parameters," (in English), *Science,* vol. 198, no. 4323, pp. 1264-1267, 1977.

[10] M. Ferrari and V. Quaresima, "A brief review on the history of human functional near-infrared spectroscopy (fNIRS) development and fields of application," (in English), *Neuroimage,* vol. 63, no. 2, pp. 921-935, Nov 1 2012.

[11] H. Ayaz, M. Izzetoglu, K. Izzetoglu, B. Onaral, and B. Ben Dor, "Early diagnosis of traumatic intracranial hematomas," *J Biomed Opt,* vol. 24, no. 5, pp. 1-10, Feb 2019.

[12] F. Scholkmann *et al.*, "A review on continuous wave functional near-infrared spectroscopy and imaging instrumentation and methodology," (in English), *Neuroimage,* vol. 85, pp. 6-27, Jan 15 2014.

[13] V. Quaresima and M. Ferrari, "A Mini-Review on Functional Near-Infrared Spectroscopy (fNIRS): Where Do We Stand, and Where Should We Go?," (in English), *Photonics,* vol. 6, no. 3, Sep 2019.

[14] X. Cui, S. Bray, D. M. Bryant, G. H. Glover, and A. L. Reiss, "A quantitative comparison of NIRS and fMRI across multiple cognitive tasks," (in English), *Neuroimage,* vol. 54, no. 4, pp. 2808-2821, Feb 14 2011.

[15] G. Pfurtscheller and C. Neuper, "Motor imagery and direct brain-computer communication," (in English), *Proceedings of the IEEE,* vol. 89, no. 7, pp. 1123-1134, Jul 2001.

[16] B. He, L. Yang, C. Wilke, and H. Yuan, "Electrophysiological Imaging of Brain Activity and Connectivity-Challenges and Opportunities," (in English), *Ieee*

Transactions on Biomedical Engineering, vol. 58, no. 7, pp. 1918-1931, Jul 2011.

[17] L. F. Nicolas-Alonso and J. Gomez-Gil, "Brain Computer Interfaces, a Review," (in English), *Sensors*, vol. 12, no. 2, pp. 1211-1279, Feb 2012.

[18] S. Waldert, L. Tushaus, C. P. Kaller, A. Aertsen, and C. Mehring, "fNIRS Exhibits Weak Tuning to Hand Movement Direction," (in English), *Plos One*, vol. 7, no. 11, Nov 8 2012.

[19] H. Girouard and C. Iadecola, "Neurovascular coupling in the normal brain and in hypertension, stroke, and Alzheimer disease," *J Appl Physiol (1985)*, vol. 100, no. 1, pp. 328-35, Jan 2006.

[20] J. A. Claassen and R. Zhang, "Cerebral autoregulation in Alzheimer's disease," *J Cereb Blood Flow Metab*, vol. 31, no. 7, pp. 1572-7, Jul 2011.

[21] R. Li, T. Nguyen, T. Potter, and Y. Zhang, "Dynamic cortical connectivity alterations associated with Alzheimer's disease: An EEG and fNIRS integration study," (in English), *Neuroimage-Clinical*, vol. 21, 2019.

[22] M. D'Esposito, L. Y. Deouell, and A. Gazzaley, "Alterations in the BOLD fMRI signal with ageing and disease: a challenge for neuroimaging," *Nat Rev Neurosci*, vol. 4, no. 11, pp. 863-72, Nov 2003.

[23] A. P. Buccino, H. O. Keles, and A. Omurtag, "Hybrid EEG-fNIRS Asynchronous Brain-Computer Interface for Multiple Motor Tasks," (in English), *Plos One*, vol. 11, no. 1, Jan 5 2016.

[24] S. Fazli *et al.*, "Enhanced performance by a hybrid NIRS-EEG brain computer interface," (in English), *Neuroimage*, vol. 59, no. 1, pp. 519-529, Jan 2 2012.

[25] F. Putze *et al.*, "Hybrid fNIRS- EEG based classification of auditory and visual perception processes," (in English), *Frontiers in Neuroscience,* vol. 8, Nov 18 2014.

[26] M. Naito, Y. Michioka, K. Ozawa, Y. Ito, M. Kiguchi, and T. Kanazawa, "A communication means for totally locked-in ALS patients based on changes in cerebral blood volume measured with near-infrared light," (in English), *Ieice Transactions on Information and Systems,* vol. E90d, no. 7, pp. 1028-1037, Jul 2007.

[27] B. Abibullaev and J. An, "Classification of frontal cortex haemodynamic responses during cognitive tasks using wavelet transforms and machine learning algorithms," (in English), *Medical Engineering & Physics,* vol. 34, no. 10, pp. 1394-1410, Dec 2012.

[28] X. X. Yin *et al.*, "A hybrid BCI based on EEG and fNIRS signals improves the performance of decoding motor imagery of both force and speed of hand clenching," (in English), *Journal of Neural Engineering,* vol. 12, no. 3, Jun 2015.

[29] R. Li, T. Potter, W. Huang, and Y. Zhang, "Enhancing Performance of a Hybrid EEG-fNIRS System Using Channel Selection and Early Temporal Features," (in English), *Frontiers in Human Neuroscience,* vol. 11, Sep 15 2017.

[30] M. J. Khan, M. J. Y. Hong, and K. S. Hong, "Decoding of four movement directions using hybrid NIRS-EEG brain-computer interface," (in English), *Frontiers in Human Neuroscience,* vol. 8, Apr 28 2014.

[31] H. D. Nguyen and K. S. Hon, "Bundled-optode implementation for 3D imaging in functional near-infrared spectroscopy," (in English), *Biomedical Optics Express*, vol. 7, no. 9, pp. 3491-3507, Sep 1 2016.

[32] M. J. Khan and K. S. Hong, "Passive BCI based on drowsiness detection: an fNIRS study," (in English), *Biomedical Optics Express*, vol. 6, no. 10, pp. 4063-4078, Oct 1 2015.

[33] H. O. Keles, R. L. Barbour, and A. Omurtag, "Hemodynamic correlates of spontaneous neural activity measured by human whole-head resting state EEG plus fNIRS," (in English), *Neuroimage*, vol. 138, pp. 76-87, Sep 2016.

[34] R. Li, C. Zhao, C. Wang, J. Wang, and Y. Zhang, "Enhancing fNIRS Analysis Using EEG Rhythmic Signatures: an EEG-informed fNIRS Analysis Study," *IEEE Transactions on Biomedical Engineering*, 2020.

[35] A. C. Ehlis, T. M. Ringel, M. M. Plichta, M. M. Richter, M. J. Herrmann, and A. J. Fallgatter, "Cortical correlates of auditory sensory gating: a simultaneous near-infrared spectroscopy event-related potential study," *Neuroscience*, vol. 159, no. 3, pp. 1032-43, Mar 31 2009.

[36] T. Takeda *et al.*, "Influence of Pleasant and Unpleasant Auditory Stimuli on Cerebral Blood Flow and Physiological Changes in Normal Subjects," *Adv Exp Med Biol*, vol. 876, pp. 303-309, 2016.

[37] H. Aghajani, M. Garbey, and A. Omurtag, "Measuring Mental Workload with EEG+fNIRS," *Front Hum Neurosci*, vol. 11, p. 359, 2017.

[38] M. Takeuchi *et al.*, "Brain cortical mapping by simultaneous recording of functional near infrared spectroscopy and electroencephalograms from the

whole brain during right median nerve stimulation," *Brain Topogr,* vol. 22, no. 3, pp. 197-214, Nov 2009.

[39] R. J. Cooper *et al.,* "Transient haemodynamic events in neurologically compromised infants: a simultaneous EEG and diffuse optical imaging study," *Neuroimage,* vol. 55, no. 4, pp. 1610-6, Apr 15 2011.

[40] F. Zennifa, J. Ide, Y. Noguchi, and K. Iramina, "Monitoring of cognitive state on mental retardation child using EEG, ECG and NIRS in four years study," in *2015 37th Annual International Conference of the IEEE Engineering in Medicine and Biology Society (EMBC)*, 2015, pp. 6610-6613: IEEE.

[41] A.-M. Marx *et al.,* "Near-infrared spectroscopy (NIRS) neurofeedback as a treatment for children with attention deficit hyperactivity disorder (ADHD)—a pilot study," *Frontiers in human neuroscience,* vol. 8, p. 1038, 2015.

[42] U. Chaudhary, N. Birbaumer, and M. R. Curado, "Brain-machine interface (BMI) in paralysis," *Ann Phys Rehabil Med,* vol. 58, no. 1, pp. 9-13, Feb 2015.

[43] T. Onitsuka, N. Oribe, and S. Kanba, "Neurophysiological findings in patients with bipolar disorder," *Suppl Clin Neurophysiol,* vol. 62, pp. 197-206, 2013.

[44] S. Schneider, L. Wagels, F. B. Haeussinger, A. J. Fallgatter, A. C. Ehlis, and A. M. Rapp, "Haemodynamic and electrophysiological markers of pragmatic language comprehension in schizophrenia," *World J Biol Psychiatry,* vol. 16, no. 6, pp. 398-410, Sep 2015.

[45] A. Mori, M. Iwadate, N. T. Minakawa, and S. Kawashima, "Game addiction," *Nihon Rinsho,* vol. 73, no. 9, pp. 1567-73, Sep 2015.

[46] J. R. Wolpaw, N. Birbaumer, D. J. McFarland, G. Pfurtscheller, and T. M. Vaughan, "Brain-computer interfaces for communication and control," (in English), *Clinical Neurophysiology,* vol. 113, no. 6, pp. 767-791, Jun 2002, Art. no. 1.

[47] B. Blankertz, G. Dornhege, M. Krauledat, K. R. Muller, and G. Curio, "The non-invasive Berlin Brain-Computer Interface: Fast acquisition of effective performance in untrained subjects," (in English), *Neuroimage,* vol. 37, no. 2, pp. 539-550, Aug 15 2007.

[48] P. Brunner, A. L. Ritaccio, J. F. Emrich, H. Bischof, and G. Schalk, "Rapid communication with a "P300" matrix speller using electrocorticographic signals (ECoG)," (in English), *Frontiers in Neuroscience,* vol. 5, 2011.

[49] K. J. Miller, G. Schalk, E. E. Fetz, M. den Nijs, J. G. Ojemann, and R. P. N. Rao, "Cortical activity during motor execution, motor imagery, and imagery-based online feedback " (in English), *Proceedings of the National Academy of Sciences of the United States of America,* vol. 107, no. 15, pp. 7113-7113, Apr 13 2010.

[50] K. Choi, "Electroencephalography (EEG)-based neurofeedback training for brain-computer interface (BCI)," (in English), *Experimental Brain Research,* vol. 231, no. 3, pp. 351-365, Nov 2013.

[51] I. Rejer, "Genetic algorithm with aggressive mutation for feature selection in BCI feature space," (in English), *Pattern Analysis and Applications,* vol. 18, no. 3, pp. 485-492, Aug 2015.

[52] M. Salvaris and F. Sepulveda, "Classification effects of real and imaginary movement selective attention tasks on a P300-based brain-computer interface," (in English), *Journal of Neural Engineering,* vol. 7, no. 5, Oct 2010.

[53] N. Naseer, F. M. Noori, N. K. Qureshi, and K. S. Hong, "Determining Optimal Feature-Combination for LDA Classification of Functional Near-Infrared Spectroscopy Signals in Brain-Computer Interface Application," (in English), *Frontiers in Human Neuroscience,* vol. 10, May 25 2016.

[54] S. M. Coyle, T. E. Ward, and C. M. Markham, "Brain-computer interface using a simplified functional near-infrared spectroscopy system," (in English), *Journal of Neural Engineering,* vol. 4, no. 3, pp. 219-226, Sep 2007.

[55] S. Coyle, T. Ward, C. Markham, and G. McDarby, "On the suitability of near-infrared (NIR) systems for next-generation brain-computer interfaces," (in English), *Physiological Measurement,* vol. 25, no. 4, pp. 815-822, Aug 2004.

[56] B. Sorger *et al.*, "Another kind of 'BOLD Response': answering multiple-choice questions via online decoded single-trial brain signals," (in English), *Coma Science: Clinical and Ethical Implications,* vol. 177, pp. 275-292, 2009.

[57] J. H. Lee, J. Ryu, F. A. Jolesz, Z. H. Cho, and S. S. Yoo, "Brain-machine interface via real-time fMRI: Preliminary study on thought-controlled robotic arm," (in English), *Neuroscience Letters,* vol. 450, no. 1, pp. 1-6, Jan 23 2009.

[58] S. Waldert *et al.*, "Hand movement direction decoded from MEG and EEG," (in English), *Journal of Neuroscience,* vol. 28, no. 4, pp. 1000-1008, Jan 23 2008.

[59] M. J. Khan and K. S. Hong, "Hybrid EEG-fNIRS-Based Eight-Command Decoding for BCI: Application to Quadcopter Control," (in English), *Frontiers in Neurorobotics*, vol. 11, Feb 17 2017.

[60] J. Lin and C. Hsieh, "A Wireless BCI-Controlled Integration System in Smart Living Space for Patients," (in English), *Wireless Personal Communications*, vol. 88, no. 2, pp. 395-412, May 2016.

[61] A. von Luhmann, C. Herff, D. Heger, and T. Schultz, "Toward a Wireless Open Source Instrument: Functional Near-infrared Spectroscopy in Mobile Neuroergonomics and BCI Applications," (in English), *Frontiers in Human Neuroscience*, vol. 9, Nov 12 2015.

[62] N. Naseer and K. S. Hong, "fNIRS-based brain-computer interfaces: a review," (in English), *Frontiers in Human Neuroscience,* vol. 9, Jan 28 2015.

[63] J. Shin, K. R. Muller, C. H. Schmitz, D. W. Kim, and H. J. Hwang, "Evaluation of a Compact Hybrid Brain-Computer Interface System," (in English), *Biomed Research International,* 2017.

[64] A. Zafar and K. S. Hong, "Detection and classification of three-class initial dips from prefrontal cortex," (in English), *Biomedical Optics Express*, vol. 8, no. 1, pp. 367-383, Jan 1 2017.

[65] Z. Li, Y. Wang, W. Quan, T. Wu, and B. Lv, "Evaluation of different classification methods for the diagnosis of schizophrenia based on functional near-infrared spectroscopy," (in English), *Journal of Neuroscience Methods*, vol. 241, pp. 101-110, Feb 15 2015.

[66] B. Blankertz, R. Tomioka, S. Lemm, M. Kawanabe, and K. R. Muller, "Optimizing spatial filters for robust EEG single-trial analysis," (in English), *Ieee Signal Processing Magazine*, vol. 25, no. 1, pp. 41-56, Jan 2008.

[67] F. Al-Shargie, M. Kiguchi, N. Badruddin, S. C. Dass, A. F. M. Hani, and T. B. Tang, "Mental stress assessment using simultaneous measurement of EEG and fNIRS," (in English), *Biomedical Optics Express*, vol. 7, no. 10, pp. 3882-3898, Oct 1 2016.

[68] M. Mihara and I. Miyai, "Review of functional near-infrared spectroscopy in neurorehabilitation," (in English), *Neurophotonics*, vol. 3, no. 3, Jul-Sep 2016.

[69] Y. Zhang, D. H. Brooks, M. A. Franceschini, and D. A. Boas, "Eigenvector-based spatial filtering for reduction of physiological interference in diffuse optical imaging," (in English), *Journal of Biomedical Optics*, vol. 10, no. 1, Jan-Feb 2005.

[70] F. Scholkmann, S. Spichtig, T. Muehlemann, and M. Wolf, "How to detect and reduce movement artifacts in near-infrared imaging using moving standard deviation and spline interpolation," (in English), *Physiological Measurement*, vol. 31, no. 5, pp. 649-662, May 2010.

[71] W. D. Penny, K. J. Friston, J. T. Ashburner, S. J. Kiebel, and T. E. Nichols, *Statistical parametric mapping: the analysis of functional brain images*. Academic press, 2011.

[72] L. Holper, M. Biallas, and M. Wolf, "Task complexity relates to activation of cortical motor areas during uni- and bimanual performance: A functional NIRS study," (in English), *Neuroimage*, vol. 46, no. 4, pp. 1105-1113, Jul 15 2009.

[73] V. J. Samar, A. Bopardikar, R. Rao, and K. Swartz, "Wavelet analysis of neuroelectric waveforms: A conceptual tutorial," (in English), *Brain and Language,* vol. 66, no. 1, pp. 7-60, Jan 1999.

[74] A. Subasi, "EEG signal classification using wavelet feature extraction and a mixture of expert model," (in English), *Expert Systems with Applications,* vol. 32, no. 4, pp. 1084-1093, May 2007.

[75] R. D. Frostig, E. E. Lieke, D. Y. Tso, and A. Grinvald, "Cortical Functional Architecture and Local Coupling between Neuronal-Activity and the Microcirculation Revealed by Invivo High-Resolution Optical Imaging of Intrinsic Signals," (in English), *Proceedings of the National Academy of Sciences of the United States of America,* vol. 87, no. 16, pp. 6082-6086, Aug 1990.

[76] A. Zafar, K. S. Hong, and M. J. Khan, "Initial dip detection based on both HbO and HbR vector-based phase analysis," (in English), *2016 55th Annual Conference of the Society of Instrument and Control Engineers of Japan (Sice),* pp. 543-548, 2016.

[77] H. Drucker, C. J. C. Burges, L. Kaufman, A. Smola, and V. Vapnik, "Support vector regression machines," (in English), *Advances in Neural Information Processing Systems 9,* vol. 9, pp. 155-161, 1997.

[78] C. C. Chang and C. J. Lin, "LIBSVM: A Library for Support Vector Machines," (in English), *Acm Transactions on Intelligent Systems and Technology,* vol. 2, no. 3, 2011.

[79] S. Strand, "100 statistical tests (3rd edition)," (in English), *British Educational Research Journal,* vol. 34, no. 1, pp. 148-150, 2008.

[80] K. S. Hong and H. Santosa, "Decoding four different sound-categories in the auditory cortex using functional near-infrared spectroscopy," (in English), *Hearing Research,* vol. 333, pp. 157-166, Mar 2016.

[81] H. Girouard and C. Iadecola, "Neurovascular coupling in the normal brain and in hypertension, stroke, and Alzheimer disease," (in English), *Journal of Applied Physiology,* vol. 100, no. 1, pp. 328-335, Jan 2006.

[82] M. T. Talukdar, H. R. Frost, and S. G. Diamond, "Modeling Neurovascular Coupling from Clustered Parameter Sets for Multimodal EEG-NIRS," (in English), *Computational and Mathematical Methods in Medicine,* 2015.

[83] S. Debener, M. Ullsperger, M. Siegel, and A. K. Engel, "Single-trial EEG-fMRI reveals the dynamics of cognitive function," (in English), *Trends in Cognitive Sciences,* vol. 10, no. 12, pp. 558-563, Dec 2006.

[84] B. He, A. Sohrabpour, E. Brown, and Z. M. Liu, "Electrophysiological Source Imaging: A Noninvasive Window to Brain Dynamics," (in English), *Annual Review of Biomedical Engineering, Vol 20,* vol. 20, pp. 171-196, 2018.

[85] G. Pfurtscheller and F. H. L. da Silva, "Event-related EEG/MEG synchronization and desynchronization: basic principles," (in English), *Clinical Neurophysiology,* vol. 110, no. 11, pp. 1842-1857, Nov 1999.

[86] N. K. Logothetis, "The underpinnings of the BOLD functional magnetic resonance imaging signal," (in English), *Journal of Neuroscience,* vol. 23, no. 10, pp. 3963-3971, May 15 2003.

[87] M. Belanger, I. Allaman, and P. J. Magistretti, "Brain Energy Metabolism: Focus on Astrocyte-Neuron Metabolic Cooperation," (in English), *Cell Metabolism,* vol. 14, no. 6, pp. 724-738, Dec 7 2011.

[88] R. Scheeringa *et al.*, "Neuronal Dynamics Underlying High- and Low-Frequency EEG Oscillations Contribute Independently to the Human BOLD Signal," (in English), *Neuron,* vol. 69, no. 3, pp. 572-583, Feb 10 2011.

[89] R. Sclocco *et al.*, "EEG-informed fMRI analysis during a hand grip task: estimating the relationship between EEG rhythms and the BOLD signal," (in English), *Frontiers in Human Neuroscience,* vol. 8, Apr 1 2014.

[90] T. Nguyen, T. Potter, T. Nguyen, C. Karmonik, R. Grossman, and Y. Zhang, "EEG Source Imaging Guided by Spatiotemporal Specific fMRI: Toward an Understanding of Dynamic Cognitive Processes," (in English), *Neural Plasticity*, 2016.

[91] D. A. Boas, C. E. Elwell, M. Ferrari, and G. Taga, "Twenty years of functional near-infrared spectroscopy: introduction for the special issue," (in English), *Neuroimage,* vol. 85, pp. 1-5, Jan 15 2014.

[92] R. Li *et al.*, "Cortical Hemodynamic Response and Connectivity Modulated by Sub-threshold High-Frequency Repetitive Transcranial Magnetic Stimulation," (in English), *Frontiers in Human Neuroscience,* vol. 13, Mar 19 2019.

[93] L. Duan, Y. J. Zhang, and C. Z. Zhu, "Quantitative comparison of resting-state functional connectivity derived from fNIRS and fMRI: A simultaneous recording study," (in English), *Neuroimage,* vol. 60, no. 4, pp. 2008-2018, May 1 2012.

[94] T. Huppert, J. Barker, B. Schmidt, S. Walls, and A. Ghuman, "Comparison of group-level, source localized activity for simultaneous functional near-infrared spectroscopy-magnetoencephalography and simultaneous fNIRS-fMRI during parametric median nerve stimulation," (in English), *Neurophotonics,* vol. 4, no. 1, Jan 2017.

[95] F. Herold, P. Wiegel, F. Scholkmann, A. Thiers, D. Hamacher, and L. Schega, "Functional near-infrared spectroscopy in movement science: a systematic review on cortical activity in postural and walking tasks," (in English), *Neurophotonics,* vol. 4, no. 4, Oct-Dec 2017.

[96] V. Quaresima and M. Ferrari, "Functional Near-Infrared Spectroscopy (fNIRS) for Assessing Cerebral Cortex Function During Human Behavior in Natural/Social Situations: A Concise Review," (in English), *Organizational Research Methods,* vol. 22, no. 1, pp. 46-68, Jan 2019.

[97] P. Lachert, D. Janusek, P. Pulawski, A. Liebert, D. Milej, and K. J. Blinowska, "Coupling of Oxy- and Deoxyhemoglobin concentrations with EEG rhythms during motor task," (in English), *Scientific Reports,* vol. 7, Nov 13 2017.

[98] R. Li, T. Nguyen, T. Potter, and Y. Zhang, "Dynamic cortical connectivity alterations associated with Alzheimer's disease: An EEG and fNIRS integration study," *NeuroImage: Clinical,* p. 101622, 2018.

[99] P. Croce, F. Zappasodi, A. Merla, and A. M. Chiarelli, "Exploiting neurovascular coupling: a Bayesian sequential Monte Carlo approach applied to simulated EEG fNIRS data," (in English), *Journal of Neural Engineering,* vol. 14, no. 4, Aug 2017.

[100] M. J. Khan, U. Ghafoor, and K. S. Hong, "Early Detection of Hemodynamic Responses Using EEG: A Hybrid EEG-fNIRS Study," (in English), *Frontiers in Human Neuroscience*, vol. 12, Nov 29 2018.

[101] C. Zich, S. Debener, A. K. Thoene, L. C. Chen, and C. Kranczioch, "Simultaneous EEG-fNIRS reveals how age and feedback affect motor imagery signatures," (in English), *Neurobiology of Aging*, vol. 49, pp. 183-197, Jan 2017.

[102] G. Pfurtscheller, I. Daly, G. Bauernfeind, and G. R. Muller-Putz, "Coupling between Intrinsic Prefrontal HbO2 and Central EEG Beta Power Oscillations in the Resting Brain," (in English), *Plos One*, vol. 7, no. 8, Aug 24 2012.

[103] L. Chen, P. Sandmann, J. Thorne, C. Herrmann, and S. Debener, "Association of Concurrent fNIRS and EEG Signatures in Response to Auditory and Visual Stimuli," (in English), *Brain Topography*, vol. 28, no. 5, pp. 710-725, Sep 2015.

[104] J. Chul, S. Tak, K. E. Jang, J. Jung, and J. Jang, "NIRS-SPM: Statistical parametric mapping for near-infrared spectroscopy," (in English), *Neuroimage*, vol. 44, no. 2, pp. 428-447, Jan 15 2009.

[105] K. J. Friston, A. P. Holmes, K. J. Worsley, J. P. Poline, C. D. Frith, and R. S. Frackowiak, "Statistical parametric maps in functional imaging: a general linear approach," *Human brain mapping*, vol. 2, no. 4, pp. 189-210, 1994.

[106] M. Okamoto *et al.*, "Three-dimensional probabilistic anatomical cranio-cerebral correlation via the international 10-20 system oriented for transcranial functional brain mapping," (in English), *Neuroimage*, vol. 21, no. 1, pp. 99-111, Jan 2004.

[107] B. Fischl *et al.*, "Automatically parcellating the human cerebral cortex," (in English), *Cerebral Cortex*, vol. 14, no. 1, pp. 11-22, Jan 2004.

[108] F. Matthews, B. A. Pearlmutter, T. E. Ward, C. Soraghan, and C. Markham, "Hemodynamics for braincomputer interfaces," (in English), *IEEE Signal Processing Magazine,* vol. 25, no. 1, pp. 87-94, Jan 2008.

[109] S. Tak and J. C. Ye, "Statistical analysis of fNIRS data: A comprehensive review," (in English), *Neuroimage,* vol. 85, pp. 72-91, Jan 15 2014.

[110] S. G. Diamond *et al.*, "Dynamic physiological modeling for functional diffuse optical tomography," (in English), *Neuroimage,* vol. 30, no. 1, pp. 88-101, Mar 2006.

[111] J. W. Barker, A. Aarabi, and T. J. Huppert, "Autoregressive model based algorithm for correcting motion and serially correlated errors in fNIRS," (in English), *Biomedical Optics Express,* vol. 4, no. 8, pp. 1366-1379, Aug 1 2013.

[112] H. Santosa, X. T. Zhai, F. Fishburn, and T. Huppert, "The NIRS Brain AnalyzIR Toolbox," (in English), *Algorithms,* vol. 11, no. 5, May 2018.

[113] R. Caldara, M. P. Deiber, C. Andrey, C. Michel, G. Thut, and C. A. Hauert, "Actual and mental motor preparation and execution: a spatiotemporal ERP study," (in English), *Experimental Brain Research,* vol. 159, no. 3, pp. 389-399, Dec 2004.

[114] J. W. Barker, A. L. Rosso, P. J. Sparto, and T. J. Huppert, "Correction of motion artifacts and serial correlations for real-time functional near-infrared spectroscopy," (in English), *Neurophotonics,* vol. 3, no. 3, Jul-Sep 2016.

[115] J. A. Hanley and B. J. Mcneil, "A Method of Comparing the Areas under Receiver Operating Characteristic Curves Derived from the Same Cases," (in English), *Radiology,* vol. 148, no. 3, pp. 839-843, 1983.

[116] C. Neuper, M. Wortz, and G. Pfurtscheller, "ERD/ERS patterns reflecting sensorimotor activation and deactivation," (in English), *Event-Related Dynamics of Brain Oscillations,* vol. 159, pp. 211-222, 2006.

[117] K. Nakayashiki, M. Saeki, Y. Takata, Y. Hayashi, and T. Kondo, "Modulation of event-related desynchronization during kinematic and kinetic hand movements," (in English), *Journal of Neuroengineering and Rehabilitation,* vol. 11, May 30 2014.

[118] R. C. Mesquita, M. A. Franceschini, and D. A. Boas, "Resting state functional connectivity of the whole head with near-infrared spectroscopy," (in English), *Biomedical Optics Express,* vol. 1, no. 1, pp. 324-336, Aug 2 2010.

[119] P. Pouliot *et al.*, "Hemodynamic changes during posterior epilepsies: An EEG-fNIRS study," (in English), *Epilepsy Research,* vol. 108, no. 5, pp. 883-890, Jul 2014.

[120] I. Tachtsidis and F. Scholkmann, "False positives and false negatives in functional near-infrared spectroscopy: issues, challenges, and the way forward," (in English), *Neurophotonics,* vol. 3, no. 3, Jul-Sep 2016.

[121] L. Gagnon, M. A. Yuecel, D. A. Boas, and R. J. Cooper, "Further improvement in reducing superficial contamination in NIRS using double short separation measurements," (in English), *Neuroimage,* vol. 85, pp. 127-135, Jan 15 2014.

[122] L. Jancke, K. Lutz, and S. Koeneke, "Converging evidence of ERD/ERS and BOLD responses in motor control research," (in English), *Event-Related Dynamics of Brain Oscillations,* vol. 159, pp. 261-271, 2006.

[123] A. Kumar, A. Singh, and Ekavali, "A review on Alzheimer's disease pathophysiology and its management: an update," (in English), *Pharmacological Reports,* vol. 67, no. 2, pp. 195-203, Apr 2015.

[124] A. s. Association, "2018 Alzheimer's disease facts and figures," *Alzheimer's & Dementia,* vol. 14, no. 3, pp. 367-429, 2018.

[125] S. Palmqvist *et al.*, "Detailed comparison of amyloid PET and CSF biomarkers for identifying early Alzheimer disease," (in English), *Neurology,* vol. 85, no. 14, pp. 1240-1249, Oct 6 2015.

[126] A. D. Cohen and W. E. Klunk, "Early detection of Alzheimer's disease using PiB and FDG PET," (in English), *Neurobiology of Disease,* vol. 72, pp. 117-122, Dec 2014.

[127] L. Canuet *et al.*, "Resting-State Network Disruption and APOE Genotype in Alzheimer's Disease: A lagged Functional Connectivity Study," (in English), *Plos One,* vol. 7, no. 9, Sep 25 2012.

[128] A. Kabbara, H. Eid, W. El Falou, M. Khalil, F. Wendling, and M. Hassan, "Reduced integration and improved segregation of functional brain networks in Alzheimer's disease," (in English), *Journal of Neural Engineering,* vol. 15, no. 2, Apr 2018.

[129] F. Vecchio *et al.*, "Human Brain Networks in Cognitive Decline: A Graph Theoretical Analysis of Cortical Connectivity from EEG Data," (in English), *Journal of Alzheimers Disease,* vol. 41, no. 1, pp. 113-127, 2014.

[130] M. Hata *et al.*, "Functional connectivity assessed by resting state EEG correlates with cognitive decline of Alzheimer's disease - An eLORETA study," (in English), *Clinical Neurophysiology,* vol. 127, no. 2, pp. 1269-1278, Feb 2016.

[131] M. S. Hamalainen and R. J. Ilmoniemi, "Interpreting Magnetic-Fields of the Brain - Minimum Norm Estimates," (in English), *Medical & Biological Engineering & Computing,* vol. 32, no. 1, pp. 35-42, Jan 1994.

[132] C. Phillips, M. D. Rugg, and K. J. Friston, "Anatomically informed basis functions for EEG source localization: Combining functional and anatomical constraints," (in English), *Neuroimage,* vol. 16, no. 3, pp. 678-695, Jul 2002.

[133] D. M. Schmidt, J. S. George, and C. C. Wood, "Bayesian inference applied to the electromagnetic inverse problem," (in English), *Human Brain Mapping,* vol. 7, no. 3, pp. 195-212, 1999.

[134] S. Kajihara, Y. Ohtani, N. Goda, M. Tanigawa, Y. Ejima, and K. Toyama, "Wiener filter-magnetoencephalography of visual cortical activity," (in English), *Brain Topography,* vol. 17, no. 1, pp. 13-25, Fal 2004.

[135] A. M. Dale *et al.*, "Dynamic statistical parametric mapping: Combining fMRI and MEG for high-resolution imaging of cortical activity," (in English), *Neuron,* vol. 26, no. 1, pp. 55-67, Apr 2000.

[136] Z. Liu, L. Ding, and B. He, "Integration of EEG/MEG with MRI and fMRI - High-resolution, multimodal neuroimaging," (in English), *IEEE Engineering in Medicine and Biology Magazine,* vol. 25, no. 4, pp. 46-53, Jul-Aug 2006.

[137] F. Babiloni *et al.*, "Linear inverse source estimate of combined EEG and MEG data related to voluntary movements," (in English), *Human Brain Mapping,* vol. 14, no. 4, pp. 197-209, Dec 2001.

[138] A. Liu, J. W. Belliveau, and A. M. Dale, "Spatiotemporal imaging of human brain activity using functional MRI constrained magnetoencephalography data: Monte Carlo simulations," (in English), *Proceedings of the National Academy of Sciences of the United States of America,* vol. 95, no. 15, pp. 8945-8950, Jul 21 1998.

[139] M. H. Lee, C. D. Smyser, and J. S. Shimony, "Resting-State fMRI: A Review of Methods and Clinical Applications," (in English), *American Journal of Neuroradiology,* vol. 34, no. 10, pp. 1866-1872, Oct 2013.

[140] T. Aihara *et al.*, "Cortical current source estimation from electroencephalography in combination with near-infrared spectroscopy as a hierarchical prior," (in English), *Neuroimage,* vol. 59, no. 4, pp. 4006-4021, Feb 15 2012.

[141] M. F. Folstein, S. E. Folstein, and P. R. McHugh, ""Mini-mental state". A practical method for grading the cognitive state of patients for the clinician," *J Psychiatr Res,* vol. 12, no. 3, pp. 189-98, Nov 1975.

[142] K. NAz and H. Epps, "Relationship between color and emotion: A study of college students," *College Student J,* vol. 38, no. 3, p. 396, 2004.

[143] J. A. Uriguen and B. Garcia-Zapirain, "EEG artifact removal-state-of-the-art and guidelines," (in English), *Journal of Neural Engineering,* vol. 12, no. 3, Jun 2015.

[144] A. Gramfort *et al.*, "MNE software for processing MEG and EEG data," (in English), *Neuroimage,* vol. 86, pp. 446-460, Feb 1 2014.

[145] V. D. Calhoun, T. Adali, V. B. McGinty, J. J. Pekar, T. D. Watson, and G. D. Pearlson, "fMRI activation in a visual-perception task: network of areas detected using the general linear model and independent components analysis," *Neuroimage,* vol. 14, no. 5, pp. 1080-8, Nov 2001.

[146] J. B. Poline and M. Brett, "The general linear model and fMRI: does love last forever?," *Neuroimage,* vol. 62, no. 2, pp. 871-80, Aug 15 2012.

[147] K. J. Worsley *et al.*, "A general statistical analysis for fMRI data," *Neuroimage,* vol. 15, no. 1, pp. 1-15, Jan 2002.

[148] C. W. Woo, A. Krishnan, and T. D. Wager, "Cluster-extent based thresholding in fMRI analyses: pitfalls and recommendations," *Neuroimage,* vol. 91, pp. 412-9, May 1 2014.

[149] A. Pothen and C.-J. Fan, "Computing the block triangular form of a sparse matrix," *ACM Trans. Math. Softw.*, vol. 16, no. 4, pp. 303-324, 1990.

[150] P. C. Hansen, "Analysis of Discrete Ill-Posed Problems by Means of the L-Curve," (in English), *Siam Review,* vol. 34, no. 4, pp. 561-580, Dec 1992.

[151] C. J. Stam, G. Nolte, and A. Daffertshofer, "Phase lag index: assessment of functional connectivity from multi channel EEG and MEG with diminished bias from common sources," (in eng), *Hum Brain Mapp,* vol. 28, no. 11, pp. 1178-93, Nov 2007.

[152] M. Vinck, R. Oostenveld, M. van Wingerden, F. Battaglia, and C. M. A. Pennartz, "An improved index of phase-synchronization for

electrophysiological data in the presence of volume-conduction, noise and sample-size bias," *NeuroImage,* vol. 55, no. 4, pp. 1548-1565, 2011/04/15/ 2011.

[153] F. Hatz, M. Hardmeier, H. Bousleiman, S. Ruegg, C. Schindler, and P. Fuhr, "Reliability of fully automated versus visually controlled pre- and post-processing of resting-state EEG," (in English), *Clinical Neurophysiology,* vol. 126, no. 2, pp. 268-274, Feb 2015.

[154] M. Rubinov and O. Sporns, "Complex network measures of brain connectivity: Uses and interpretations," (in English), *Neuroimage,* vol. 52, no. 3, pp. 1059-1069, Sep 2010.

[155] K. R. Daffner, D. M. Rentz, L. F. M. Scinto, R. Faust, A. E. Budson, and P. J. Holcomb, "Pathophysiology underlying diminished attention to novel events in patients with early AD," (in English), *Neurology,* vol. 56, no. 10, pp. 1377-1383, May 22 2001.

[156] H. Saito *et al.*, "Visual event-related potential in mild dementia of the Alzheimer's type," (in English), *Psychiatry and Clinical Neurosciences,* vol. 55, no. 4, pp. 365-371, Aug 2001.

[157] X. W. Sun *et al.*, "Age-dependent brain activation during forward and backward digit recall revealed by fMRI," (in English), *Neuroimage,* vol. 26, no. 1, pp. 36-47, May 15 2005.

[158] F. Tian, A. Yennu, A. Smith-Osborne, F. Gonzalez-Lima, C. S. North, and H. Liu, "Prefrontal responses to digit span memory phases in patients with post-

traumatic stress disorder (PTSD): A functional near infrared spectroscopy study," (in English), *Neuroimage-Clinical,* vol. 4, pp. 808-819, 2014.

[159] C. Babiloni *et al.*, "Hippocampal volume and cortical sources of EEG alpha rhythms in mild cognitive impairment and Alzheimer disease," (in English), *Neuroimage,* vol. 44, no. 1, pp. 123-135, Jan 1 2009.

[160] D. H. Salat, J. A. Kaye, and J. S. Janowsky, "Selective preservation and degeneration within the prefrontal cortex in aging and Alzheimer disease," (in English), *Archives of Neurology,* vol. 58, no. 9, pp. 1403-1408, Sep 2001.

[161] S. C. Johnson *et al.*, "The relationship between fMRI activation and cerebral atrophy: Comparison of normal aging and Alzheimer disease," (in English), *Neuroimage,* vol. 11, no. 3, pp. 179-187, Mar 2000.

[162] E. J. Sanz-Arigita *et al.*, "Loss of 'Small-World' Networks in Alzheimer's Disease: Graph Analysis of fMRI Resting-State Functional Connectivity," *PLOS ONE,* vol. 5, no. 11, p. e13788, 2010.

[163] P. J. Visser, F. R. J. Verhey, P. A. M. Hofman, P. Scheltens, and J. Jolles, "Medial temporal lobe atrophy predicts Alzheimer's disease in patients with minor cognitive impairment," (in English), *Journal of Neurology Neurosurgery and Psychiatry,* vol. 72, no. 4, pp. 491-497, Apr 2002.

[164] V. Jelic *et al.*, "Quantitative electroencephalography in mild cognitive impairment: longitudinal changes and possible prediction of Alzheimer's disease," (in English), *Neurobiology of Aging,* vol. 21, no. 4, pp. 533-540, Jul-Aug 2000.

[165] L. Pini *et al.*, "Brain atrophy in Alzheimer's Disease and aging," (in English), *Ageing Research Reviews,* vol. 30, pp. 25-48, Sep 2016.

[166] D. J. Watts and S. H. Strogatz, "Collective dynamics of 'small-world' networks," (in English), *Nature,* vol. 393, no. 6684, pp. 440-442, Jun 4 1998.

[167] D. S. Bassett and E. T. Bullmore, "Small-world brain networks," (in English), *Neuroscientist,* vol. 12, no. 6, pp. 512-523, Dec 2006.

[168] D. S. Bassett and E. T. Bullmore, "Small-World Brain Networks Revisited," (in English), *Neuroscientist,* vol. 23, no. 5, pp. 499-516, Oct 2017.

[169] P. J. Toussaint *et al.*, "Characteristics of the default mode functional connectivity in normal ageing and Alzheimer's disease using resting state fMRI with a combined approach of entropy-based and graph theoretical measurements," (in English), *Neuroimage,* vol. 101, pp. 778-786, Nov 1 2014.

[170] Z. Q. Wang, M. Zhang, Y. Han, H. Q. Song, R. J. Guo, and K. C. Li, "Differentially disrupted functional connectivity of the subregions of the amygdala in Alzheimer's disease," (in English), *Journal of X-Ray Science and Technology,* vol. 24, no. 2, pp. 329-342, 2016.

[171] M. M. A. Engels, C. J. Stam, W. M. van der Flier, P. Scheltens, H. de Waal, and E. C. W. van Straaten, "Declining functional connectivity and changing hub locations in Alzheimer's disease: an EEG study," (in English), *Bmc Neurology,* vol. 15, Aug 20 2015.

[172] C. J. Stam *et al.*, "Graph theoretical analysis of magnetoencephalographic functional connectivity in Alzheimers disease," (in English), *Brain,* vol. 132, pp. 213-224, Jan 2009.

[173] O. Adeoye *et al.*, "Recommendations for the Establishment of Stroke Systems of Care: A 2019 Update A Policy Statement From the American Stroke Association," (in English), *Stroke,* vol. 50, no. 7, pp. E187-E210, Jul 2019.

[174] R. Teasell, N. A. Bayona, and J. Bitensky, "Plasticity and reorganization of the brain post stroke," *Top Stroke Rehabil,* vol. 12, no. 3, pp. 11-26, Summer 2005.

[175] C. Grefkes and G. R. Fink, "Reorganization of cerebral networks after stroke: new insights from neuroimaging with connectivity approaches," (in English), *Brain,* vol. 134, pp. 1264-1276, May 2011.

[176] J. Chen *et al.*, "Alterations of static functional connectivity and dynamic functional connectivity in motor execution regions after stroke," (in English), *Neuroscience Letters,* vol. 686, pp. 112-121, Nov 1 2018.

[177] C. H. Park *et al.*, "Longitudinal Changes of Resting-State Functional Connectivity During Motor Recovery After Stroke," (in English), *Stroke,* vol. 42, no. 5, pp. 1357-1362, May 2011.

[178] A. K. Rehme, S. B. Eickhoff, L. E. Wang, G. R. Fink, and C. Grefkes, "Dynamic causal modeling of cortical activity from the acute to the chronic stage after stroke," (in English), *Neuroimage,* vol. 55, no. 3, pp. 1147-1158, Apr 1 2011.

[179] L. Cheng *et al.*, "Reorganization of Motor Execution Networks During Sub-Acute Phase After Stroke," (in English), *IEEE Transactions on Neural Systems and Rehabilitation Engineering,* vol. 23, no. 4, pp. 713-723, Jul 2015.

[180] X. Zheng *et al.*, "The plasticity of intrinsic functional connectivity patterns associated with rehabilitation intervention in chronic stroke patients," (in English), *Neuroradiology,* vol. 58, no. 4, pp. 417-427, Apr 2016.

[181] G. R. Philips, J. J. Daly, and J. C. Principe, "Topographical measures of functional connectivity as biomarkers for post-stroke motor recovery," (in English), *Journal of Neuroengineering and Rehabilitation,* vol. 14, Jul 6 2017.

[182] A. M. Golestani, S. Tymchuk, A. Demchuk, B. G. Goodyear, and V.-S. Grp, "Longitudinal Evaluation of Resting-State fMRI After Acute Stroke With Hemiparesis," (in English), *Neurorehabilitation and Neural Repair,* vol. 27, no. 2, pp. 153-163, Feb 2013.

[183] A. R. Carter *et al.*, "Resting Interhemispheric Functional Magnetic Resonance Imaging Connectivity Predicts Performance after Stroke," (in English), *Annals of Neurology,* vol. 67, no. 3, pp. 365-375, Mar 2010.

[184] L. Wang *et al.*, "Dynamic functional reorganization of the motor execution network after stroke," (in English), *Brain,* vol. 133, pp. 1224-1238, Apr 10 2010.

[185] M. R. Borich, K. E. Brown, B. Lakhani, and L. A. Boyd, "Applications of Electroencephalography to Characterize Brain Activity: Perspectives in Stroke," (in English), *Journal of Neurologic Physical Therapy,* vol. 39, no. 1, pp. 43-51, Jan 2015.

[186] R. D. Pascualmarqui, C. M. Michel, and D. Lehmann, "Low-Resolution Electromagnetic Tomography - a New Method for Localizing Electrical-Activity in the Brain," (in English), *International Journal of Psychophysiology,* vol. 18, no. 1, pp. 49-65, Oct 1994.

[187] Y. Zhang, W. van Drongelen, and B. He, "Estimation of in vivo brain-to-skull conductivity ratio in humans," (in English), *Applied Physics Letters,* vol. 89, no. 22, Nov 27 2006.

[188] Y. Zhang, S. Zhu, and B. He, "A second-order finite element algorithm for solving the three-dimensional EEG forward problem," (in English), *Physics in Medicine and Biology,* vol. 49, no. 13, pp. 2975-2987, Jul 7 2004.

[189] Y. Zhang, W. van Drongelen, M. Kohrman, and B. He, "Three-dimensional brain current source reconstruction from intra-cranial ECoG recordings," (in English), *Neuroimage,* vol. 42, no. 2, pp. 683-695, Aug 15 2008.

[190] Y. Zhang, L. Ding, W. van Drongelen, K. Hecox, D. M. Frim, and B. He, "A cortical potential imaging study from simultaneous extra- and intracranial electrical recordings by means of the finite element method," (in English), *Neuroimage,* vol. 31, no. 4, pp. 1513-1524, Jul 15 2006.

[191] T. Nguyen, T. Potter, C. Karmonik, R. Grossman, and Y. Zhang, "Concurrent EEG and Functional MRI Recording and Integration Analysis for Dynamic Cortical Activity Imaging," (in English), *Jove-Journal of Visualized Experiments,* no. 136, Jun 2018.

[192] T. Nguyen, T. Potter, R. Grossman, and Y. Zhang, "Characterization of dynamic changes of current source localization based on spatiotemporal fMRI constrained EEG source imaging," (in English), *Journal of Neural Engineering,* vol. 15, no. 3, Jun 2018.

[193] T. Nguyen, T. Zhou, T. Potter, L. Zou, and Y. Zhang, "The Cortical Network of Emotion Regulation: Insights from Advanced EEG-fMRI Integration Analysis," *IEEE Trans Med Imaging,* Feb 22 2019.

[194] B. Molavi and G. A. Dumont, "Wavelet-based motion artifact removal for functional near-infrared spectroscopy," (in English), *Physiological Measurement,* vol. 33, no. 2, pp. 259-270, Feb 2012.

[195] M. P. A. van Meer *et al.*, "Recovery of Sensorimotor Function after Experimental Stroke Correlates with Restoration of Resting-State Interhemispheric Functional Connectivity," (in English), *Journal of Neuroscience,* vol. 30, no. 11, pp. 3964-3972, Mar 17 2010.

[196] F. Quandt *et al.*, "The functional role of beta-oscillations in the supplementary motor area during reaching and grasping after stroke: A question of structural damage to the corticospinal tract," (in English), *Human Brain Mapping,* vol. 40, no. 10, pp. 3091-3101, Jul 2019.

[197] J. R. Carey *et al.*, "Analysis of fMRI and finger tracking training in subjects with chronic stroke," (in English), *Brain,* vol. 125, pp. 773-788, Apr 2002.

[198] N. S. Ward, M. M. Brown, A. J. Thompson, and R. S. J. Frackowiak, "Neural correlates of outcome after stroke: a cross-sectional fMRI study," (in English), *Brain,* vol. 126, pp. 1430-1448, Jun 2003.

[199] S. S. Kantak, J. W. Stinear, E. R. Buch, and L. G. Cohen, "Rewiring the Brain: Potential Role of the Premotor Cortex in Motor Control, Learning, and Recovery of Function Following Brain Injury," (in English), *Neurorehabilitation and Neural Repair,* vol. 26, no. 3, pp. 282-292, Mar-Apr 2012.

[200] S. Vogt *et al.*, "Prefrontal involvement in imitation learning of hand actions: Effects of practice and expertise," (in English), *Neuroimage,* vol. 37, no. 4, pp. 1371-1383, Oct 1 2007.

[201] N. Sharma, J. C. Baron, and J. B. Rowe, "Motor imagery after stroke: relating outcome to motor network connectivity," *Ann Neurol,* vol. 66, no. 5, pp. 604-16, Nov 2009.

[202] P. Nachev, C. Kennard, and M. Husain, "Functional role of the supplementary and pre-supplementary motor areas," (in English), *Nature Reviews Neuroscience,* vol. 9, no. 11, pp. 856-869, Nov 2008.

[203] C. Grefkes *et al.*, "Cortical connectivity after subcortical stroke assessed with functional magnetic resonance imaging," (in English), *Annals of Neurology,* vol. 63, no. 2, pp. 236-246, Feb 2008.

[204] C. Calautti, F. Leroy, J. Y. Guincestre, and J. C. Baron, "Dynamics of motor network overactivation after striatocapsular stroke - A longitudinal PET study using a fixed-performance paradigm," (in English), *Stroke,* vol. 32, no. 11, pp. 2534-2542, Nov 2001.

[205] C. Gerloff *et al.*, "Multimodal imaging of brain reorganization in motor areas of the contralesional hemisphere of well recovered patients after capsular stroke," (in English), *Brain,* vol. 129, pp. 791-808, Mar 2006.

[206] M. Lotze, J. Markert, P. Sauseng, J. Hoppe, C. Plewnia, and C. Gerloff, "The role of multiple contralesional motor areas for complex hand movements after internal capsular lesion," (in English), *Journal of Neuroscience,* vol. 26, no. 22, pp. 6096-6102, May 31 2006.

[207] B. Hordacre, B. Moezzi, and M. C. Ridding, "Neuroplasticity and network connectivity of the motor cortex following stroke: A transcranial direct current

stimulation study," (in English), *Human Brain Mapping*, vol. 39, no. 8, pp. 3326-3339, Aug 2018.